공학박사학위논문

A study on required toughness of CO_2 pipeline by fluid structure interaction

유동 구조 연계 해석을 통한
CO_2 배관의 필요 인성치 분석

2018년 02월

서울대학교 대학원

재료공학부

염 규 정

A study on required toughness of CO2 pipeline by fluid structure interaction

유동 구조 연계 해석을 통한
CO2 배관의 필요 인성치 분석 고찰

지도 교수 오 규 환

이 논문을 공학박사 학위논문으로 제출함
2018년 2월

서울대학교 대학원
재료공학부
염 규 정

염규정의 공학박사 학위논문을 인준함
2018년 2월

위 원 장	한 홍 남	(인)
부위원장	오 규 환	(인)
위 원	선 정 윤	(인)
위 원	김 우 식	(인)
위 원	조 재 형	(인)

Abstract

Kyu Jung Yeom

Department of Materials Science and Engineering

The Graduate School

Seoul National University

In this thesis, the CO_2 pipeline of required toughness is discussed. In order to analysis of CO_2 pipeline for appropriate geometries, the fluid structure interaction (FSI) is used by combination of ABAQUS and Fluent. The natural gas has experienced with single-phase decompression when the crack occurs during operation. Otherwise, CO_2 pipeline mostly operates with two phase of supercritical or dense phase for efficiency with high density and low viscosity. It is caused phase transition when the crack propagation is occurred with suddenly drop the pressure and temperature which is plateau curve behavior.

The two cases of CO_2 pipeline have studied in thesis. Firstly, the different crack sizes ratio analyzes from 10 % to 90 % for critical internal pressure. The initiation crack located in longitudinal direction from outside of diameter. The 3 m length of CO_2 pipeline considers the appropriated flow of 100 % CO_2. At last, the crack propagation of two successive sections with girth weld took into account for analysis of toughness required.

The material properties of API X70 pipeline was acquired by the results of tensile test. The fracture toughness was converted the fracture energy based on the BS 7910 with plane strain condition from Charpy v-notch impact test. In part of crack propagation, the Traction-Separation theory applied based on comparison with experiment and simulation. The girth weld effect is supposed to be conducted the simulation based on the experimental shape of base, heat affected zone, and girth weld of API X70 pipe.

The fluid of 100 % CO_2 recognized with homogeneous equilibrium model, enhanced wall treatment, and Real Peng-Robison equation of state with confirmation followed dense phase of CO_2. The interaction surface with fluid and structure is found to be consistent for FSI, the iteration has conducted to analyze with 100 % fluid at first, then simulated structure analysis by XFEM.

The crack with the maximum principle stress is predicted over yield strength of materials for crack propagation. The crack propagation studied by XFEM, which is not required with direction of crack and remeshed. Otherwise, seam crack needs to propagate of crack. The failure theory was used maximum principle stress, which predicts the propagated.

The critical internal pressure was acquired depending on the crack size ratio. Even though the crack existence with 10 % crack size, the critical internal pressure dropped in a short time. It causes the integrity of pipeline. The results of crack

propagation with FSI is lower than the structure analysis. It is reason that the high pressure was initiated with inlet of CO_2 fluid.

The simulation results of basic study of crack size ratio and measurement of pressure with crack propagation by FSI, the FEED will affect for decreasing cost of construction of CO_2 pipeline.

Keywords: CO_2 pipeline, Crack propagation, Girth weld, Traction-separation, Crack tip opening displacement, Charpy V-notch impact test, Fluid structure interaction, Critical internal pressure, XFEM, Maximum principle stress

Student Number: 2010-20616

Contents

List of Tables

List of Figures

1. Introduction

1.1 Needs and Scope of CCS Project

Electricity generation is one of the major sources of carbon dioxide emissions and fossil fuel power plants play major roles in global warming. Due to global warming, the temperature is increasing and glaciers are melting at the South and North Poles, leading to a rise in sea levels. In 2010, industrialized countries announced the Kyoto Protocol in an agreement to reduce the production of carbon dioxide (CO_2) by 2050. Furthermore, the 2015 United Nations Climate Change Conference was held in Paris in order to negotiate a reduction in climate change. Carbon capture and storage (CCS) is the process of CO_2 transport using pipelines, ships, and trucks to deposit CO_2 and prevent it from entering the atmosphere.

Oil and gas industry has similar with CO_2 pipeline transportation. But the mechanism and operation condition are different from the compression stations and design of pipeline and etc. For the selection of pipeline, high strength low-alloy steels (HSLA) are commonly used for transportation from 1960's for large diameter and thickness.

In order to prevent from tear and crack propagation of steel pipeline, stainless steel is alternative case of prevent from fracture. However, the weld of pipeline needs more money to develop the technique for quick and easy to way of connection with

pipeline of seam weld and girth weld. Moreover, the finding of defects in pipeline is difficult to find the locations and geometries. Otherwise, the steel pipeline uses the pigging system to analyze with defect shapes and locations. In conclusion, the use the stainless pipeline could cause an amount of money to design for CO_2 pipeline.

In order to develop the CO_2 pipelines with appropriate thickness, diameter and toughness, it is important to predict the flow and fracture behavior of the pipelines. The trend of flow is different from those of liquid and gas pipelines. The tendency of liquid pipeline fractures is short and narrow while gas pipeline fractures are long and wide. The CO_2 pipeline decompression is also different from those of liquid and gas pipelines and crack initiation and propagation in CO_2 pipelines show different behaviors [1]. It is unclear whether cracks in CO_2 pipelines lead to ruptures similar to liquid or gas pipelines.

In the view of fracture behavior of pipeline, pipelines contained defects sometimes fail. Pipelines transport with gaseous fluid, two-phase fluid, dense-phase fluids, or liquid. The fracture behavior must analyze the toughness or other effects before operation of pipeline. The assessment of brittle fracture was assessed by semi-empirical equation which developed by NG-18 early 1970's and the drop-weight tear test (DWTT) could solve the problem of brittle fracture propagation.

In order to evaluate the fracture propagation of ductile behavior, there is a developed Battelle two curve method (BTCM) by Battelle Memorial Institute (BMI). This is developed in the 1970s by Keinfer, using the actual size pipe, which is artificially generated cracks using various experimental conditions, determined the either fracture propagation and arrest. However, BTCM used in the 1970s with API X65 pipe, which was lower than 100 Joule of fracture energy. The comparisons with high strength and toughness of pipeline and CO_2 pipeline would not appreciate with based on the BTCM assessment. The researchers have found to need correction factor for assessing the crack propagation. The trend of pipeline in recently uses with high strength and toughness pipeline due to reduce the cost of construction. The results of charpy v-notch (CVN) impact test would above the capacity of CVN tester and newly produced pipeline is higher than elderly produced pipeline when are equalized with compositions.

Because natural gas (NG) is different from the CO_2 pipeline with operational pressure and condition as shown in Fig. 1.1. When NG is decompressed, the pressure and temperature is decreased slowly but the behavior of CO_2 considers the two phase region. This region would be difficult to transport through the pipe when fracture is occurred caused instantly widespread of CO_2 under the ground. The density is safe even if the rupture because NG is lighter than air. Otherwise the density is NG is CO_2 is known as heavier than air and remained the ground with CO_2. CO_2 is more likely to be toxic if the CO_2 pipeline is ruptured. [2]

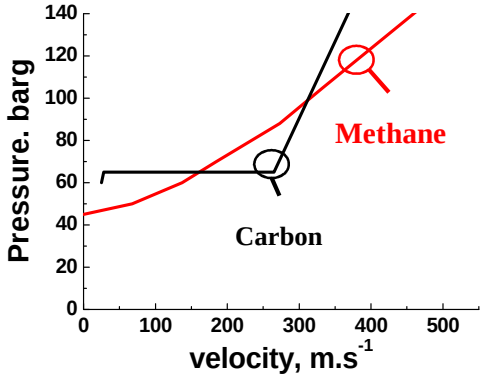

Fig. 1.1. Comparison decompression curve with CO_2 and Methane

The operational condition of the NG is different CO_2 pipeline with operational pressure and the temperature. The design of thickness and diameter is applied different view of consideration. NG operates with 5.12 MPa and - 77.3 ^oC at critical point, otherwise the 96% CO_2 operates 7.247 MPa and 31 ^oC at critical point as shown in Fig. 1.2. General operating pressure of NG is 8.5 MPa, CO_2 is transported with temperature of 8.5 ~ 15 MPa and 70 ^oC or more with dense phase or supercritical phase for high density and low viscosity efficiently. Therefore, when designing CO_2 pipeline, it must be needed to assess other approaches.

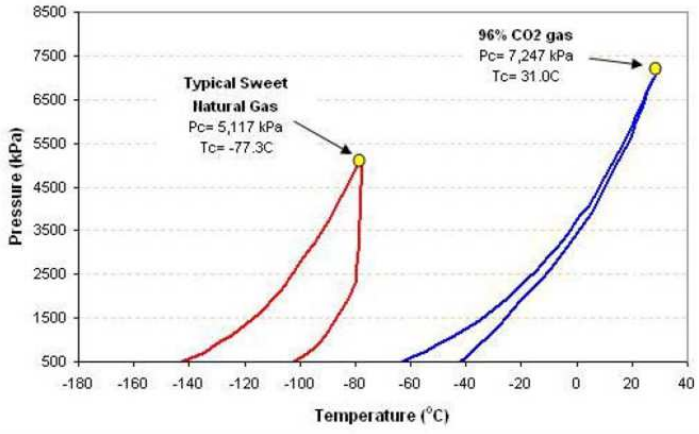

Fig. 1.2. Difference of phase envelope with NG and CO_2 [2]

Therefore, finite element method (FEM) can simulate similarly to the actual situation in order to be analyzed with structural analysis and fluid analysis of CO_2 pipeline by fluid structure interaction (FSI) connected at the same time. In this study, the minimum toughness required value of the CO_2 pipeline was studied for efficient design.

A small-scale test specimens was used to analyze the crack propagation through the structural analysis for acquiring the fracture theory to simulate three-dimension model of fracture propagation which is measured by CVN impact test and crack tip opening displacement (CTOD) test of API X 70 pipe. The crack propagation with girth weld was considered to simulate the actual shape of pipeline. An analysis of the impact of flow analysis CO_2 with equation of state (EOS) due to the flow by

applying flow behavior at the same time with Peng-Robison, viscosity, thermal conductivity, and specific heat capacity (C_P).

2. Background and literature review

2.1 CCS and CO_2 Transportation

2.1.1 Captured method

CO_2 transportation consists of tanks, ships, and pipelines for gases and liquids [3] as shown in Fig 2.1. In order to transport CO_2, the pipeline is a continuous method that allows Megatons of transports per year. Otherwise, trucks and ships are used, but they need storage sites and equipment for evaporation to deposit into the ground [4]. When liquid volume of CO_2 transports 3million/m3 per year, road and rail is inefficient. LNG-type vessels are very costly and will result in high unit cost of transport. Thus, the most reasonable transportation is by pipelines [5]. Transporting captured of CO_2 with trucks, rails and ships are relatively limited quantities. LNG-type vessels are very costly and will result in high unit cost of transport. Transporting captured of CO_2 with trucks, rails and ships are relatively limited quantities. However, the pipeline network could be transport the enormous quantities of CO_2 [6]. However, the pipeline network could be transport the enormous quantities of CO_2 [4]. The pipeline network can transport enormous quantities of CO_2 [3] while trucks and rails cost more than twice as much as the pipeline method [5].

Fig. 2.1. The method of transportation of CO_2

Existed of carbon steel are suitable to transport CO_2 with low level of moisture content for approximately 500 ppm. CO_2 pipeline considers containing with lower H_2S for transportation [3].

In the case of CCS, it is divided into three large cases with capture technology of CO_2 emissions, such as the power plant and etc., CO_2 recovery method that is discharged from the mass emission sources which power plants is divided into three large following depending on where and how to collect the CO_2 as shown in Fig 2.1.

- Post-combustion capture: Before the burning of fossil fuels, separated hydrogen and CO_2 then capture.

- Pre-combustion capture: After the burning of fossil fuels, separated nitrogen and CO_2 then capture.

- Oxyfuel: Injection of oxygen to the combustor, trapped by CO_2 emissions.

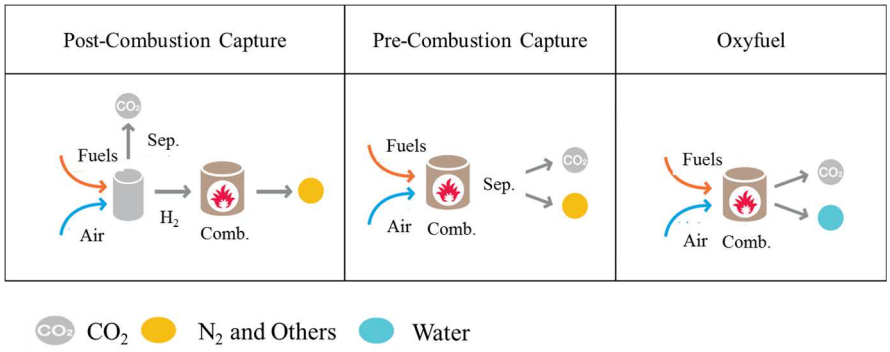

Fig. 2.2. Three method of captured CO_2.

As shown in Table 2.1, procedure of post-combustion need to decrease of amount of SO_2, and Pre-combustion and Oxfuel are predicted the economic method despite of their procedure owns the Sulphur according to IPPC report. However, since never decided yet for method of capturing CO_2, it is necessary to consider with various impurities depending on the generation of CO_2 and other impurities.

Table. 2.1. The expectation of CO_2 and impurity composition to occur in the chemical factory [3]

Coal Fired Power Plants	Component	Coal Fired % Volume	Gas Fired % Volume

Post-Combustion Capture	SO_2	<0.01	<0.01
	NO	<0.01	<0.01
	$N_2/Ar/O_2$	0.01	0.01
Pre-Combustion Capture	H_2O	0.01-0.6	<0.01
	H_2	0.8-2.0	1
	CO	0.03-0.4	0.04
	CH_4	0.01	2
	$N_2/Ar/O_2$	0.03-0.6	1.3
Oxyfuel	SO_2	0.5	<0.01
	NO	0.01	<0.01
	$N_2/Ar/O_2$	3.7	4.1

The tendency of liquid-vapor affects with different compositions of CO_2 pipeline. As it can be seen as shown in Fig. 2.3 which CO_2 and other impurities affect the phase envelope curve. Therefore, it is necessary evaluation flow, structure, and design of CO_2 pipeline.

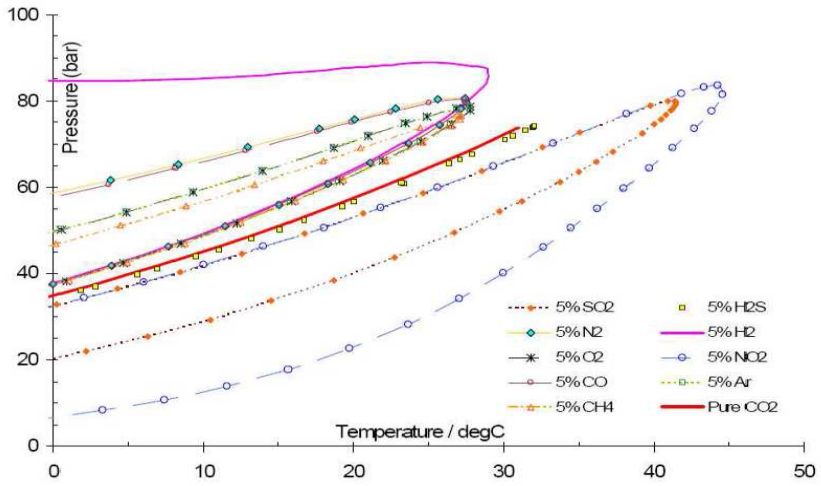

Fig. 2.3. Phase envelope curve depending on the CO_2 and other impurities

In case of CO_2 transportation of U.S.A and Canada, the CO_2 pipeline has been operating far from the cities with short term operation. NG is lighter than the air and it is distributed into the air in case of accident, otherwise the flow of CO_2 is high concentration, it is undergone under the ground which it causes the death from asphyxia. Recently there is no consideration of operation in CO_2 pipeline otherwise the operation of NG has experienced with over 40 years including design and construction. There might have operated for short length to transport from factories in South Korea. There is no experience of operation CO_2 pipeline, therefore, it is required to study of design with CO_2 pipeline in order to acquire the proper thickness, diameter, and toughness for preventing from crack propagation.

The consideration of design CO_2 pipeline is described as below

- Transport with condition of dense phase or supercritical phase in order to obtain of efficiencies.

- Transport from 15 MPa to ambient pressure for crack propagation, or reverse of pressure in case of burst pressure test

- Need to define the fracture behavior of CO_2 pipeline

- Operates dense phase or supercritical phase with 15 MPa and 330 K

- Calculate thermal conductivity, C_P for dense phase of CO_2 fluid

2.1.2 Analysis of CO_2 project

The CO_2 pipeline operates very short term compared with NG and installed the Enhanced Oil Reservoir (EOR) in the century of middle 19^{th,} There is summary of projects of CO_2 pipeline from now on as shown in Table 2.2.

Table. 2.2. CCS projects of North America and Europe [7].

a : Country codes: AU=Australia, CA=Canada, CN=China, DE=Germany, DZ=Algeria, FR=France NL=Netherlands, NO=Norway, UK=United Kingdom, US=United States

b : Legend status: P=Planned, O=Operational and C=Cancelled

c : EOR=Enhanced Oil Recovery, ECBMR=Enhanced Coal Bed Methane Recovery)

Project name	Country code[a]	Status[b]	Length (km)	Capacity (Mton/y)	Onshore /Offshore	Sink[c]
North-America						
CO_2 Slurry	CA	P	Unknown	Unknown	Onshore	EOR
Quest	CA	P	84	1.2	Onshore	Saline aquifer
Alberta Trunk Line	CA	P	240	15	Onshore	Unknown
Weyburn	CA	O	330	2	Onshore	EOR
Saskpower Boundary Dam	CA	P	66	1.2	Onshore	EOR

Beaver Creek	US	O	76	Unknown	Onshore	EOR
Monell	US	O	52.6	1.6	Onshore	EOR
Bairoil	US	O	258	23	Onshore	Unknown
Salt Creek	US	O	201	4.3	Onshore	EOR
Sheep Mountain	US	O	656	11	Onshore	CO2 hub
Slaughter	US	O	56	2.6	Onshore	EOR
Cortez	US	O	808	24	Onshore	CO2 hub
Central Basin	US	O	231.75	27	Onshore	CO2 hub
Canyon Reef Carriers	US	O	354	Unknown	Onshore	Unknown
Choctaw (NEJD)	US	O	294	7	Onshore	EOR
Decatur	US	O	1.9	1.1	Onshore	Saline aquifer
Europe						
Snøhvit	NO	O	153	0.7	Both	Porous Sandstone formation
Peterhead	UK	P	116	10	Both	Depleted oil/gas field
Longannet	UK	C	380	2	Both	Depleted oil/gas field
White Rose	UK	P	165	20	Both	Saline aquifer
Kingsnorth	UK	C	270	10	Both	Depleted oil/gas field
ROAD	NL	P	25	5	Both	Depleted oil/gas field
Barendrecht	NL	C	20	0.9	Onshore	Depleted oil/gas field

OCAP	NL	O	97	0.4	Onshore	Greenhouses
Jänschwalde	DE	C	52	2	Onshore	Sandstone formation
Lacq	FR	O	27	0.06	Onshore	Depleted oil/gas field
Rest of the World						
Rhourde Nouss-Quartzites	DZ	P	30	0.5	Onshore	Depleted oil/gas field
Qinshui	CN	P	116	0.5	Onshore	ECBMR
Gorgon	AU	P	8.4	4	Onshore	Sandstone formation

The general composition of CO_2 pipeline has been informed as shown in Table 2.3 for CCS projects.

Table. 2.3. Tendency of CO_2 and other impurities for CCS projects [8].

	Canyon Reef Carriers	Central Basin	Sheep Mt. Source	Weyburn	Cortez
CO_2	95%	98.50%	95.80%	96%	95%
CH_4	5%	0.20%	1.70%	0.70%	1-5%
N_2	<0.5%	1.30%	0.90%	<300ppm	4%
H_2S	100ppm	-	-	0.90%	0.00%

$C2^+$	-	-	0.60%	2.30%	Trace
CO_2	-	-	-	0.10%	-
O_2	-	-	-	<50ppm	-
Src_2	Anthropogenic	Natural	Natural	Anthropogenic	Natural
H_2O	50ppm wt	257ppm wt	129ppm wt	20 ppm vol	257ppm wt

It is known the important effect for controlling of lowering N_2 in EOR, but the CCS is not considerate effect. The CO_2 pipeline considers limiting of contains of H_2S for transportation [3].

2.1.3 Analysis of CO_2 standards

Although CO_2 pipelines are actively used along with enhanced oil recovery, NG pipelines, and liquid pipelines, there are some differences in the operating conditions and design of pipelines. Moreover, the transportation of CO_2 in pipelines occurs in a dense or supercritical phase to ensure highly efficient transportation with high density and low viscosity, which are required for CCS [9].

CO_2 pipelines should be conformed to design based on the standards and regulations. Although CO_2 transport by pipelines can be performed like Weyburn CO_2 pipelines from Benlah, North Dakota, USA, to the Weyburn oil field in Sakatchewan, Canada project in 2000. The guidelines and standards for CO_2 pipelines are still considered inadequate. The main reason is that CO_2 pipelines are located and operated in remote areas such as Texas and New Mexico.

In the USA, CO_2 pipelines are subject to federal regulation under the Department of Transportation 49 Code of Federal Regulations Part 195 [10. The US Department of Transportation sets the minimum safety standards for pipelines transporting hazardous liquids, which includes CO_2.

ASME B31.4 [11] is a code intended for liquid pipelines that considers CO_2 compressed above its critical pressure as a liquid. Otherwise, ASME B31.8 [12] is a code for gas pipelines that excludes CO_2 pipelines used for transportation. Codes like ASME B31.4, DNV-OS-F101 [9] and ISO 13623 [13] may be applicable for CO_2 pipelines, but they do not consider anthropogenic CO_2 in dense or supercritical phases.

Det Norske Veritas (DNV) launched a supported Joint Industry Project called CO2PIPETRANS with the objective to develop a DNV Recommended Practice (RP) for transportation of CO_2 in onshore and offshore pipelines in 2008 [9].

DNV-RP-J202 [2] was issued in 2010 to standardize CO_2 pipelines and provides guidelines for the design, construction, and operation of steel pipelines for CO_2 transportation. The objective of RP is to provide guidance for the safe and reliable design, construction, and operation of pipelines intended for large scale transportation of CO_2 and to supplement existing standards such as ISO 13623, DNV-OS-F101, and ASME B31.4, as shown in Table 2.4.

Table 2.4. Standards comparison among ISO 13623, DNV-OS-F101 and ASME B31.4 for ductile fracture.

Standards	ISO 13623	DNV-OS-F101	ASME B31.4
5. Materials and pipeline design	Sec.8 Materials and Coatings Sec.10 Construction	Sec.7 Construction- Linepipe Sec.8 Construction- Components and Assemblies Sec.9 Construction -Corrosion Protection and Weight Coating Sec.10 Construction -Installation	-
5.5 Running ductile fracture control	Sec.8.1.6 Shear Fracture Toughness	Sec.7 I 200 Supplementary requirement, fracture arrest properties	Sec.402.5 (Specific for CO_2 pipelines)

2.2 Design of CO_2 pipeline

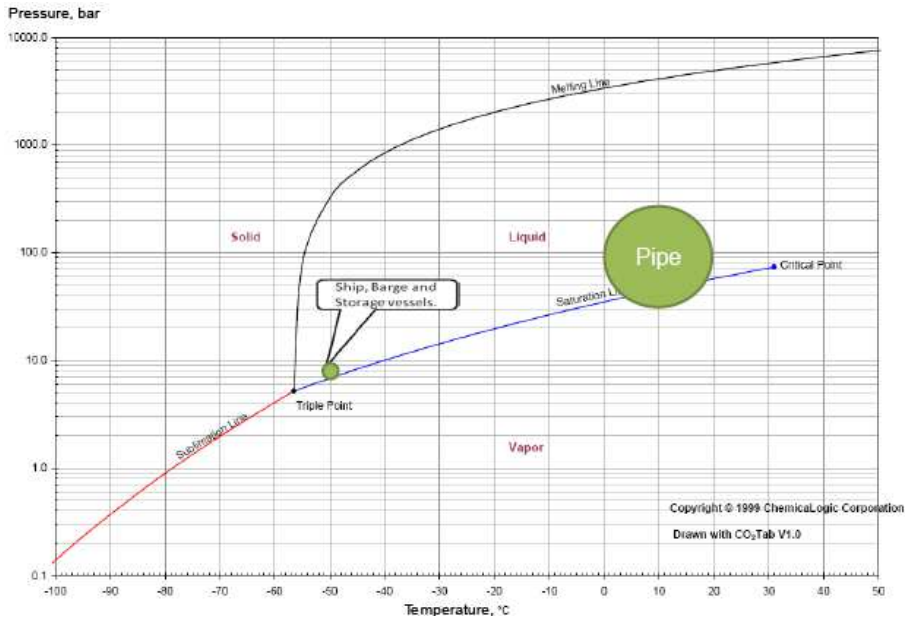

Fig. 2.4. Phase diagram of CO_2 [14]

In the above of Fig, 2.4., CO_2 is transported near the triple point when transporting CO_2 to the ship. It is known that transporting from -9 ^oC to 31 ^oC and from 9 MPa to 15 MPa. This status is the most efficient due the phase of dense or supercritical which is more high density and low viscosity of CO_2. If a leak occurs during transportation, the pressure is reduced along the saturated line. In this case, the two phase has

occurred in one phase, and the CO_2 pipeline is fractured, and CO_2 may be exposed to the outside and cause serious death of human life.

2.2.1 Determined of pipe thickness

Before determining the pipe thickness, the pipe diameter should be determined according to the pressure drop allowance per unit length, friction, CO_2 density, and CO_2 mass flow rate. The following equation is an example of how to calculate the pipe diameter.

$$\frac{\Delta P}{\Delta L} = \frac{32 f \dot{m}^2}{\pi^2 \rho D^5}$$

D : Pipeline diameter

$\Delta P/\Delta L$: Maximum allowable pressure drop

m : CO_2 mass flow rate

ρ : CO_2 density

f : Fanning friction pressure

Using the above equation, the mass flow rate to pipe diameter ratio is calculated as shown in Fig. 2.5.

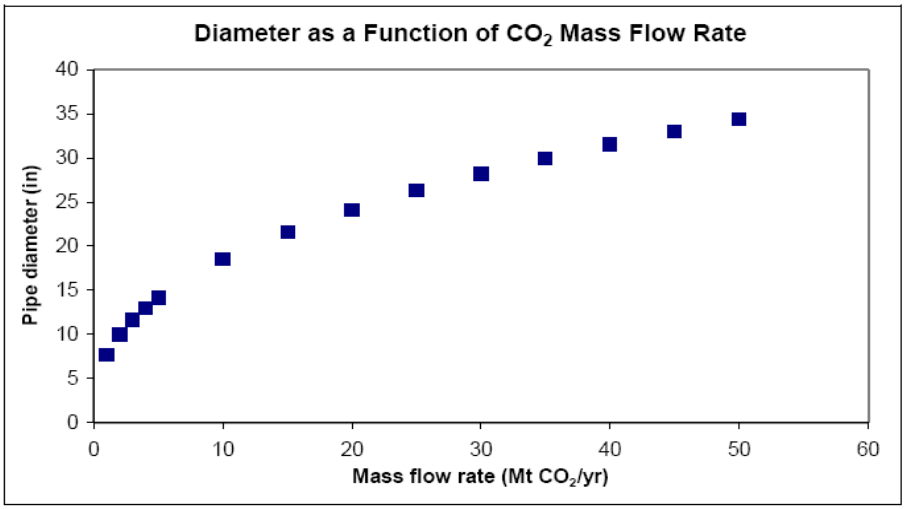

Fig. 2.5 Maximum mass CO_2 flow rate as a function of pipeline diameter [15].

In addition to the above equation, there are various evaluation methods according to the mass flow of the pipeline as shown in Table. 2.5. The pipe diameter is calculated from the results obtained through the flow assurance analysis.

Table.2.5 Equations for the calculation of pipeline diameter.

Contents	Evaluation	Formula
Hydraulic equations for turbulent flow	No topographic height Friction factor independent of flow rate Fluid & pipeline characteristics into account	$D^5 = \frac{32 \cdot f_F \cdot Q_m^2}{p\pi^2 (\Delta p / L)}$
	- Topographic height into account - Avoids use of iterative calculations	$D = \left(\frac{8 \cdot f \cdot Q_m^2 \cdot L}{\rho\pi^2 [\rho g (z_1 - z_2) + (p_1 - p_2)]} \right)^{1/5}$
	Iterative calculations Friction factor in function of diameter	$D = \left(\frac{-64 Z_{ave}^2 R^2 T_{ave}^2 \cdot f_F \cdot Q_m^2 \cdot L}{\pi^2 [M Z_{ave} R T_{ave} (p_1 - p_2) + 2 g P_{ave}^2 M^2 (h_2 - h_1)]} \right)^{1/5}$
	Steady friction factor	$\Delta p = 2.252 \frac{f \cdot L \cdot \rho \cdot Q^2}{D^5}$
Hydraulic equations with velocity as parameter	Average velocity has to be assumed Does not take pressure drop into account	$D = \sqrt{\frac{4 Q_m}{v\pi\rho}}$
Optimal design	Pressure not taken into account Economic pipe diameter calculation	$D_{opt} = 0.363 \left(\frac{Q_m}{\rho} \right)^{0.45} \rho^{0.13} \mu^{0.025}$

When the diameter of pipeline is determined using the above equation, the pipe thickness is calculated below equation which is described in the ASME and BS

specifications. Otherwise the standard of DVN is not stated of calculation of pipeline thickness.

$$t = \frac{PD_0}{2SEFT}$$

t : Minimum of pipe thickness (mm)

P : Design internal pressure (MPa)

D_0 : Diameter of pipeline (mm)

S : Yield strength of pipeline (MPa)

E : Longitudinal joint factor

T : Temperature factor

F : Design factor

Pipe are based on nominal pipe size (NPS). For NPS 14 and higher pipes, the nominal diameter is equal to the outer diameter. The NPS method represents the standard size of the tube in inches such as and NPS 1/2 and NPS 10.

Determine the structural factor (F) is described as below. The structural factor of ASME B31 [16] and BS 8010 [17] is described as shown in Table 2.6.

Table. 2.6. Design factor of standards.

Design factor/Standard	ASME B31.8	ASME B31.4	BS 8010
Design factor (liquid)	-	0.72	0.72
Design factor (Gas)	0.4 ~ 0.8	-	0.3 ~ 0.72

There is not stated of DNV standard for predicting of thickness measurement. The structure factor with onshore pipeline is described in ISO 13623; Annex B [13] as shown in Table. 2.7.

Table. 2.7 Utilization factors onshore in DNV-RP-J202

Location	Fluid Category C	Fluid category D and E				
		Location Class (Population density)				
		LC1	LC2	LC3	LC4	LC5
General Route	0.77 0.83	0.77 0.83	0.77	0.67	0.55	0.45
Crossings and Parallel encroachments						
Minor roads	0.77	0.77	0.77	0.67	0.55	0.45
Major roads, railways, canals, rivers, diked flood defenses and lakes	0.67	0.67	0.67	0.67	0.55	0.45
Pig traps and multi-pipe slug catchers	0.67	0.67	0.67	0.67	0.55	0.45
Special constructions such as fabricated assemblies and pipeline on bridges	0.67	0.67	0.67	0.67	0.55	0.45

In the case of non-human areas which located in tundra and desert, the design factor is 0.83 to determine the pipe thickness.

In this study, design factor was evaluated by applying 0.4, which is mainly applied to domestic gas piping design, and 0.72, which is the liquid transport piping

coefficient. Temperature derating factor of pipeline is described as shown in Table 2.8.

Table 2.8. Temperature derating factor, T, for steel pipe [12]

Temperature, °F(℃)	Temperature derating Factor, T
250 (121) or less	1.000
300 (149)	0.967
350 (177)	0.933
400 (204)	0.900
450 (232)	0.867

If the temperature is a medium value, calculate the T value according to the proportional method. The temperature coefficient for a given pipeline is value 1. Longitudinal joint factor is described as shown in Table 2.9.

Table 2.9 Longitudinal joint factor, E [12].

Spec. No	Pipe Class	E factor
ASTM A 53	Seamless Electric-Resistance-Welded Furnace-Butt Welded, Continuous Weld	1.00
ASTM A 106	Seamless	1.00
ASTM A 134	Electric-Fusion Arc-Welded	0.60
ASTM A 135	Electric-Resistance - Welded	1.00
ASTM A 139	Electric-Fusion Arc-Welded	0.80
ASTM A 333	Seamless Electric-Resistance – Welded	1.00
ASTM A 381	Submerged-Arc-Welded	0.80
ASTM A 671	Electric-Fusion-Welded Classes 13,23,33,43,53 Classes 12,22,32,42,52	0.80
ASTM A 672	Electric-Fusion-Welded Classes 13,23,33,43,53 Classes 12,22,32,42,52	1.00
ASTM A 691	Electric-Fusion-Welded Classes 13,23,33,43,53 Classes 12,22,32,42,52	0.80
ASTM A 984	Electric-Resistance - Welded	1.00
ASTM A 1005	Double Submerged-Arc-Welded	1.00

ASTM A 1006	Laser Beam Welded	1.00
API 5L	Electric Welded	1.00
	Seamless	1.00
	Submerged-Arc-Welded	1.00
	(Long, Seam or Helical seam)	
	Furnace-Butt Welded, Continuous Weld	0.60

The welding efficiency of a given longitudinal joint factor is determined by the above table and is '1' given. (CASE A, B)

Mill Torrance of pipeline is described the domestic pipeline as shown in Table 2.10. (unit :mm)

Table. 2.10 Mill Torrance of pipeline for domestic

Thickness of pipe	Tolerance
≤5.0 (0.197")	±0.5 (0.020")
>5.0 (0.197") to < 15.0 (0.591")	±0.1t
≥15.0 (0.591")	±1.5 (0.060")

The Mill Torrance is considered below Table 2.11. in standard of API 5L [18] and Table 2.12 in standard of ISO 3183 [13].

Table. 2.11 Tolerances for wall thickness [18]

Size	Type of pipe	Tolerance (% of specified wall thickness)	
		Grade B or Lower	Grade X42 or Higher
≤2 7/8	All	+20.0 – 12.5	+15.0 – 12.5
>2 7/8 and < 20	All	+15.0 – 12.5	+15.0 – 12.5
≥ 20	Welded	+17.5 – 12.5	+19.5 – 8.0
≥ 20	Seamless	+15.0 – 12.5	+17.5 – 10.0

Table. 2.12 Tolerances for wall thickness, Table J.4 [13]

Wall thickness (t) mm (in)	Tolerances mm (in)
SMLS pipe	
< 4.0 (0.157)	+ 0.6 (0.024) - 0.5 (0.020)
> 4.0 (0.157) to < 10.0 (0.394)	+ 0.15 t - 0.125 t
> 10.0 (0.157) to < 25.0 (0.984)	+ 0.125 t - 0.125 t
> 25.0 (0.984)	+ 3.7 (0.146) or + 0.1 t, whichever is the greater + 3.0 (0.120) or - 0.1 t, whichever is the greater
HFW pipe	
< 6.0 (0.236)	± 0.4 (0.016)
	± 0.7 (0.028)
	± 1.0 (0.039)
SAW pipe	
< 6.0 (0.236)	± 0.5 (0.020)
> 6.0 (0.236) to < 10.0 (0.394)	± 0.7 (0.028)
> 10.0 (0.394) to < 20.0 (0.787)	± 0.7 (0.028)
> 20.0 (0.787)	+ 1.5 (0.060) - 1.0 (0.039)

The Kingsnorth Carbon Capture & Storage Project, which carried out the CCS demonstration project and carried out the basic design of CO_2 pipeline in the UK, was evaluated using ISO 3183, Table J.4 [13] to use the 1.5mm.

Corrosion-resistant depth prevents the pipe thickness from decreasing with considering the extra pipe thickness due to corrosion. The allowable corrosion depth of the pipe is designed to be set to 1.5 mm [19].

2.2.2 Determined of pipe toughness

Development of the ductile fracture propagation control technology is critical to ensure structural integrity and supply of gas. Moreover, understanding for requirement toughness of pipelines is one of the important design factors for preventing the brittle and ductile fracture. Since 1970s, the brittle fracture arrest criterion was developed by Maxey. Otherwise, the ductile fracture criterion does not exist [20]. Running ductile fracture may cause a catastrophic failure of gas pipeline Fracture resistance is important to design factor and consider Charpy impact energy to prevent propagation.

In order to research the requirement of toughness for ductile fracture, there are existed representatively methods as CVN impact test and CTOD.

CVN uses v-notched specimen to measure the absorbed energy during fracture. The absorbed energy is a measure of toughness for materials and temperature-dependent ductile-brittle transition widely used in industry as it is easy to prepare and conduct. The results of the CVN impact test can be obtained quickly and cheaply [21]. The CTOD suggested fracture concept with δ_t as the characteristic parameter of CTOD [22, 23]

The CTOD criterion states that in ductile materials crack initiation starts, if the crack tip opening displacement δ_t exceeds a critical materials specific limit value δ_{tc}, as shown below equation

$$\delta_t = \delta_{tc}$$

This assessment assumes that atomic interaction forces across the faces an opening crack as cohesive zone. This method is more reliable to compare CVN because it is the limited to specimen size for understand of ductile crack propagation. The CTOD used for preparation with conventional method and relatively inexpensive to testify the toughness of pipe. Therefore, the conditions must be tested when utilized as supplement pipelines according to the British Standards Institution and American Society for Testing and Materials [24, 25].

2.2.2.1 CVN

Charpy impact testing also known as CVN test considered with hammer to strike the specimen to measure the toughness of pipe with pendulum from height. Since it is easy to make the specimen and testify, the swing with pendulum measure the height of the swing for absorbed energy of the specimen as shown in Fig. 2.6. The test has conducted with a range of low and high temperature for predicting the ductile to brittle transition temperature (DBTT) curve.

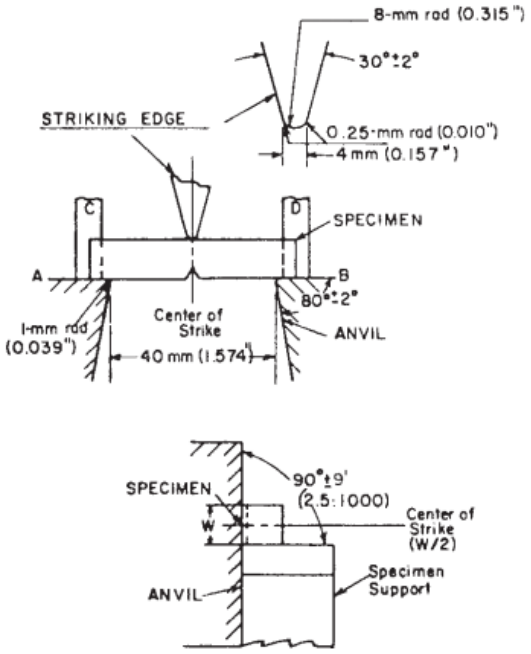

Fig. 2.6 Charpy (Simple-Beam) Impact Test [26].

The specimen of testify with CVN test is described with 10 mm × 10mm × 55 mm for standard size, 10 mm × 7.5 mm × 55mm, 10 mm × 6.7 mm × 55 mm, 10 mm × 5 mm × 55 mm, 10 mm × 3.3 mm × 55 mm, and 10 mm × 2.5 mm × 55 mm for

subsize specimen according to the ASTM A370 as shown in Fig. 2.7 (Standard Test Method and Definitions for Mechanical Testing of Steel Products).

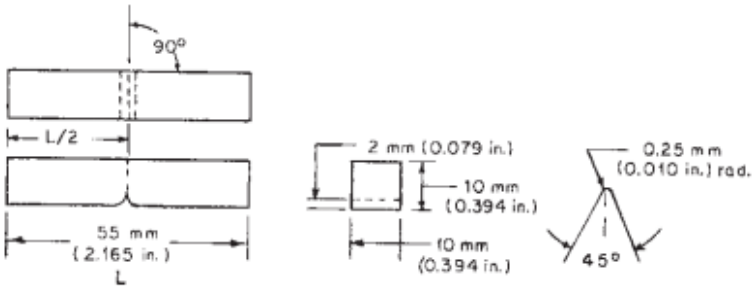

(a) Standard Full Size Specimen

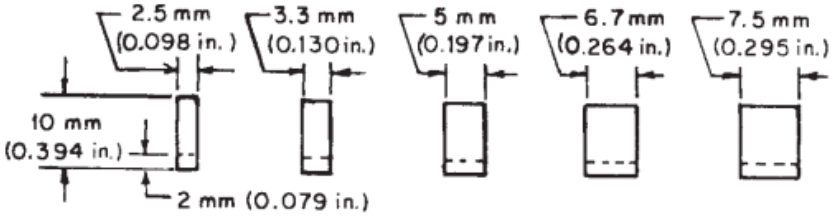

(b) Standard Subsize Specimens

Fig. 2.7. Charpy V-notch Impact Test Specimens with standard and subsize [26].

The DBTT curve is important the curvature due to changed fracture energy suddenly. The curve is hardly measure the precisely point the change material properties. The DBTT is derived by empirically way to measure. When the high strength and toughness of pipeline conduct to testify of CVN. The CVN energy goes up to the maximum allowable energy for the test machine. Even though the equivalent material properties of pipeline with production of past and present, the present

pipeline would higher than the past pipeline. Since these reason and CVN test did not cover up the whole thickness of pipeline, there is demand to apply another method to acquire the proper toughness of pipeline such as DWTT or CTOD.

2.2.2.2 DWTT

The DWTT has been proposed as a fracture parameter that can be used to characterize material toughness. The size of specimens of the charpy test and the Izod test are comparatively smaller than DWTT specimen [27] and therefore the length of fracture ligament is not long enough to reach steady state fracture [28]. DWTT method is one of the suitable methods to allocate the fracture behavior to real pipe lines application [29, 30] as shown in Fig. 2.8. The DWTT predicts of transition temperature and fracture behavior of pipeline. According to the American Petroleum Institute (API), press notch (PN) DWTT uses for low toughness of pipeline and Chevron notch(CN) DWTT is recommended for high toughness. The specimen of DWTT process with transverse-longitudinal direction for reducing the thickness of pipeline as 19 mm and makes test with PN or CN DWTT specimen.

The assessment of DWTT is predicted the 85 % of shear fracture proportion from preventing brittle fracture.

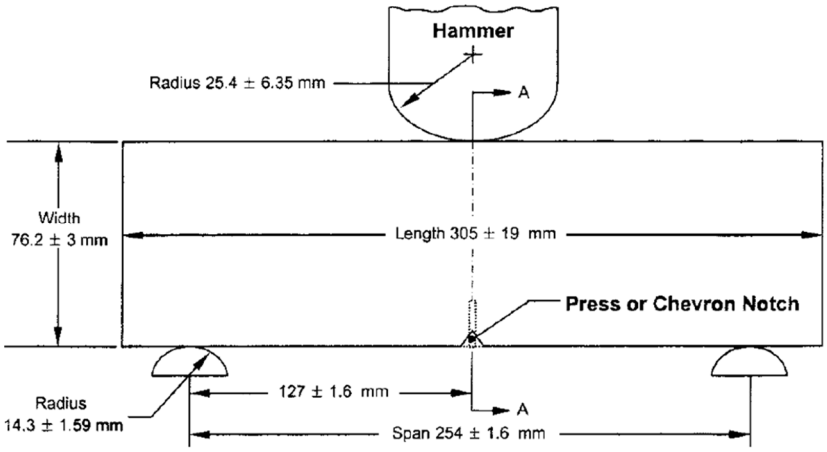

Fig.2.8 Geometry of DWTT experiment [31].

2.2.2.3 CTOD

Fracture mechanism specimens made of ductile materials are loaded, it can be observed that the tip of the originally sharp crack undergoes with wide stretching, and blunting due to plastic deformation, even before the crack initiates.

Opening displacement of crack faces exceeds by far that crack opening due to purely elastic deformation. Local measure of the plastic strain around the crack tip. This parameter δt is called CTOD. Wells and Burdekin & Stone suggested a fracture concept that the crack tip opening displacement δ_t as characteristic parameter. The CTOD criterion states that in ductile materials crack initiation starts, if the crack tip opening displacement δ_t exceeds a critical, materials specific limit value δt_c.

Cohesive zone model is based on the assumption that the material's failure process during fracture occurs only in a narrow strip-shaped zone in front of the main crack. The first model from Barenblatt is assume that atomic interaction forces across the faces of an opening crack as cohesive zone. All cohesive zone model is needed as a consequence of unrealistic stress singularity at the crack tip disappear. A similar

model was developed by Dugdal to simulated a strip-shaped plastic zone ahead of the crack in ductile metal sheets.

This assessment assumes that atomic interaction forces across the faces an opening crack as cohesive zone. This method is more reliable to compare CVN because it is the limited to specimen size for understand of ductile crack propagation as shown Fig. 2.9. The B and W was determined according to longitudinal and circumferential direction as shown in Fig. 2.10.

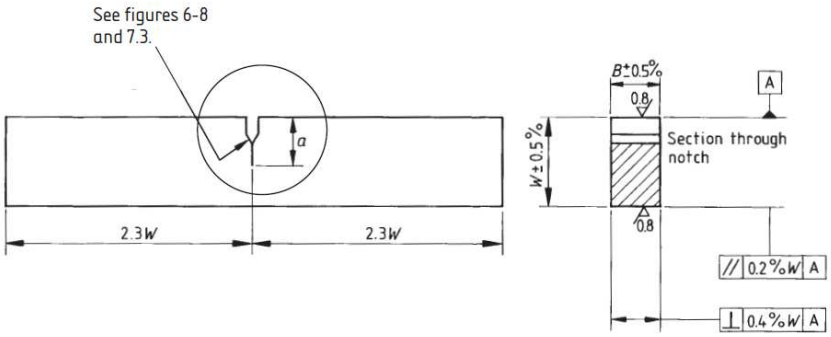

Fig. 2.9. Geometry of CTOD specimen [24, 25]

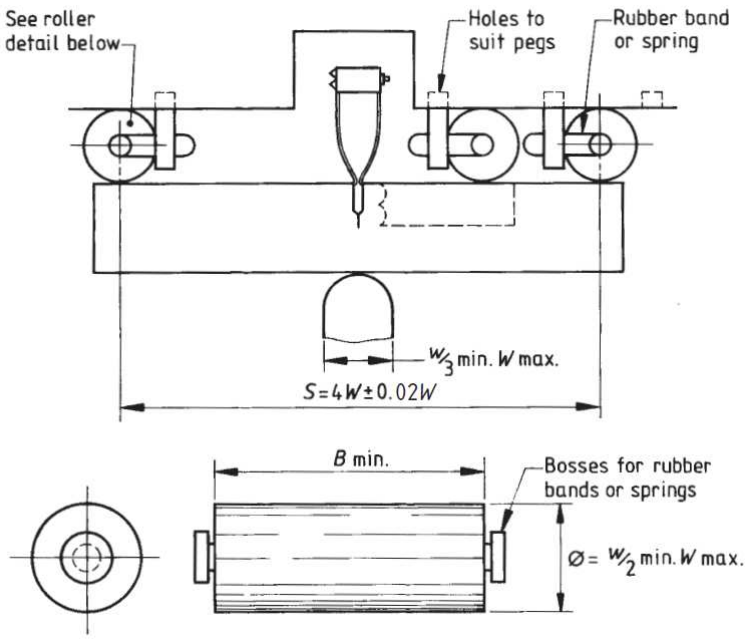

Fig. 2.10. Geometry and set position of holder [24, 25]

B : Thickness

W : 2 x (B) thickness ($1.0 < W/B \leq 4.0$)

a : Crack length ($0.45W < a < 0.55W$)

The pre-cracking condition was described with room temperature and fatigue precracking force accuracy of ± 2.5 %. The maximum fatigue precracking force F_f is considered the final 1.3 mm or 50 % length.

$$F_f = \frac{B(W-a)^2(\sigma_{YSP} + \sigma_{TSP})}{4S}$$

σ_{YSP} : 0.2 % proof strength at the temperature of fatigue precracking (MPa)

σ_{TSP} : Tensile strength at the temperature of fatigue precracking (MPa)

S : Span length

Growth and coalescence of microvoids, a geometric shortening of the remaining ligaments occurs. The cohesive zone model (CZM) assumes that growth and coalescence of microvoids, a geometric shortening of the remaining ligaments occurs [32] as shown in Fig. 2.11. In this study, CTOD simulation was applied the bilinear behavior for FEA. In order to establish the damage theory of CTOD, equations derived for damage initiation, evolution and fracture energy. Damage initiation of material starts at the point when the stress or strain reaches the user defined damage initiation criterion. Maximum nominal stress criterion (MAXS) used for in this Traction Separation (TS) law in mode I [28, 33].

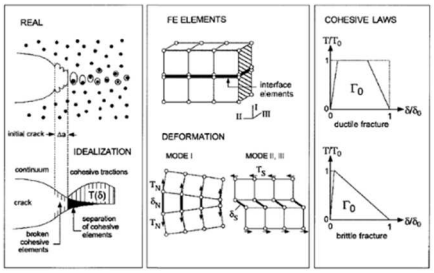

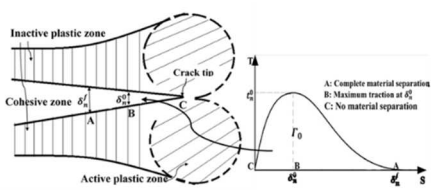

Figure 2.7: Embedded cohesive process zone and typical traction-separation (TS) curve, (Li & Chandra, 2003).

Fig. 2.11. Representation of the Ductile Failure Process by CZM

Damage initiation

The material starts at the point when the stress or strain reaches the user defined damage initiation criterion. In this study, we consider criterion with maximum nominal stress criterion (MAXS). The value of K_{nn} is taken 10,000,000 MPa in TS laws [28]. K_{nn}, K_{ss}, and K_{tt} are uncoupled traction-separation law which is equal to Knn2(1+ν) *(*Poisson's ratio ν : 0.3) for values of K_{ss} and K_{tt}. The material starts at the point when the stress or strain reaches the user defined damage initiation criterion. A TS law is a progressive damage model that defines the maximum traction based on the separation or strain history of the element. The bilinear TS laws has been chosen to analyze the CTOD simulation and experiment. The interface between two CTODs was considered zero thickness of specimen.

$$max\left\{\frac{\langle t_n \rangle}{t_n^o}, \frac{t_s}{t_s^o}, \frac{t_t}{t_t^o}\right\} = 1$$

T^o_n (nominal stress) : 3-4 x σ_y [28, 33]

T^o_s, T^o_t (shear strength) : 0.75 x T^o_n

Damage evolution

$$D = \frac{\delta_n^f \left(\delta_n^{\max} - \delta_n^o\right)}{\delta_n^{\max}\left(\delta_n^f - \delta_n^o\right)}$$

D : Damage scalar

δ^f_n : Effective displacement at complete failure

δ^o_n : Effective displacement at damage initiation

α : Non-dimensional material parameter that define the rate of damage evolution

The fracture energy is equal to the area under the traction-separation curve. The fracture toughness of the cohesive zone model in terms of fracture energy can be expressed to represent the traction-separation law as shown in Fig. 2.12

$$G_c = \tau_0 = \frac{1}{2} t_n^0 \delta_n^f$$

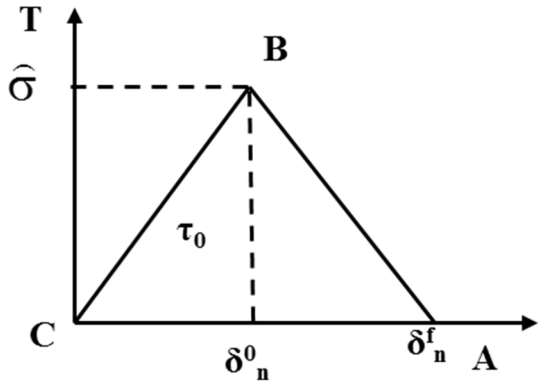

Fig. 2.12. Bilinear traction-separation law [28].

$\hat{\sigma}$, (t^o_n): Maximum traction (B)

δ^f_n, (δ_c): Final separation (A)

τ_0: Fracture toughness

2.3 BTCM and other approaches

As below of Table 2.13, there is comparison of brittle and ductile fracture of pipeline.

Table. 2.13. Comparison of brittle and ductile fracture

	Brittle fracture	Ductile fracture
Fracture propagation speed	365m/s ~ 914m/s	400~800ft/sec
Fracture propagating	Simultaneous along the axis of the pipeline are common	Straight line along the axis
Fracture surface pattern	Sinusoidal pattern (due to fracture and elastic stress wave)	Shear facture through the thickness and local wall thinning.
Fracture surface	Narrow ‘lips’ on the internal and external surfaces on the pipe(No global plastic deformation effect)	Extensive global plastic deformation with the pipe ahead of the fracture oversized and the pipe behind the fracture flattened.

In order to develop the design with CO_2 pipeline, it is important to predict the decompression curve and fracture behavior of CO_2 pipelines. The decompression curve is different from liquid and gas pipelines. The liquid pipelines would fracture

with short and narrow and gas pipeline with long and wide as shown in Fig. 2.13. However, CO_2 pipeline of decompression are also different from liquid and gas pipelines, crack initiation and propagation of CO_2 pipelines could show different behavior [1]. It is unclear that cracks with CO_2 pipelines could rupture as a liquid pipeline or gas pipeline.

Fig. 2.13. (a) Gas and (b) liquid pipelines fracture behavior.

When the pipeline occurs the fracture, pipeline consist of rupture and leak and dispose the gas into the air. The pipeline does not require the proper toughness in order to prevent from the crack propagation result in the propagation or arrest as shown in Fig. 2.13.

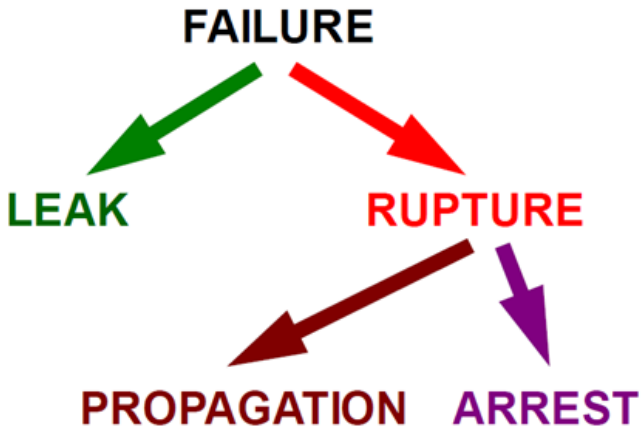

Fig. 2.13. Leaks, ruptures and propagating fractures [1]

The mechanism occurs for the gas and liquid pipeline. However, the CO_2 pipeline contains the different gas decompression and fracture behavior occurs different behavior of fracture initiation or propagation. The standard of CO_2 pipeline issued only the DNV-RP-J202 (2012) by Det Norske Veritas (DNV) which called Design and operation of CO_2 Pipelines. This standard consist of design, fatigue, and assessment of CO_2 pipeline. The most of these subjects cite from other standards with ASME or ISO. This standard need to predict for more information in order to design of CO_2 pipeline.

The supplement existing standards such as ISO 13623 [13] (Petroleum and natural gas Industries-Pipeline transportation systems), DNV-OS-F101 [9] (Submarine

Pipeline Systems) and ASME B31.4 [11] (Pipeline Transportation Systems for Liquid Hydrocarbons and Other Liquids)).

The study of ductile fracture is necessary to confirm the method which conducts with based on the engineering or simulation but these standards are discussed with details of conduction for verification of ductile fracture.

2.3.1 Assessment of BTCM

BTCM is based on the semi-empirical analysis which could predict the minimum of requirement toughness combined with decompression curve and crack fracture. This method predict the critical axial crack length depended on the solution of modified Dugdale plastic zone correction.

The development of axial through-wall-crack equations described with the mechanism of axial through-wall-cracked pipe fracture by Maxey and Kiefner. The driving force of crack used the plane stress intensity factor as blow.

$$\frac{\pi K_c^{\,2}}{8c\sigma_f^{\,2}} = \ln\left\{\sec\left(\frac{\pi\sigma}{(2\sigma_f)}\right)\right\}$$

2c : Total axial through-wall crack length (inch)

σ_f : Flow stress (ksi)

σ : Hoop stress at failure, (ksi)

K_c : Critical plane-stress stress-intensity factor, (ksi-in$^{0.5}$)

The driving force could predict when axial crack is larger than the crack of flat-plate. In case of axial crack, Folias bulging factor (M_T) is applied as below.

$$\frac{\pi K_c^{\,2}}{8c\sigma_f^{\,2}} = In\left\{ sec\left(\frac{\pi M_T \sigma_h}{(2\sigma_f)} \right) \right\}$$

K_c : Plane stress fracture toughness (according to the experiment data)

σ_h : Hoop stress at failure

M_T : Folias bulging factor for a through-wall axial crack

In order to estimate above the equation, the correlation analyze between K_c and CVN energy. This equation could anticipate using between initial crack length and Charpy toughness for acquiring empirical relationship as shown in Fig. 2.14.

$$\frac{12C_V}{A_C} = \frac{K_C^2}{E} = G_C$$

C_v : Charpy V-notch impact energy, ft-lb

A_C : Net-section area of the Charpy specimen, i.e., 0.124 in^2

E : Elastic modulus, psi

K_c : Plane-stress critical stress intensity factor, $psi\text{-}in^{0.5}$

G_c : Plane-stress strain energy release rate, $in\text{-}lb/in^2$

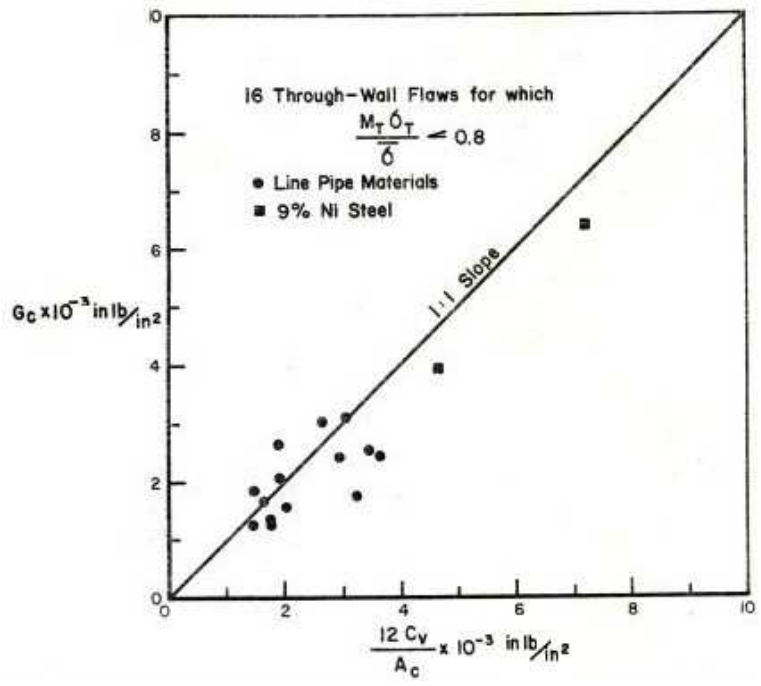

Fig. 2.14. The relationship between Gc and CV from full-scale fracture initiation tests to Charpy upper-shelf energy.

The relationship equations of driving force and correlation analyze between Kc and CVN energy combine equation as below.

$$\frac{12C_V E}{(8c\sigma_f^2 A_C)} = In\left\{ sec\left(\frac{\pi M_T \sigma_h}{(2\sigma_f)} \right) \right\}$$

This equation could be adaptation through K to J as below.

$$\frac{\pi JE}{(8c\sigma_f^2)} = In\left\{ sec\left(\frac{\pi M_T \sigma_h}{(2\sigma_f)} \right) \right\}$$

The curve of J-R manages to forecast with crack growth and maximum load. The definition of M_T (Bulging factor) is yield strength + 68.95MPa. The axial crack stability analyses were related to the decompression curve. The speed of brittle fracture was from 1000 to 1500 m/s of crack propagation, 350 m/s for the NG. The speed of brittle fracture is faster than the decompression curve, the crack is propagated (otherwise speed of water is slower). Brittle fracture arrest criteria were proposed other studies related with CVN energy and DWTT. However, the speed of ductile fracture is slower than brittle fracture for propagation. the effect of

decompression curve in the internal flow is important to predict the fracture behavior of pipeline.

In the case of decompression behavior of flow applied with pressure, the flow suffered from 1) ideal gas, 2) two phase, or 3) single phase gas as shown in Fig. 2.15.

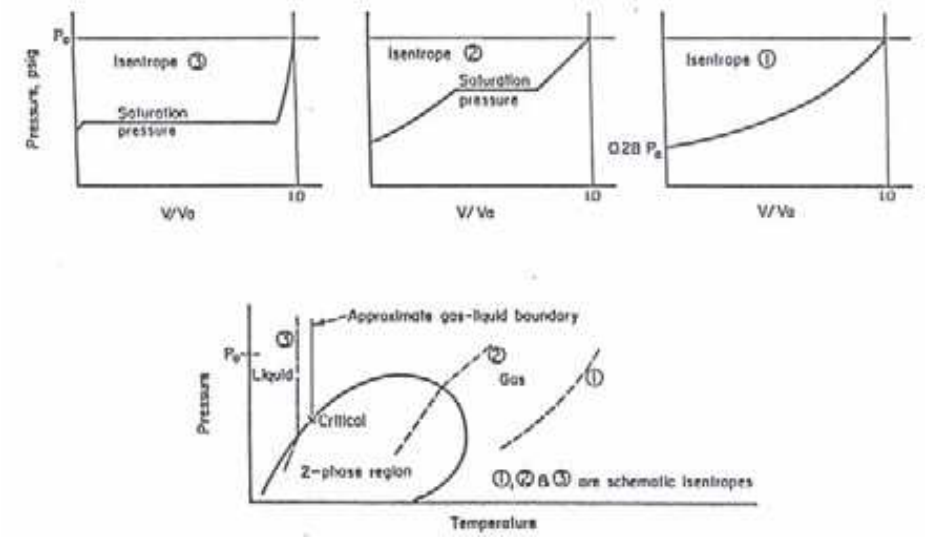

Fig. 2.15. Schematic of decompression behavior for ductile fracture arrest conditions.

In the case of above figure, the x axis describes the depressurization pressure (Pd), the y axis describes instantaneous pressure sound speed (Va) / the initial sound speed (V) (Va / V). In case of methane, it shows the ideal gas behavior with 405 m/s for the initial sound speed. Rich NG shows decompression behavior in two phases. Therefore, it is necessary to increase the toughness in order to prevent ductile

fracture. The speed of wave is immediately sound speed, which gas decompression lowers temperature and sound speed decreases, may rupture by decreasing gas velocity. Velocity of decompression pressure gas with immediate sonic velocity is related to the rate which ductile fracture develops.

Based on the ideal gas the expansion is isentropic, which leads to a cross section of the pipe. The ideal gas proposes an evaluation formula assuming homogeneous in case of flow. The equation was proposed with relationship between wave velocity and pressure as below equation.

$$P_d = P_i \left[\frac{2}{\gamma+1} \left(\frac{\gamma-1}{\gamma+1} \right) \frac{V}{V_a} \right]^{\frac{2\gamma}{\gamma-1}}$$

P_d : Decompressed pressure level

P_i : Initial line pressure,

V : Pressure wave velocity,

V_a : Acoustic velocity of gas at initial pressure and temperature

γ : Initial specific heat of gas.

The pressure slowly decreases due to the full-bore opening rapidly grows, it is possible to know with 1) slit occurrence, 2) decompression. Decompression of decreasing cause increase the in near the location where the original rupture had begun, and toughness for preventing from crack propagation is required.

NG containing hydrocarbons heavier than methane is referred to rich gas. The hydrocarbon tends the behavior of two-phase and more complex than the ideal gas. In order to assess the rich gas, the assessment is used the GASDECOM. BMI was developed with empirical equation as below

$$V_f = \left[\frac{C_B \sigma_f}{\sqrt{CVP}}\right]\left[\frac{\sigma_d}{\sigma_a} - 1\right]^{\frac{1}{6}}$$

V_f : Fracture speed, m/s

C_B : Backfill constant backfill constant (2.76 for no backfill, 2.00 for soil backfilled and 1.71 for water backfilled pipe)

σ_f : Flow stress (SMYS + 68.9MPa), MPa

CVP : Charpy V-notch upper-shelf energy for a 2/3-thickness specimen, J

σ_d : Decompressed hoop stress (PdRm/t), MPa

σ_a : Arrest stress, MPa

$$\sigma_a = \left[\frac{2\sigma_f}{3.33\pi}\right] arccos\left\{exp\left[-\frac{(18.75CVPE\pi)}{24\sigma_f^2 (R_m t)^{0.5}}\right]\right\}$$

P_d : Decompressed pressure, MPa

R_m : Mean pipe radius, mm

t : Pipe or tube thickness, mm

E : Elastic modulus, MPa

In order to define of ductile fracture, Battelle was conducted full scale hydrostatic burst test used low toughness and strength pipe in the early 1970's by Maxey. The approach of BTCM was assessed the crack propagation when the driving force for propagation fracture is presented by decompression curve. When BTCM analyzed for crack propagation, the gas decompression curve was determined by GASDECOM program which developed by Kenneth E. Starling on behalf of the

BMI 1970's to analyze with different gas mixtures. The crack propagation is predicted when the crack resistance curve and decompression of gas are tangent

The crack resistance curve concluded with semi-empirical equation as shown in below equation.

$$V_f = C\frac{\sigma_f}{\sqrt{R}}\left(\frac{P}{P_a}-1\right)^{\frac{1}{6}}$$

V_f : Crack propagation velocity (m/s)

C : Backfill parameter (2.75)

σ_f : σ_y+69MPa

R : C_v/A_c (C_v : Charpy impact energy, A_c : 80mm^2(area of Charpy specimen)

P : Instant decompressed pressure near the crack tip (MPa)

P_a : $2t\sigma_a/D$ (arrest pressure at the crack tip (MPa)

$$P_a = \frac{\sigma_a t}{R}$$

t : Pipe thickness (mm).

$$\sigma_a = \frac{2\bar{\sigma}}{3.33\pi_0} \cos^{-1} \exp\left(-\frac{CVN \cdot E\pi}{24A\bar{\sigma}^2\sqrt{Rt}} \right)$$

E : Elastic modulus (GPa)

D : Pipe diameter (mm)

$\bar{\sigma}$: Flow stress which is $(\sigma_y + \sigma_{UTS})/2$

The above equations were based on the full scale hydrostatic burst tests used NG.

The prediction of crack propagation assumes with tangent between gas decompression curve and crack resistance curve as shown in Fig. 2.16

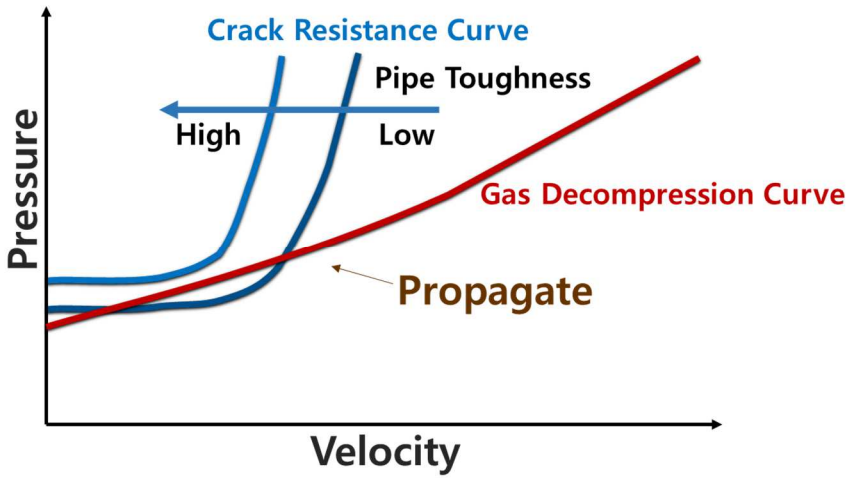

Fig. 2.16. The assessment of BTCM

The gas decompression curve obtained used GASDECOM with variety of impurities. The GASDECOM describes the simple decompression models for predicting the decompression behavior of fluid with involving lean and rich gas. The EOS uses Benedict, Webb, Rubin, Sratling (BWRS) and developed to use the Span-Wagner for CO_2 and GERG-2008 for CO_2-rich mixture [1]. The GASDECOM was developed in early 1970's and used results of full scale hydrostatic burst test with low strength and toughness pipelines

2.3.2 Limitations of BTCM

DNV-RP-J202 states about the BTCM especially for understanding of ductile fracture that need to confirm with appropriate verification based on BTCM and engineering method.

BTCM approach assumed that pipelines with cracks would propagate when the crack resistance curve and gas decompression curve were tangent each other. It is very simple way to calculate when the pipelines of geometries, grade and toughness are known. However, it was based on the semi-empirical method, low toughness and strength of pipeline such as API X65 and below. Problems could be anticipated to analyze with pipelines of high strength and toughness.

The study of trend with toughness of pipeline is increasing of CVN energy, which the crack propagation could be preventing from fracture. In this Fig. 2.27., it can be seen that the high strength and toughness pipe is applied from 100 Joule with CVN energy.

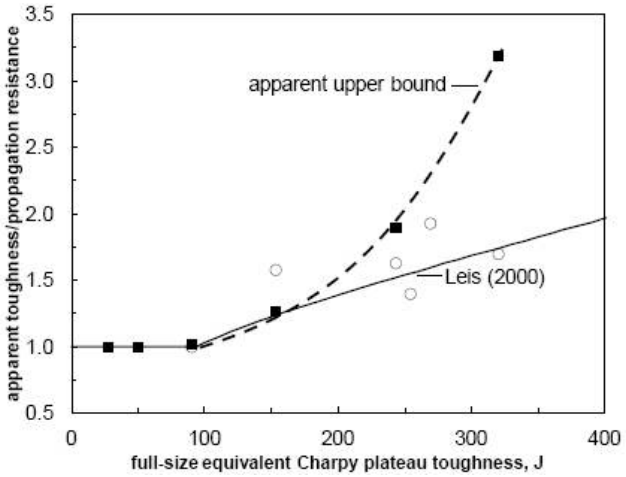

Fig. 2.17. The trend of CVN energy of pipeline [36].

When pipelines are used to transport with CO_2, it is needed to test with full scale fracture propagation test for adapting BTCM approach.

In the late 1970's, Japanese researchers started a large research program High-strength Line Pipe (HLP) and conducted a series of full-scale fracture propagation tests for X70 gas pipeline steels at pressure up to 80% SMYS and at temperature of -5 ^{o}C by Iron and Steel Institute of Japan (ISIJ) with HLP [37, 38]. Series of full scale burst tests, X70, 48in, 18.3mm, dry air, and NG. They are considered with simply extended the BTCM by curve fitting with pre-cracked DWTT energy and

recalibration is needed for the new fluids and new materials with modern steel with high strength and toughness as below equations.

$$V_f = 0.670 \frac{\sigma_f}{\sqrt{R}} \left(\frac{P}{P_a} - 1 \right)^{0.393}$$

$$P_a = \left[0.382 \frac{t\sigma_f}{D} \right] cos^{-1} \left[exp \left[- \frac{3.81 \times 10^{-7} R}{\sigma_f{}^2 \sqrt{Dt}} \right] \right]$$

V_f : Crack velocity(m/s)

σ_f : $(\sigma_{ys} + \sigma_{uts})/2$ (MPa)

R : D_p/A_p (J/mm^2)

D_p : Total energy of PC DWTT (J)

A_p : Fracture area (mm^2)

P : Decompressed pressure (MPa)

P_a : Arrest pressure (MPa)

$D_p(\text{estimate}) = 3.29t^{1.5}C_V^{0.544}$

The Japanese researcher developed HLP to predict final crack length. HLP considered with correlation between PC-DWTT and CVN energy. They found the recalibration is needed for the new fluids and new materials with modern steel with high strength and toughness. However, it needs to revise the equation of applied crack velocity [39], and problems similar to the BTCM for API X80 and above [40].

Researchers have studied the correction factors to analyze the CO_2 pipeline by using GASDECOM [35, 36, 41, 42]. However, The BTCM predicts unconservative correction factors of 1.4 to 1.7 for X80 and X100, respectively [39] as shown in Fig. 2.17.

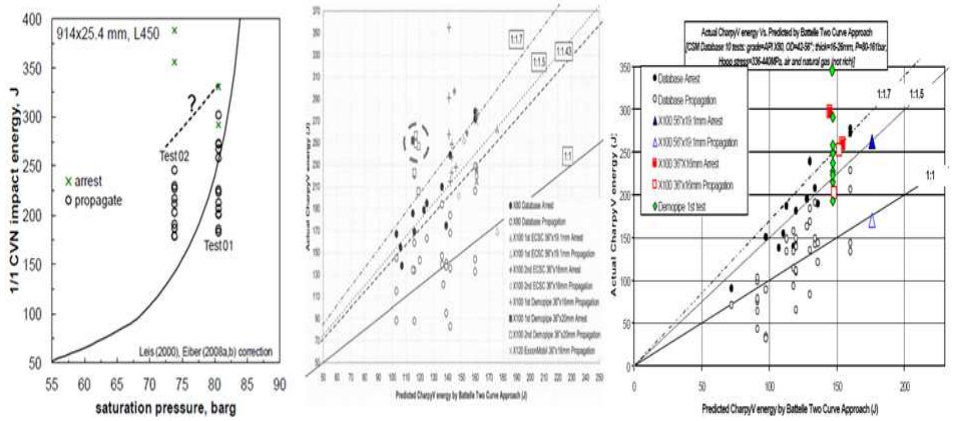

Fig. 2.17. The comparisons the BTCM and results of burst pressure test, result in the not the appropriate method by BTCM

The requirements for Safe and Reliable CO_2 Transportation Pipeline study the ductile fracture propagation [43]. The purpose of the project is to predict the crack initiation and leak by releasing a large quantity of CO_2 to test corrosion and stress corrosion events (DNV, 2011). The full scale burst propagation test with initial crack is conducted to predict the arrest of the long ductile fracture propagation. The test condition is 24 inches in diameter, 14.11 mm in thickness, and 15 MPa in internal

pressure. Furthermore, the pipeline was buried in 1 m depth of soil at 10 ºC. The assessment combines the centro sviluppo materiali model with BTCM to predict the arrest condition and propagation of GASMISC. The use of this model predicts the crack propagation of the CO_2 pipeline underwater water [24] as shown in Fig. 2.18.

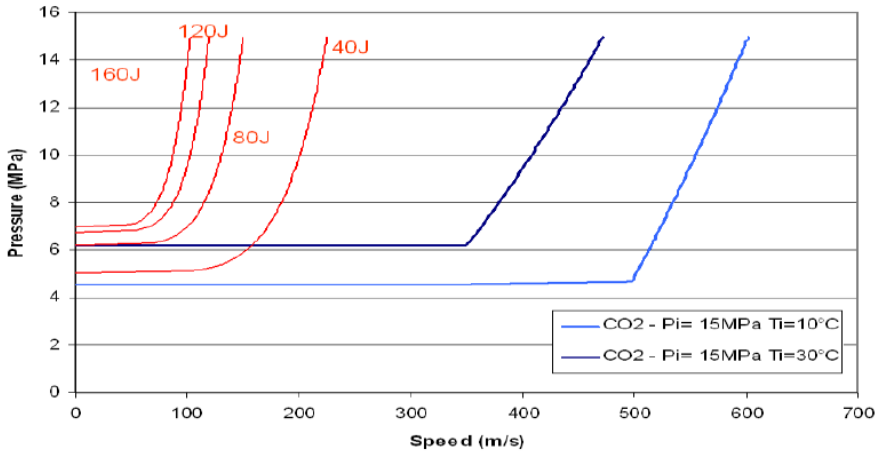

Fig. 2.18. The results of decompression model of CSM for study of arrest/propagation for CO_2 pipeline

Tensor Engineering developed the BTCM for the installation of CO_2 pipelines in Abu Dhabi as shown in Fig. 2.19. The toughness calculation used BTCM with a decompression curve and dragged the conclusion effective pipe with thicker walls rather than crack arrest due to the costly arrest ductile fracture [45].

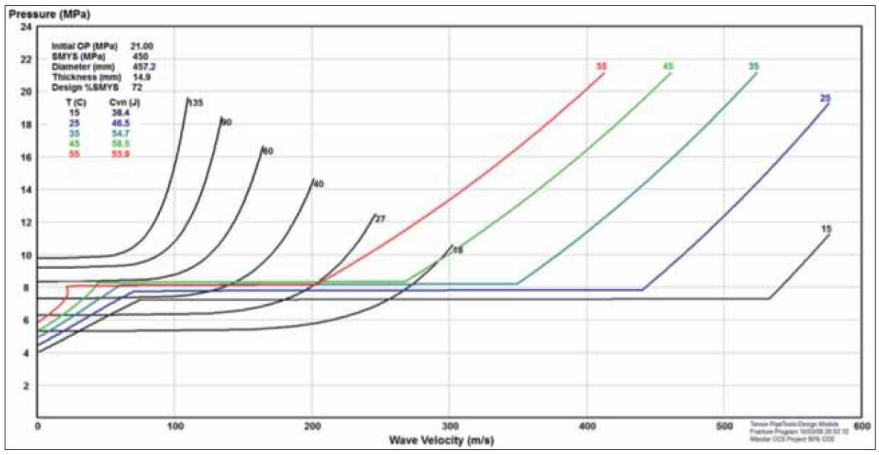

Fig. 2.19. The results of BTCM with varied toughness of pipeline by Tensor Engineering.

Full scale test or engineering method will remain the standard by which to prove the viability of a pipelines design [9, 12] Fracture propagation tests had done with CO_2 pipelines, but the tests were used with pipelines of small diameter, thin wall and low toughness [34]. These were subjected to test with crack arresters effectively. It was not clear to prove the fracture propagate with BTCM. West Jefferson test which conducted by National grid was performed with high toughness and CO_2 rich mixture to confirm that initial defect becomes be long and wide ruptures as shown through Fig.2.20 to 2.21 and Table 2.14 to 2.17. These tests were successful to

achieve the both arrest and propagate CO_2 pipelines. The results of West Jefferson test were compared with BTCM for appropriate the measurement of toughness of pipeline. The conclusion was not analytically predicting the arrest or propagation of crack.

Table 2.14 The average yield and tensile strength, and average Charpy V-notch impact energy of each pipe [1].

Test No.	Pipe No.	yield strength (N/mm^2)	tensile strength (N/mm^2)	CVN (J)	K_{ic} ($MPa\sqrt{m}$)	G (MPA.mm)
1	3553	533.3	610.7	201	216	157
2	44993 (W)	491	582.2	184	206	143
3	44992 (E)	511	589	194	212	152

Table. 2.15. The test condition of CO_2 pipeline

No.	Impurities (mol, %)		Pressure (MPa)	Buried depths (m)
	CO_2	N_2		
01	100	-	14.82	1.0
02	100	-	15.09	1.3
03	87.5	12.5	14.90	1.3

Fig.2.20 The picture of West Jefferson tests with CO_2 (GL Noble Denton)

Table 2.16. The length of the test vessel

Test No.	length of vessel, m
1	16.16
2	16.97 (8.43+8.54)
3	22.71 (5.955+10.80+5.955)

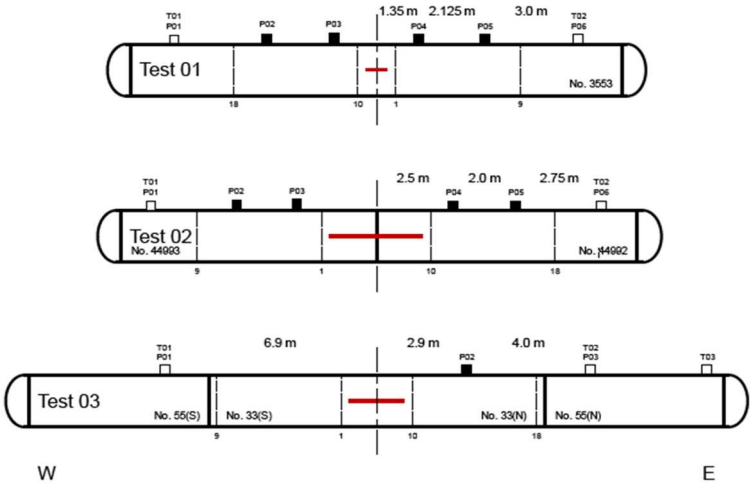

Fig. 2.21. Schematic diagram of CO2 pipeline with crack position and length.

Table. 2.17. The results of crack propagation test with CO_2 pipeline

No.	Length of crack initiation (m)	Length of crack propagation (m)	Fracture behavior
01	0.7	3.045	Fish-mouth shape
02	3.0	5.600	Fish-mouth shape
03	1.8	15.665	Long and wide shape

The condition of pipeline used API X65 (Grade L450), 914 mm of diameter, and 25.4 mm of thickness. The arrest with green 'X' mark is supposed to be above the line and propagation is under the line as shown in Fig. 2.22 for appropriate prediction. Even though the correction factor used with 1.2 for Test 01 and 1.8 for Test 02 did not match with arrest and propagation marks as shown in Fig. 2.22.

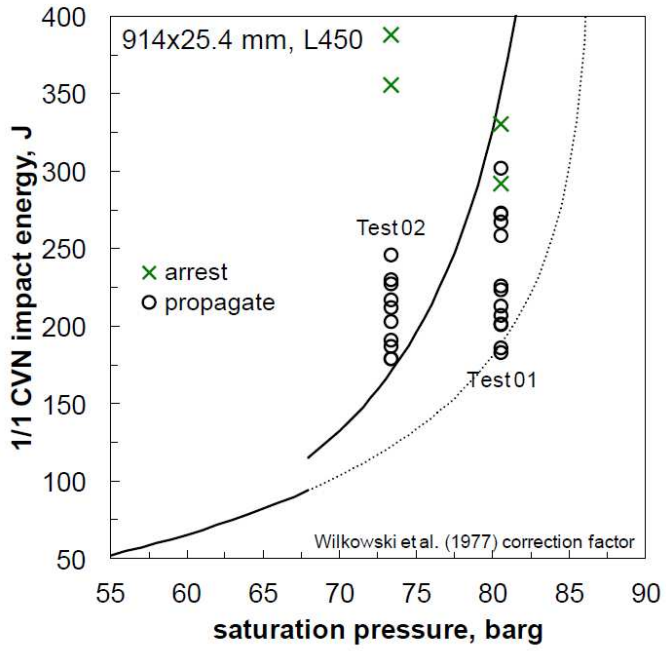

Fig. 2.22. The relationship between saturate pressure and requirement toughness of pipeline

The most conservative of the various correction factors has been used and still the predictions of BTCM is non-conservative. The pressure at the crack tip in both tests was significantly lower than the observed or predicted plateau (saturation pressure), but the fracture in the two tests still propagated further than predicted. As a result of these, The BTCM is not applicable to liquid or dense phase CO_2 or CO_2-rich mixtures for predicting of crack propagation. The driving force appears to be higher than predicted.

2.4 Thermodynamic

2.4.1 Equation of state

One of the simplest equations of state for this purpose is the ideal gas law, which is roughly accurate for gases at low pressures and high temperatures. However, this equation becomes increasingly inaccurate at higher pressures and lower temperatures, and fails to predict condensation from a gas to a liquid.

Introduced in 1949, the Redlich-Kwong EOS was a considerable improvement over other equations of that time. It is an analytic cubic EOS and is still of interest primarily due to its relatively simple form. The original form is

$$p = \frac{RT}{V-b} - \frac{a_0}{V(V+b)T_r^{0.5}}$$

P : Pressure (Pa)

R : Universal gas constant

V : Molar volume (m^3/kmol)

T : Temperature (K)

a_0, b : Pressure and temperature, in certain circumstances

The simply equation of Equation of State is ideal gas law, which is not quietly accurate equation for low pressure and high pressure. The researchers studied the failure of prediction of condensation from a gas to liquid. In order to improve equation of state, the equation has proposed with Soave-Redlich-Kwong, Peng-Robinson equation, Aungier-Redlich-Kwong [46].

The Peng-Robinson EOS used in order to determine of the phase behavior with various mixtures of impurities compared to pure CO_2. This equation developed in 1976 with Ding-Yu Peng and Donald Robinson, which is applicable to all calculations of all fluid properties in NG processes. The equation is similar to the Soave equation.

$$p = \frac{RT}{V_m - b} - \frac{a\alpha}{V^2{}_m + 2bV_m - b^2}$$

$$a = \frac{0.45724R^2T_e^2}{P_c}$$

$$b = \frac{0.07780RT_c}{P_c}$$

$$\alpha = (1 + 0.37464 + 1.54226\omega - 0.26992\omega^2)(1 - T_r^{0.5}))^2$$

$$T_r = \frac{T}{T_e}$$

V_m : Molar volume

Z : PV/RT

α : Related to the critical temperature Tc,

P_c : Critical pressure,

ω : Acentric factor of the species

2.4.2 Homogenous equilibrium method for transport of CO_2 flow

The CO_2 flow of fluent need to treats homogeneous gas method (HEM) phase in chemical reactions for equivalent as a single-phase chemical reaction. Otherwise, the flow could not flow equivalently in a diameter of pipeline. The reaction rate scaled by the volume fraction of the particular phase in the cell. Specify mass fraction of each species considered in Fluent [47].

$$\frac{\partial}{\partial t}(\rho Y_i) + \nabla \cdot (\rho \bar{v} Y_i) = -\nabla \cdot \bar{J}_i + R_i + S_i$$

R_i : Net rate of production of species i by chemical reaction

S_i : Rate of creation by addition from the dispersed phase plus any user-defined sources

2.4.3 Estimation of Gas Viscosities

We predicted of viscosity with gas mixture from theoretical models before simulating 100 % CO_2 flow. The molecular theory of gases has been sufficiently developed to allow the prediction of transport properties. The viscosity of gases may be accurately estimated by the viscosity of quasi-spherical molecules.

$$\mu = 26.7 \times 10^{-6} \frac{(MT)^{1/2}}{\sigma_c^2 \Omega_\mu}$$

μ : Gas viscosity, Poise (0.1 kg/ms)

M : Molecular weight (g)

T : Absolute temperature (K)

σ_c : Collision diameter

Ω_μ : Collision integral

$$\frac{\varepsilon}{k} = 1.92 T_m \text{ , } \qquad \sigma_c = 1.222 V m^{1/3}$$

k : Boltzmann constant (=1.38×10^{-23} J/mol·k)

ε : Energy parameter for interaction between molecules ($kgm^2/s^2\cdot mol$)

T_m : Melting temperature (K)

V_m : Boiling temperature (K)

$$\mu_{mix} = \frac{\sum X_i \mu_i (M_i)^{1/2}}{\sum X_i (M_i)^{1/2}}$$

X_i : Mole fraction of component *i* of viscosity μ_i

M_i : Molecular weight of component *i*

The confirmation of gas viscosity is used multi species with Zn of 20 M, N_2 of 50 M, and CO of 30 M. The estimation of gas viscosity is calculated with 3.2610^{-04} kg/ms by above equations.

The viscosity of the fluid is calculated by the semi-empirical equation for thermal conductivity.

$$K= \mu(C_p+1.25R)$$

The conclude with viscosity, specific heat capacity (Cp), and thermal conductivity is 1.8945×10^{-5} kg/ms, 40.816 KJ/KmolK, and 0.00097 W/mK for 100 % of CO_2 fluid in this study.

Table 2.19. Force constants for the Lennard-Jones Potential model [48]

Species	σ, Å	$\frac{\epsilon}{k}$, °K	Species	σ, Å	$\frac{\epsilon}{k}$, °K	Species	σ, Å	$\frac{\epsilon}{k}$, °K
Al	2.655	2750	CH_3CCH	4.761	252	Li_2O	3.561	1827
AlO	3.204	542	C_3H_8	5.118	237	Mg	2.926	1614
Al_2	2.940	2750	n-C_3H_7OH	4.549	577	N	3.298	71
Air	3.711	79	n-C_4H_{10}	4.687	531	NH_3	2.900	558
Ar	3.542	93	iso-C_4H_{10}	5.278	330	NO	3.492	117
C	3.385	31	n-C_5H_{12}	5.784	341	N_2	3.798	71
CCl_2	4.692	213	C_6H_{12}	6.182	297	N_2O	3.828	232
CCl_2F_2	5.25	253	n-C_6H_{14}	5.949	399	Na	3.567	1375
CCl_4	5.947	323	Cl	3.613	131	NaCl	4.186	1989
CH	3.370	69	Cl_2	4.217	316	NaOH	3.804	1962
$CHCl_3$	5.389	340	H	2.708	37	Na_2	4.156	1375
CH_3OH	3.626	482	HCN	3.630	569	Ne	2.820	33
CH_4	3.758	149	HCl	3.339	345	O	3.050	107
CN	3.856	75	H_2	2.827	60	OH	3.147	80
CO	3.690	92	H_2O	3.737	32	O_2	3.467	107
CO_2	3.941	195	H_2O_2	4.196	289	S	3.839	847
CS_2	4.483	467	H_2S	3.623	301	SO	3.993	301
C_2	3.913	79	He	2.551	10	SO_2	4.112	335
C_2H_2	4.033	232	Hg	2.969	750	Si	2.910	3036
C_2H_4	4.163	225	I_2	5.160	474	SiO	3.374	569
C_2H_6	4.443	216	Kr	3.655	179	SiO_2	3.706	2954
C_2H_5OH	4.530	363	Li	2.850	1899	UF_6	5.967	237
C_2N_2	4.361	349	LiO	3.334	450	Xe	4.047	231
$C_2H_2CHCH_3$	4.678	299	Li_2	3.200	1899	Zn	2.284	1393

[a] Taken largely from R. A. Svehla, NASA TR R-132, 1962.

Table 2.20. Collision integrals for the Lennard-jones potential model [49]

$\frac{kT}{\epsilon}$	$\Omega_\mu = \Omega_k$	$\Omega_\mathcal{D}$	$\frac{kT}{\epsilon}$	$\Omega_\mu = \Omega_k$	$\Omega_\mathcal{D}$	$\frac{kT}{\epsilon}$	$\Omega_\mu = \Omega_k$	$\Omega_\mathcal{D}$
0.30	2.785	2.662	1.60	1.279	1.167	3.80	0.9811	0.8942
0.35	2.628	2.476	1.65	1.264	1.153	3.90	0.9755	0.8888
0.40	2.492	2.318	1.70	1.248	1.140	4.00	0.9700	0.8836
0.45	2.368	2.184	1.75	1.234	1.128	4.10	0.9649	0.8788
0.50	2.257	2 066	1.80	1.221	1.116	4.20	0.9600	0.8740
0.55	2.156	1.966	1.85	1.209	1.105	4.30	0.9553	0.8694
0.60	2.065	1 877	1.90	1.197	1.094	4.40	0.9507	0.8652
0.65	1.982	1.798	1.95	1.186	1.084	4.50	0.9464	0.8610
0.70	1.908	1.729	2.00	1.175	1.075	4.60	0.9422	0.8568
0.75	1.841	1.667	2.10	1.156	1.057	4.70	0.9382	0.8530
0.80	1.780	1.612	2.20	1.138	1.041	4.80	0.9343	0.8492
0.85	1.725	1.562	2.30	1.122	1.026	4.90	0.9305	0.8456
0.90	1.675	1.517	2.40	1.107	1.012	5.0	0.9269	0.8422
0.95	1.629	1.476	2.50	1.093	0.9996	6.0	0.8963	0.8124
1.00	1.587	1.439	2.60	1.081	0.9878	7.0	0.8727	0.7896
1.05	1.549	1.406	2.70	1.069	0.9770	8.0	0.8538	0.7712
1.10	1.514	1.375	2.80	1.058	0.9672	9.0	0.8379	0.7556
1.15	1.482	1.346	2.90	1.048	0.9576	10.0	0.8242	0.7424
1.20	1.452	1.320	3.00	1.039	0.9490	20.0	0.7432	0.6640
1.25	1.424	1.296	3.10	1.030	0.9406	30.0	0.7005	0.6232
1.30	1.399	1.273	3.20	1.022	0.9328	40.0	0.6718	0.5960
1.35	1.375	1.253	3.30	1.014	0.9256	50.0	0.6504	0.5756
1.40	1.353	1.233	3.40	1.007	0.9186	60.0	0.6335	0.5596
1.45	1.333	1.215	3.50	0.9999	0.9120	70.0	0.6194	0.5464
1.50	1.314	1.198	3.60	0.9932	0.9058	80.0	0.6076	0.5352
1.55	1.296	1.182	3.70	0.9870	0.8998	90.0	0.5973	0.5256
						100.0	0.5882	0.5170

Table 2.21. Constant-Pressure specific heats of various ideal gases [50]

$\bar{C}_{p0}$=kJ/kmol K θ=T(Kelvin)/100

Gas		Range K	Max Error %
N_2	$\bar{C}_{p0} = 39.060 - 512.79\,\theta^{-1.5} + 1072.7\,\theta^{-2} - 820.40\,\theta^{-3}$	300–3500	0.43
O_2	$\bar{C}_{p0} = 37.432 + 0.020\,102\,\theta^{1.5} - 178.57\,\theta^{-1.5} + 236.88\,\theta^{-2}$	300–3500	0.30
H_2	$\bar{C}_{p0} = 56.505 - 702.74\,\theta^{-0.75} + 1165.0\,\theta^{-1} - 560.70\,\theta^{-1.5}$	300–3500	0.60
CO	$\bar{C}_{p0} = 69.145 - 0.704\,63\,\theta^{0.75} - 200.77\,\theta^{-0.5} + 176.76\,\theta^{-0.75}$	300–3500	0.42
OH	$\bar{C}_{p0} = 81.546 - 59.350\,\theta^{0.25} + 17.329\,\theta^{0.75} - 4.2660\,\theta$	300–3500	0.43
NO	$\bar{C}_{p0} = 59.283 - 1.7096\,\theta^{0.5} - 70.613\,\theta^{-0.5} + 74.889\,\theta^{-1.5}$	300–3500	0.34
H_2O	$\bar{C}_{p0} = 143.05 - 183.54\,\theta^{0.25} + 82.751\,\theta^{0.5} - 3.6989\,\theta$	300–3500	0.43
CO_2	$\bar{C}_{p0} = -3.7357 + 30.529\,\theta^{0.5} - 4.1034\,\theta + 0.024\,198\,\theta^{2}$	300–3500	0.19
NO_2	$\bar{C}_{p0} = 46.045 + 216.10\,\theta^{-0.5} - 363.66\,\theta^{-0.75} + 232.550\,\theta^{-2}$	300–3500	0.26
CH_4	$\bar{C}_{p0} = -672.87 + 439.74\,\theta^{0.25} - 24.875\,\theta^{0.75} + 323.88\,\theta^{-0.5}$	300-2000	0.15
C_2H_4	$\bar{C}_{p0} = -95.395 + 123.15\,\theta^{0.5} - 35.641\,\theta^{0.75} + 182.77\,\theta^{-3}$	300–2000	0.07
C_2H_6	$\bar{C}_{p0} = 6.895 + 17.26\,\theta - 0.6402\,\theta^{2} + 0.007\,28\,\theta^{3}$	300–1500	0.83
C_3H_8	$\bar{C}_{p0} = -4.042 + 30.46\,\theta - 1.571\,\theta^{2} + 0.031\,71\,\theta^{3}$	300–1500	0.40
C_4H_{10}	$\bar{C}_{p0} = 3.954 + 37.12\,\theta - 1.833\,\theta^{2} + 0.034\,98\,\theta^{3}$	300–1500	0.54

Source: From T.C. Scott and R.E. Sonntag. University of Michigan, unpublished 1971, except C_2H_6, C_3H_8, and C_4H_{10} from K.A. Kobe, Petroleum Refiner, 28, No. 2, 113 (1949).

In this simulation, we considered to use the solver with density-based in the CFD model for high-pressure CO_2 flow. The density-based solver predicts better accuracy than shock and acoustic wave otherwise pressure-based solver predicts incompressible flows.

3. Research approach

The studies are discussed for crack propagation and crack behavior.

BS 7910 & R6 procedures for impact of the plastic collapse solution on the crack driving force are comparison. The crack dimension is considered with external circumferential surface breaking flaws which is considered the geometries with depths (3 mm, 6 mm, 9 mm and 12 mm) and lengths (30 mm, 60 mm and 90 mm) which is not semi-elliptical. The dimension of pipeline is 3.3m long, 14.3 mm t, and D 273.1mm. The material property is 207 GPa of Elastic modulus, 0.3 of Poisson's ratio, and 450 MPa of yield strength. The condition of simulation considered with perfectly plastic, C3D20R, and fine mesh was used for the crack ligament as shown in Fig. 3.1 and 3.2 [51].

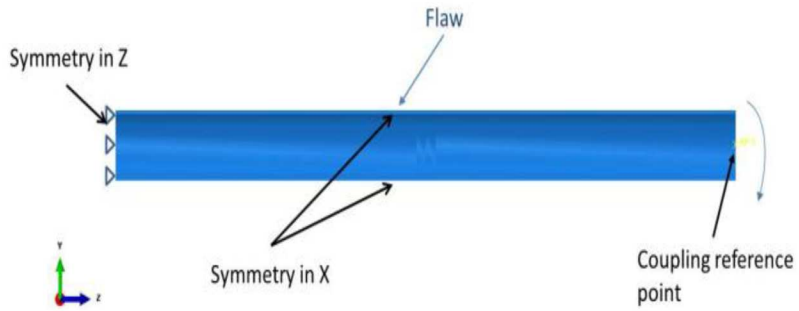

Fig. 3.1. FEA boundary conditions for pure bending of the pipe.

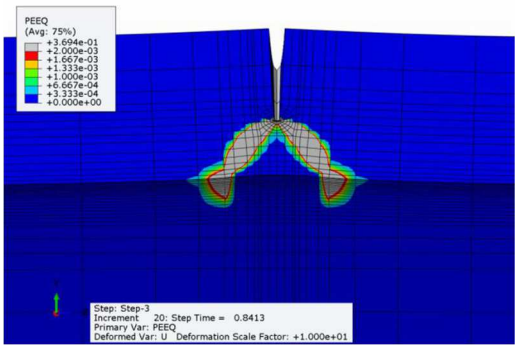

Fig. 3.2. PEEQ strain with local collapse of a pipe with flaw of 9×60 mm under tensile loading.

The results of comparison with impact of the plastic collapse solution considered with symmetry condition even though the crack existed middle of pipeline. The flaw cracks are considered with crack depths and lengths. The axial crack with depths is reasonable to understand of pipeline for acquire appropriate of toughness.

Other study considered with external axial crack for acquired the stress intensity factor (SIF) but there is limitation application which R0/Ri is equal to 2.0 as shown in Fig. 3.3 [52].

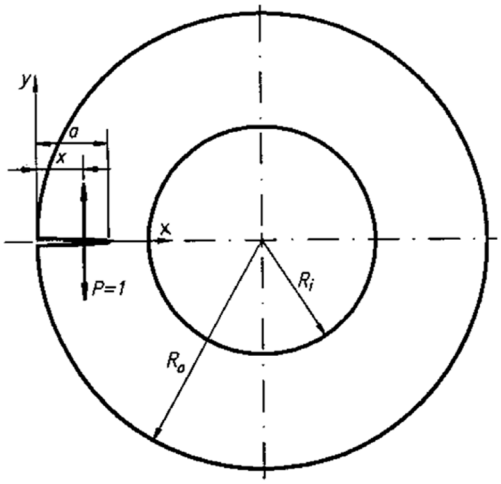

Fig. 3.3. External axial edge crack in a thick cylinder

The SIF can be determined by below equation [53, 54]

$$K_I = M_T \sigma_\varphi \sqrt{\pi c}$$

$$M_T = \sqrt{1 + 1.255\frac{c^2}{Rt} - 0.0135\frac{c^4}{R^2 t^2}}$$

$$\frac{K_I}{\sigma\sqrt{\pi a}} = \frac{K_I t}{RP\sqrt{\pi a}}$$

σ_ϕ : PD/(2 x t) is the hoop stress,

M_T : Folias correction factor, taking account of curvature of a pipe

R : mean radius of the pipe

t : pipe wall thickness

According to the above equation of SIF, the crack with axial direction was determined, But the value of SIF may limit to pipe with geometry of crack.

The study of crack propagation considered with seam crack which predict the crack direction and length with demanded of users by LS-DYNA as shown in Fig. 3.4 and 3.5 [55].

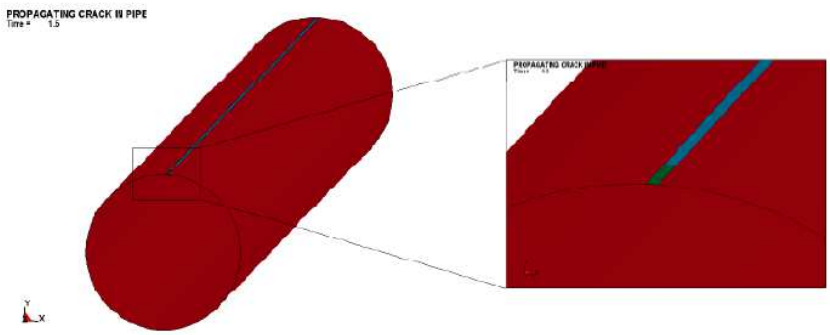

Fig. 3.4. The 3 parts of the pipe in LS-DYNA: main pipe wall (red), "explosive charge" (green), crack path (blue).

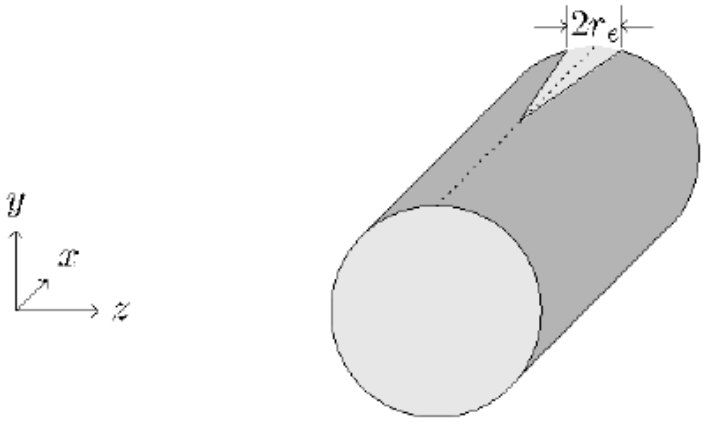

Fig. 3.5. The crack propagates along the *x*-direction, leaving behind a growing opening of width 2*re*(*x*) in the pipe.

As the crack symmetrically propagates in both directions, only half of the domain is shown.

This study used one dimensional finite volume method with shell element used, explosive (seam crack) used by LS-DYNA. The fracture theory of crack propagation has to use for crack propagation. The simulation dealing with crack need to use the hexagonal element which considers the different element thickness of pipeline. but shell element used one thickness element.

Other studies of crack used smoothed particle hydrodynamics-finite element method

(SPH-FEM) with meshless method. A coupled SPH-FEM method is developed to simulate the dynamic fracture of cylindrical shell subjected to internal explosion as shown in Fig. 3.6 and 3.7 [56].

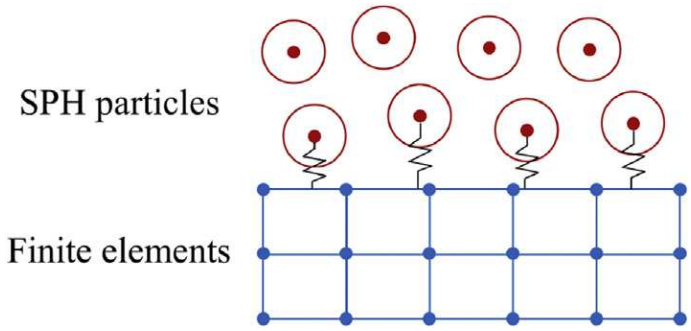

Fig. 3.6. SPH particles coupled with finite elements.

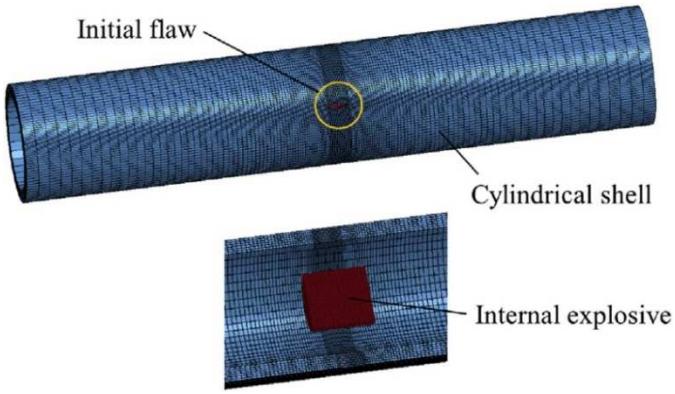

Fig. 3.7. Coupled SPH-FEM simulation model

But this study did not consider the fracture theory of crack propagation and flow of air or CO_2 fluid. The decompression or fracture theory for preventing from crack propagation are important effects as discuss of BTCM section.

Structural Integrity of CO_2 Transportation Infrastructures projected by MATTRAN (Materials for Next Generation CO_2 Pipeline Transport Systems) which conducted to research the control corrosion, stress corrosion cracking and fracture propagation for understanding of supercritical CO_2 in U.K.

This study considered with fracture mechanics behavior of CO_2 pipeline with longitudinal crack in the pipeline. Due to very low temperature during decompression, low temperature fracture toughness tests linked to a detailed finite element based stress analysis. Outflow model results show the temperature in front of the crack may drop as low as – 70 ^{o}C as shown in Fig. 3.8 and 3.9 [57]. This study simply applied yield strength of pipeline and temperature at the front of crack. The effect of CO_2 pipeline has to consider with fracture theory and flow of CO_2 and other imputers in real condition of CO_2 flow.

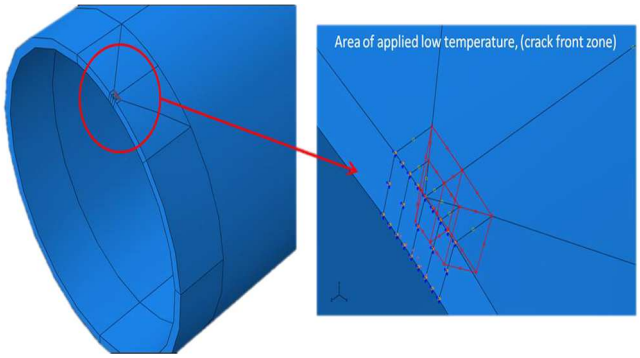

Fig. 3.8. Crack front area, applied low temperature zone.

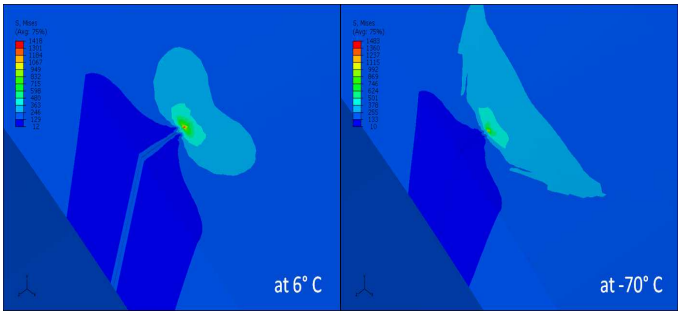

Fig. 3.9. Ambient, low temperature in front of the crack of CO_2 pipeline.

The crack propagation assumed with certain shape in pipeline as show in Fig. 3.10 and Fig. 3.11 for 3D simulation of pressure distribution behind the crack tip. The model of pipeline was implement GERG-2008 of in Fluent. The boundary condition of simulation was set with ambient pressure for outlet and no condition for inlet. The simulation condition was used with adiabatic wall, no-slip, Advection Upstream Splitting Method (AUSM), and density-based solver. But this study was no consideration of fracture toughness, material properties, welds [58]. The experimental results or other results need for verification of crack propagation.

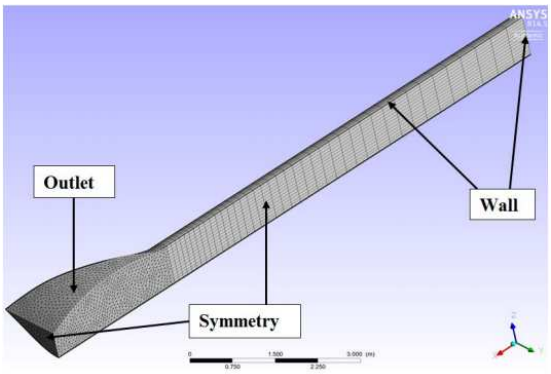

Fig. 3.10. 3D computational mesh and boundary conditions

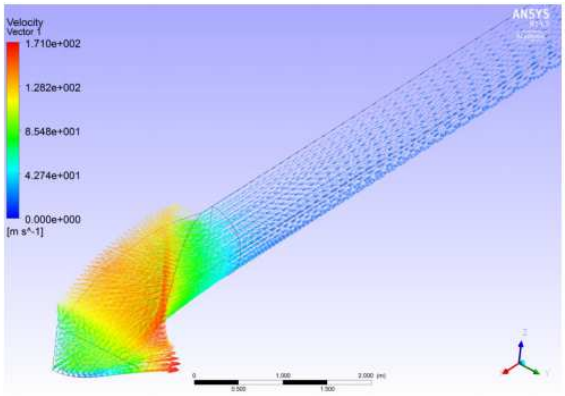

Fig. 3.11. Flow velocity field close to the fracture opening

3.1 Problem with FEM and CFD analysis

FEM used to predict the over-simplistic transient fluid flow models and limit to various EOS [59]. CFD did not deal with impact of pipe wall heat transfer and friction effect [60, 61]. Moreover, increased pressure and reducing the pipe diameter if pipe friction ignored. In this study of crack propagation with CO_2 pipeline the decompression behavior, flow and fracture analysis are important to understand for acquiring the appropriate the requirement of toughness. It is need to couple both structure and fluid analysis.

The flow of CO_2 transports as supercritical or dense phase for efficiency with high density and low viscosity. Brittle fracture could be solved with low temperature in order to deviate the ductile to brittle transition temperature. Brittle fracture is well known to prevent from fracture for increasing temperature. Otherwise, ductile fracture is not well understudied. Originally the equation of BTCM was assessed the crack propagation which is developed by Battelle in early 1960's with low toughness and strength pipe. HLP was developed their equation for ductile fracture based on the BTCM. But, high strength and toughness of pipeline are limited to apply their consideration. Other for predicting the ductile facture is based on the BTCM with correction factor. Ductile fracture need to study for further in order to predict the fracture propagation. In this study, we consider the FSI coupled with structure and

fluid to better understand of behavior with crack propagation of high strength and toughness CO_2 pipeline. Aims is for measurement of requirement toughness of CO_2 pipeline by FSI.

3.2 Structural analysis by FEM

The geometry of API X70 pipe is a 762 mm in diameter, 15.9 mm in wall thickness, respectively. The details of mechanical properties are shown in Table 3.1 and detail of composition of API X70 describes in Table 3.2.

Table 3.1. Mechanical properties of API X70 pipeline.

Mechanical properties	API X70
Young’s modulus (MPa)	207000
Poisson’s ratio	0.3
Yield strength (MPa)	532.2
Tensile strength (MPa)	626.8
Charpy impact energy (J)	464

Table 3.2. Chemical compositions of API X70 pipeline.

Element (wt. %)				
C	P	Mn	S	Si
0.07	-	1.73	0.003	0.12

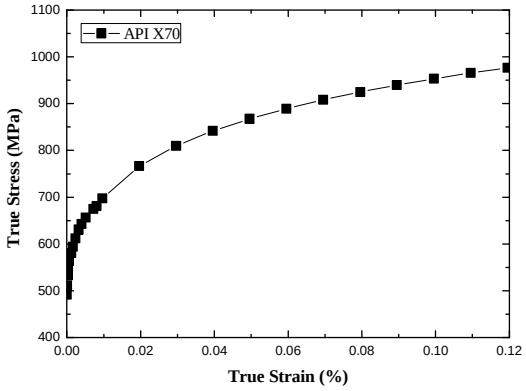

Fig. 3.12 True stress-strain curves of API X70 pipeline for used in XFEM.

Charpy impact test was conducted to measure the fracture energy which is correlated with the pipe ductile tearing resistance. The specimen was taken from the in API X70 pipeline of base metal and made as 10 x 10 x 55 mm as standard size of API 5L [18]. The result of Charpy impact energy is 464 Joule as shown in Table 3.1 and applied with XFEM simulation to analyze how crack is resistance with difference crack propagation of API X70 pipeline.

Before considering of crack propagation with API X70 pipe, the stress distribution should measure the hoop stress [62] of none existed of cracks in pipe. The API X70 pipe was modeled three dimension and symmetry condition. The hoop stress simulated with internal pressure of 8 MPa which is design pressure in API X70 pipe. The results show that the stress was concentrated from outside to inside of pipe as shown Fig. 3.13

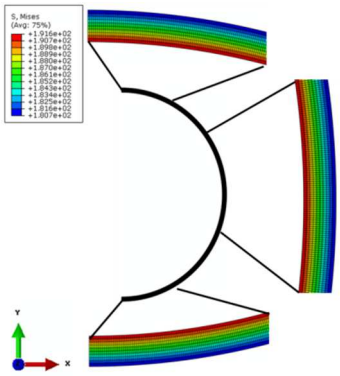

Fig. 3.13. Result of hoop stress analysis of pipeline

The hoop stress measured around 192 MPa in FEM and obtained with below equation.

$$\sigma_{hoop} = \frac{1}{2}\left(\frac{D}{t}\right)p_i \quad (6)$$

σ_{hoop} : Hoop stress

D : Diameter of pipe

t : Thickness of pipe

p_i : Internal pressure of applied in pipe

The result of hoop stress measurement could apply the simulation condition of crack sizes studies and crack propagation, respectively.

The charpy energy has acquired by CVN impact test with 100% upper shelf of API X70 pipe and weld metal.

Manual weldment was used for the HAZ for girth and seam welds. The weld consumables and welding parameters are shown for API X70 pipe in Table 3.3. The joint designs of the girth and seam weld are shown in Fig. 3.14. The microstructures of the API X70 pipe with seam and girth welds are shown as Fig. 3.15. In the case of domestic pipelines, the implement of radiographic testing is conducting after welding of the pipeline. Thus, the pipelines were assumed to initially have no defects.

Table 3.3. Weld consumables and welding parameters of API X70 pipe.

Weld	Layer No.	Welding Process	Filler metal		Polarity	Amperage (A)	Voltage (V)	Welding Speed (cm/min)
			Class	Diameter (mm)				
Girth weld	1	GTAW	ER70S-G	2.4	DCSP	100–170	12–20	6–12
	2	GTAW	ER70S-G	2.4	DCSP	170–240	15–24	8–14
	3	SMAW	E9016-G	3.2	DCRP	80–150	20–40	3–12
	4 & 5	SMAW	E9016-G	4	DCRP	100–180	20–42	3–12
Seam weld	1	GMAW	ER70S-G	1.6	DCEN	520	28	17
	2	SAW	F8A4-EA2	4	DCEP	820	37	105
					AC	660	42	
	3	SAW			DCEP	890	37	115
					AC	710	42	

GTAW : Gas tungsten arc welding

SMAW : Shielded metal arc welding

GMAW : Gas metal arc welding

SAW : Submerged arc welding

DCSP : Direct current straight-polarity

DCRP : Direct current reverse-polarity

DCEN : Direct current electrode negative

DCEP : Direct current electrode positive

AC : Alternating Current

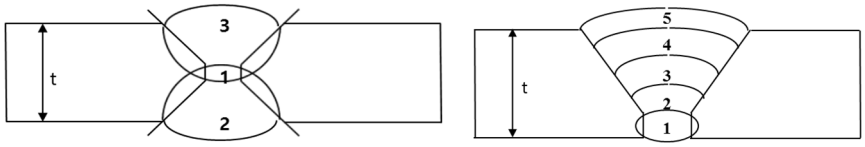

(a) Joint design of seam weld (b) Joint design of girth weld

Fig. 3.14. Joint design of seam and girth welds of API X70 pipe.

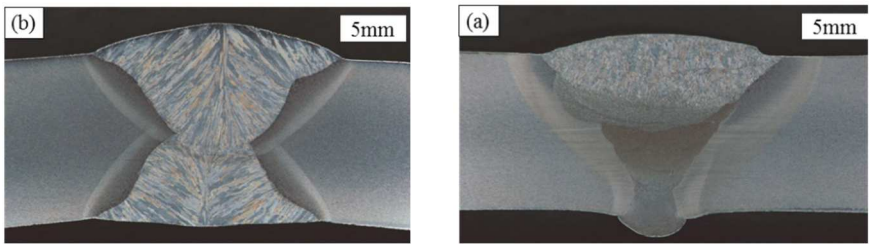

(a) Seam weld in API X70 pipe (b) Girth weld in API X70 pipe

Fig. 3.15. Microstructures of API X70 pipes with seam and girth welds.

A plate-type subsize specimen (6.3 mm in width and 2.0 mm in thickness) with girth weld [26] used for the tensile test of HAZ. The tensile test specimens of base metal, weld metal, and HAZ were polished and etched, and their microstructures were

observed, as shown Fig. 3.15 accordingly, the acquired tensile test specimens of 100% base metal, weld metal, and HAZ are shown in Fig.3.16.

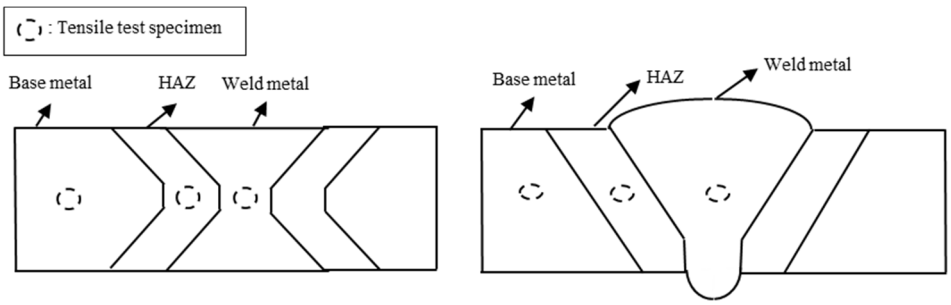

(a) Seam weld (b) Girth weld

Fig. 3.16. Diagrams of tensile specimen with seam and girth welds of API X70 pipe.

3.3 Toughness energy conversion

There is standard of conversion fracture energy through the British Standard. Stress intensity factor K is measured in this study (or called as the elastic energy release rate G). Elastic crack-tip solution and the energy theory of established relationship between K_I and G [63].

$$G = \frac{K_I^{\,2}}{E'}$$

K_I : Stress intensity factor

G : Elastic energy release rate

E' : E for plane stress conditions

E' : E/(1-ν) for plane strain conditions

SIF is valid for a through crack in an infinite plate in tension. Resistance parameters crack-tip conditions and in measuring fracture resistance is considered.

The conversion of fracture energy described in two methods. Method 1 is described with 100% shear, upper shelf behavior is present CVN energy correlation with $K_{IC,}$ K_{mat} fracture toughness corresponding to a ductile crack extension of 0.2 mm, $K_{J0.2}$ [64],

$$k_{J0.2} = \sqrt{\frac{E\left(0.53C_{V\,us}^{\,1.28}\right)\left(0.2^{\,0.133C_{v\,us}^{\,0.256}}\right)}{1000\left(1-v^2\right)}}$$

$K_{J0.2}$: MPa√m,

C_V: Charpy upper shelf energy (J)

E : Young's Modulus (MPa)

ν : Poisson’s Ratio.

Second method is based on the upper shelf CVN energy correlation with K_{IC} which provided for guidance from BS PD 6539 [65]

$$\left(\frac{K_{mat}}{\sigma_y}\right)^2 = 0.52\left(\frac{C_V}{\sigma_y} - 0.02\right)$$

σ_Y : Yield Strength(MPa)

C_v : CVN energy (J)

K_{mat} : MPa/$m^{0.5}$

Verification is conducted by curve fitting with value of 450 MPa (Yield strength) and C_v (140 Joule). The value is acquired with 175 K_{mat} comparison as shown in Fig. 3.17.

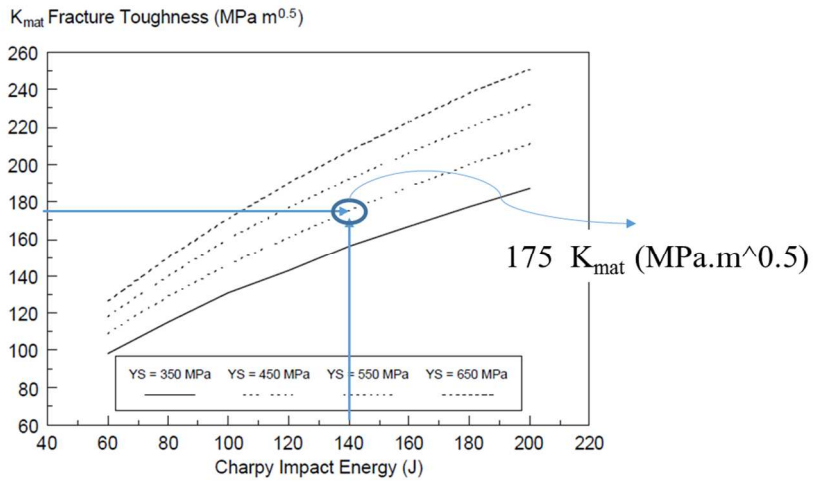

Fig. 3.17. Confirmation CVN energy by method 2 with upper shelf correlation.

The unit conversion is described as below equations

$$G = \frac{K_I^{\,2}((MPa \cdot \sqrt{m})^2)}{E^{'}(MPa)}$$
$$= \frac{MPa^2 \cdot m}{MPa}$$
$$= MPa \cdot m$$
$$= MPa \cdot mm \times 10^{-3}$$

Method 1 is appropriate method of conversion with charpy energy according to comparison equations. The method 1 will use for conversion of CVN energy for different crack sizes.

3.4 XFEM

In the XFEM, two additional displacement functions are enriched in finite element solution space: [67] One is a discontinuous function that represents the displacement jump across the crack surface while the other is the near-tip asymptotic functions that capture the singularity around the crack-tip field. The displacement function is written as

$$u = \sum_{I=1}^{N} N_1(x)\left[u_1 + H(x)a_1 + \sum_{a=1}^{4} F_a(x)b_i^a \right]$$

where $N_I(x)$ is the general nodal shape function, u_I is the general nodal displacement vector associated with the continuous part of the finite element solution, H(x) is the associated discontinuous jump function across the crack surfaces, a_I is the product of the enriched degree of freedom vector, $F_a(x)$ is the associated elastic asymptotic crack-tip function, b_I a is the product of the enriched freedom degree. The discontinuous jump function H(x) across the crack surfaces is given by

$$H(x) = \begin{cases} 1 & if\ (x - x^*) \cdot n \geq 0 \\ -1 & otherwise \end{cases}$$

here x is a sample Gauss point, x^* is the point on the crack closet to x, and n is the unit outward normal to the crack at x^*, respectively. The asymptotic crack tip functions in an isotropiwc elastic material $F_a(x)$ are

$$F_\alpha(x) = \left[\sqrt{r}\sin\frac{\theta}{2}, \sqrt{r}\cos\frac{\theta}{2}, \sqrt{r}\sin\theta\sin\frac{\theta}{2}, \sqrt{r}\sin\theta\sin\theta\frac{\theta}{2}\right]$$

where (r, h) is a polar coordinate system with its origin at the crack tip, and h = 0 is tangent to the crack surface around the tip. The cohesive segment method is based on traction-separation cohesive behavior that is given by

$$t = \begin{Bmatrix} t \\ t_n \\ t_t \end{Bmatrix} = \begin{bmatrix} K_{SS} & & \\ & K_{NN} & \\ & & K_{tt} \end{bmatrix} \begin{Bmatrix} \delta_s \\ \delta_n \\ \delta_t \end{Bmatrix} = K\delta$$

where t is the nominal traction stress vector which consists three components: t_s, t_n, and the corresponding displacements are δ_s, δ_n, and δ_t, respectively.

The failure criterion for propagation can be defined as below

$$f = \left\{ \frac{\langle \sigma_{\max} \rangle}{\sigma^0_{\max}} \right\}$$

where f is maximum principle stress ratio, σ_{max} is maximum principle stress and σ^0_{max} is maximum allowable principle stress, respectively.

ASME B31 and Subsections NC and ND (Classes 2 and 3) of Section III of the ASME Boiler and Pressure Vessel Codes [68] states that yielding in a piping component occurs when the magnitude of any of the three mutually perpendicular principle stresses exceeds the yield point strength of the material.

In this study, we used the maximum principle stress theory with Charpy impact test result for crack initiation and propagation of pipeline in XFEM. This is most commonly used when describing the strength of piping systems [67, 69, 70]

3.5 Variable of Crack sizes study

The following flow chart is considered for FSI simulation as follows. In order to analysis of different crack sizes and crack propagation, the work flow has been proposed as shown in Fig. 3.18. Before conducting of structure and fluid analysis, the surface of FSI has to be consistent of each other. The convergence is obtained through iteration of the fluid analysis, and then the FSI analysis is considered by performing the XFEM.

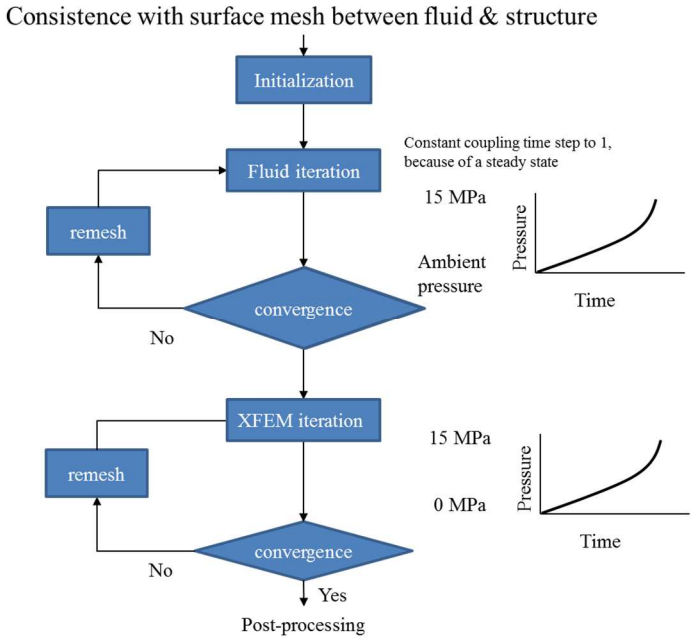

Fig. 3.18. Workflow for FSI simulation.

The CO_2 pipeline was considered by understanding the behavior of the crack depths using MpCCI [71] which facilitated cooperation in both structural and fluid analyses. The dynamic mesh used a rigid body type. The coupling time was set to value '1.0' in order to simulate ABAQUS with Fluent a consistent by MpCCI. The FSI method is method of interaction with structure and fluid by serial coupling method uses for Gauss-Seidel Algorithm which one code runs the other code waits for simulation as shown in Fig. 3.19. This is method of numerically calculating simultaneous equations which is equivalent of the iteration of the equations. Gauss-Seidel method uses a combination of iterative equations and approximation. This method is executed when one code, that is ABAQUS, is executed, the other code Fluent waits for it, and the Fluent is given to ABAQUS to give information. The method of coupling is considered the one-way coupling which gives the information of pressure and position with fluent to ABAQUS.

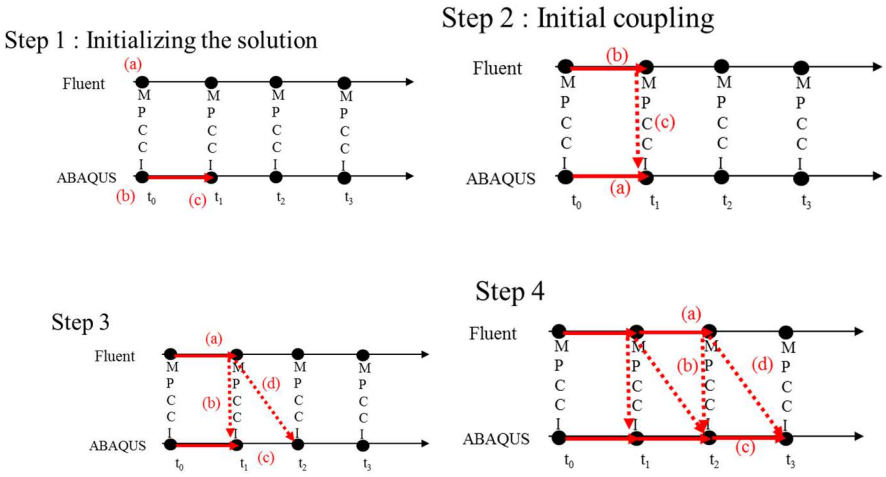

Fig.3.19. Gauss-Seidel Algorithm for consistency of ABAQUS and Fluent

The results of CTOD studied with comparison between experiment and simulation for acquirement of fracture toughness. The different crack sizes ratio was analyzed by internal pressure by structure and FSI simulation in order to recognize the critical internal pressure. The proposed model in this study are described as shown in Table 3.5 with CTOD and CVN

Table. 3.5. The proposed model with CTOD and CVN

	CTOD	CVN
Thickness of pipe	B : Thickness W : 2 x (B) thickness ($1.0 < W/B \leq 4.0$)	10 mm × 10mm × 55mm 10 mm × 7.5 mm × 55mm (subsize)
Theory in FEM	Traction-separation	Maximum principle energy
Verification	Compared experiment and simulation	Hoop stress equation

The structure model for the pipe considers a variety of surface axial cracks [51, 72] as shown in Table 3.6 using XFEM, which is not dependent on the mesh and crack direction

Table. 3.6. The depths of the crack with surface axial in API X70 pipe thickness.

Crack depth ratios according to thickness (%)								
10	20	30	40	50	60	70	80	90
Crack lengths according to thickness (mm)								
1.59	3.18	4.77	6.36	7.95	9.54	11.13	12.72	14.31

The structure and fluid analysis applied surface were confirmed by applied with inner surface of structure and outer surface of fluid. The condition of boundary and load were equivalent with hoop stress verification. The model of crack not only considered with 3 m length of three dimension due to boundary conditions and the length of pipeline but also considers the appropriate flow of CO_2 with 3 m length of pipeline for conducting burst pressure test [73, 74]. The density of elements used the 10 % crack depth from outer surface thickness of pipeline. When the element density is 2,318,509 with C3D8R (8-node linear brick element with reduced-integration points) as shown in Fig. 6, the critical internal pressure was constant at 14.44 MPa. We determined this element density in order to study variant crack depths from the outer surface thickness for structural and fluid analysis. The crack depths varied for the outer thickness from 10 % to 90 % pipe thickness, as shown in Table 3.6. The true stress-strain curve and fracture energy were evaluated at a variety of crack

depths. According to the true stress-strain curve, the maximum principle stress for the API X70 pipe was 532 MPa for crack propagation.

3.6 Crack propagation study of API X70 pipe by FSI

The crack propagation prediction with BTCM is required for correction factors and additional studies [38, 41, 58, 75]. These studies considered the non-effect of girth weld to understand crack propagation and did not apply the damage theory for crack propagation with simulation of ductile crack growth based on cohesive zone models [76]. The crack propagation forecasting is demanding to understand both structure and fluid with EOS.

In order to take into account the crack propagation prediction of the CO_2 pipeline, we established a flow chart, as shown in Table 3.6. The fracture considers the CTOD results by comparing the experiment and simulation according to the CZM. The CO_2 flow and girth weld were analyzed to predict the required toughness.

Table 3.6. The sequence simulation of FSI for predicting the requirement toughness of the CO_2 pipeline.

No.	Sequence for analysis of crack propagation analysis	
1	Fracture	Acquire fracture theory (Traction-Separation law)
2		Verify between CTOD Experiment and simulation
3	FSI	Acquire FSI simulation method : identification of mesh, surface of FSI
4	Fluid	Fluid analysis of CO_2 & impurities of pipeline
5	FSI	Combine fracture theory of structure analysis with fluid of CO_2 condition
6		Conclude the requirement of CO_2 pipeline toughness

For the purpose of decreasing internal pressure of pipeline, the time step used the exponential decay in ABAQUS in order to decrease time step from 1.0 to 0.0. According to the equation of exponential decay, the decay effect was controlled to decrease the internal pressure very instantly by using value of 0.05 as shown in Fig. 3.20.

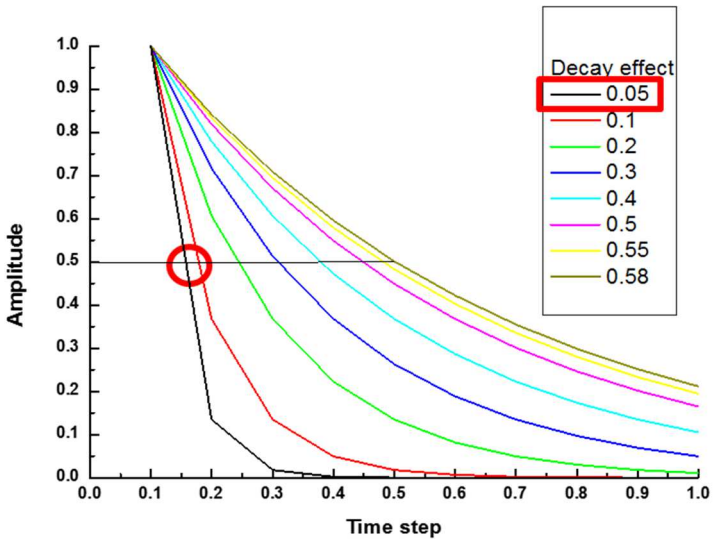

Fig. 3.22. Calculated drop of internal pressure.

$$a = A_0 + A\exp\left(-\left(t - t_0\right)/t_d\right) \quad \text{for} \quad t \geq t_0$$
$$a = A_0 \quad \text{for} \quad t < t_0$$

In order to verify the decreasing, the internal pressure in ABAQUS, we used tabular amplitude set the of time step from 1.0 of relative load with 0.0 time to 0.0 of relative load with 1.0 of time which internal pressure is increased with decreasing the total time of structure. The total time and decreasing the inlet and outlet condition of fluent is consistent with step time of structure analysis. The comparison of time amplitude was shown in Fig. 3.21 with 10 % of crack size. The condition time amplitude was applied with of Fig. 3.21 (a) with time amplitude from 0 MPa to 15 MPa and (b)

Time amplitude from 15 MPa to 0 MPa. The results of time step were 0.9780 and 0.0218, which equal to 14.67 MPa and 14.673 MPa, respectively.

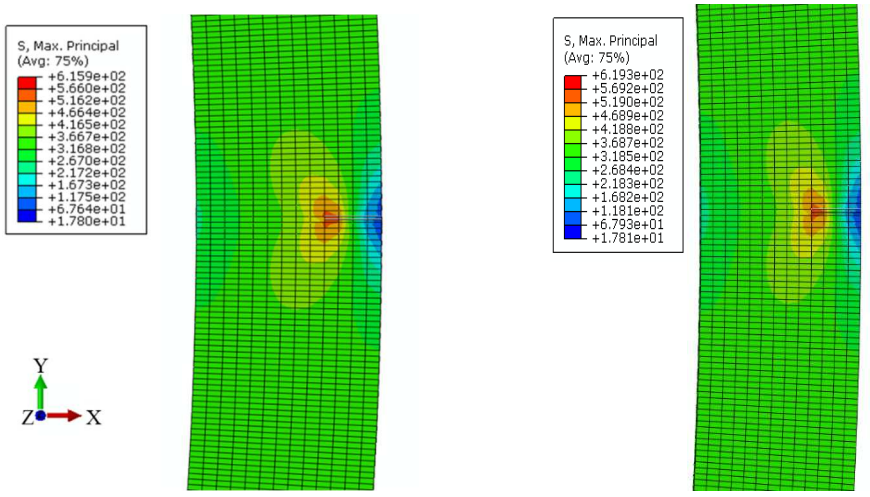

(a)Time amplitude from 0 MPa to 15 MPa (b) 15 MPa to 0 MPa

Fig. 3.22. Stress analysis of AW 10% for verification of time amplitude compared between (a) 0 MPa to 15 MPa (b) 15 MPa to 0 MPa

The three dimensional model for crack propagation is described as below. The structure model was simulated with 1/2 scale. The time step was applied the time amplitude in order to decrease the internal pressure 1 to 0 in step with 15 MPa of inner surface which considered high inlet and outlet pressure of CO_2 pipeline [58, 72]. The boundary condition was applied with y symmetry at the front of crack and pin condition at end of pipe. The element was used C3D8R as equivalent with CTOD simulation of 96,063 element number. The geometry of CTOD is based on the experiment for simulation as shown in Table 3.7.and Fig. 3.22.

Table 3.7. The geometries and experimental condition of CTOD.

	Temperature (℃)	a_0 (mm)	B (mm)	W (mm)	F (Pm, kg)
Base metal of API X70	20.00	14.80	14.97	30.00	2,721.70

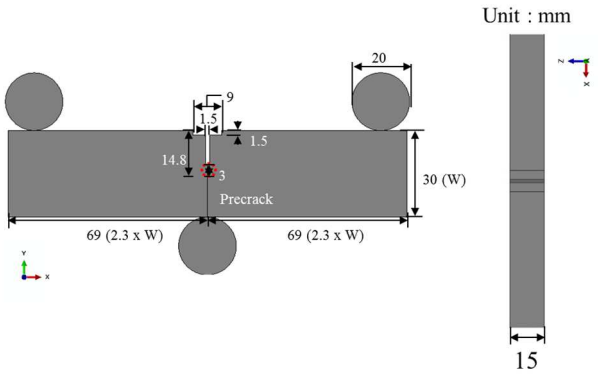

(a) Front view of CTOD model (b) Top view

Fig. 3.22. The modeling of CTOD specimen by ABAQUS.

The FEA used C3D8R (8-node linear brick element with reduced-integration points) element and three-dimensional model. The experiment and simulation of CTOD are conducted to be based on the three-point bending test (BS7448, 2005; ASTM E1290-08, 2008).

The boundary condition of CTOD with two anvils is encased and one holder above the specimen set to x and z direction with zero displacement in order to move to propagate the crack with y direction. The specimen of CTOD set the z direction with zero displacement. The interaction contact and properties of CZM is considered for surface based cohesive behavior. The viscosity coefficient is set to 10^{-5} for stabilization. The a_o is made to use surface cohesive method.

In order to apply the true stress-strain curve, the tensile test conducted with base metal, HAZ, and weld. The base metal and weld was used rod-type subsize specimens (A: 32 mm, D: 6.25mm, R: 6mm). The HAZ with girth weld used plate-type subsize specimen (width: 6.3mm, t: 2.0mm) (ASTM A370, 2010). The tensile specimen of base metal, HAZ, and weld were grinded and polished to acquire the proper position of each specimen. The true stress-strain curve of base metal, HAZ, and weld are shown in Fig. 3.23

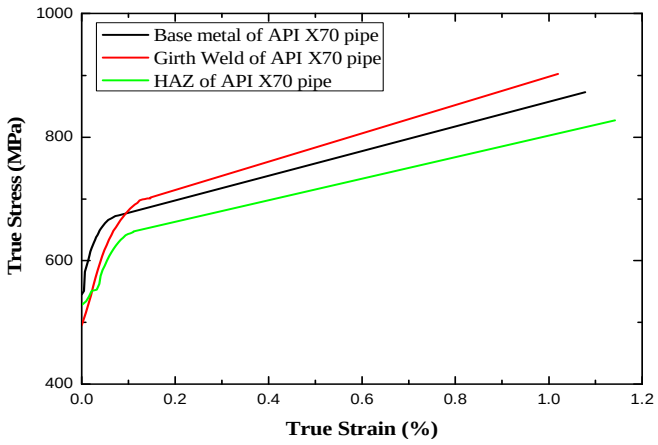

Fig. 3.23. True stress–strain curve of the base metal with API X70 pipe for base, HAZ, and girth weld.

The comparison of CTOD results with experiment and simulation is shown in Fig. 3.24. The results of load and displacement curve was measured by ABAQUS. The results obtained from the CTOD experiment were compared and analyzed with cases which the true stress-strain curve was not only applied through the tensile test, and material properties but also applied with traction-separation in this simulation. The result of true stress-strain curve was well agreed with experiment, otherwise the result of elastic property was not detached with pre-cracks which the curve is deeply increased more than elastic modulus as shown in Fig. 3.25. The coupling is conducted with XFEM of structure analysis and Fluent of fluid analysis with considering CO_2 based on the CZM of fracture criterion.

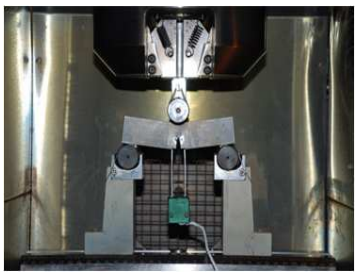

(a) CTOD experiment

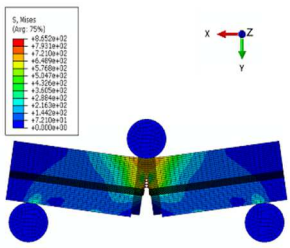

(b) Results of CTOD by FEM

Fig. 3.24**.** The comparison CTOD between experiment and simulation.

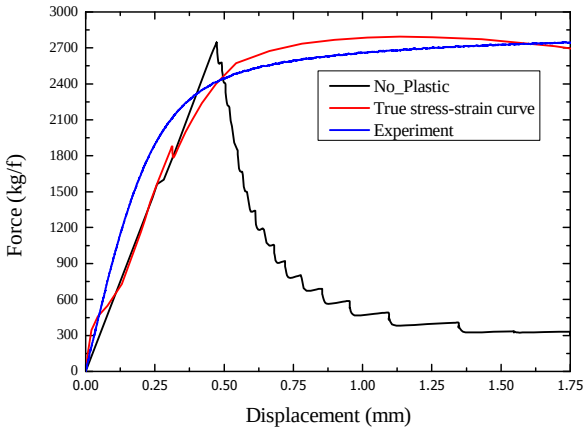

Fig. 3.25. The comparison with results of load and displacement of experiment and simulation.

The structure analysis used XFEM with 1250 mm through-wall crack length with two successive sections of API X70 pipe. The total length of the CO_2 pipeline was 15,050 mm, which takes into account an arbitrary length of 50 mm with base metal at the end of the two girth welds. Consideration is given to the complete crack propagation of the girth weld. The length and crack initiation of CO_2 pipeline considered to simulate based on High Strength Line Pipe Research Committee which is organized by the Iron and Steel Institute of Japan in 1978.

The initial crack size has an important influence for simulation of crack propagation. Therefore, the length and height of the initial crack were verified with the Table 3.8 and the mesh of the CO_2 pipeline was confirmed while changing the mesh size of the thickness and the diameter.

Table 3.8. Consideration of crack propagation.

Subjects	Check list	
Element	Mesh size in pipeline	
	1	Depth
	2	Length
Crack size	Dimension of crack	
	1	Depth
	2	Length

The API X70 pipeline was based on the diameter of 762 mm, thickness of 15.9 mm was determined to set up the mesh more than 5 seeds in thickness direction. The mesh near the crack tip was established a few more meshes due to the accuracy of the analysis. The is the important effect of crack propagation is needed to set the initial crack between meshes in order to propagate the crack in XFEM otherwise the crack propagation is not simulated in ABAQUS as shown in Fig. 3.26.

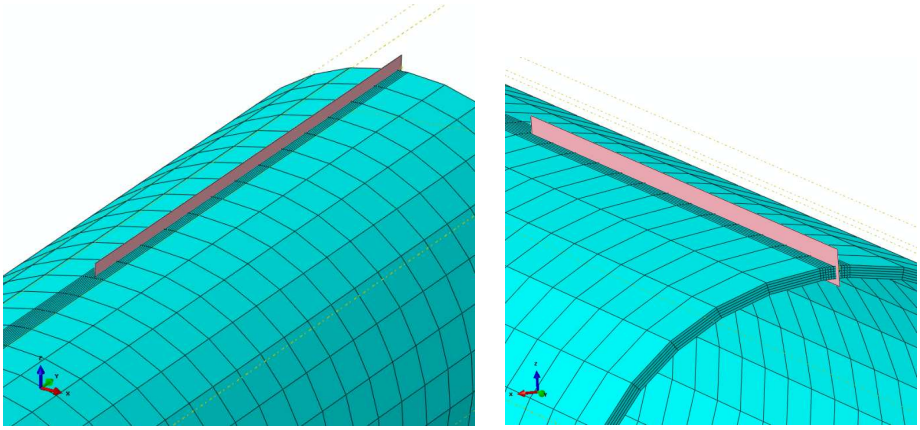

Fig. 3.26. Shape of detail initial crack size in ABAQUS.

The CO_2 pipeline was modeled with 1/2 scale due to boundary condition and load. The boundary condition was set with Y symmetry at the start of crack propagation, and the X and Z direction at the bottom of pipeline. The FEM model with CO_2 pipeline of two sections girth welds is as shown in Fig. 3.27.

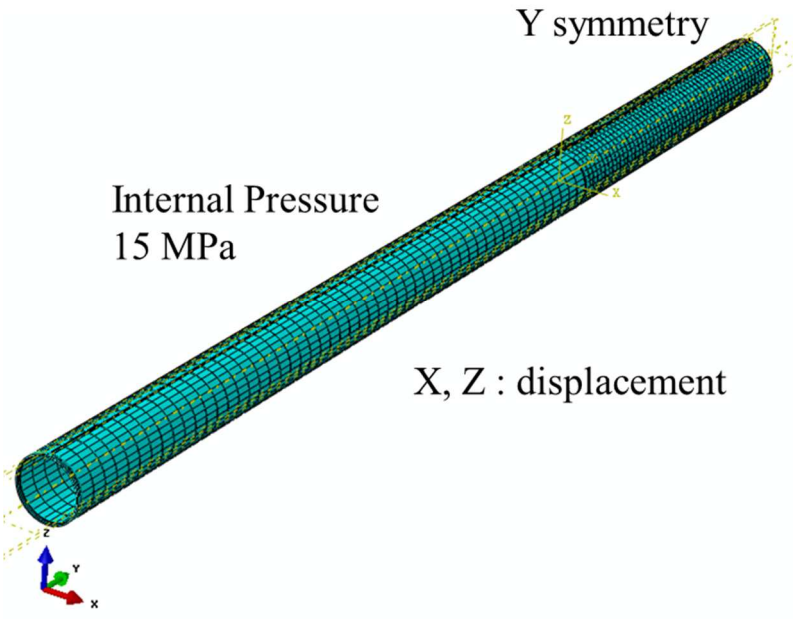

Fig. 3.27. whole model of API X70 pipe with 2 section of girth weld.

The simulation was conducted with results of experimental data from girth weld of API X70 pipeline. The effect of girth weld influences the crack propagation, which predict the direction and toughness of pipeline. This suggests that crack propagation can be predicted with effect of the girth weld, which were not applied by other researchers as shown in Fig. 3.28. The Fig. 3.28 described the weld, HAZ and base metal were merged to connect each other in order to prevent separation during applied internal pressure of pipe.

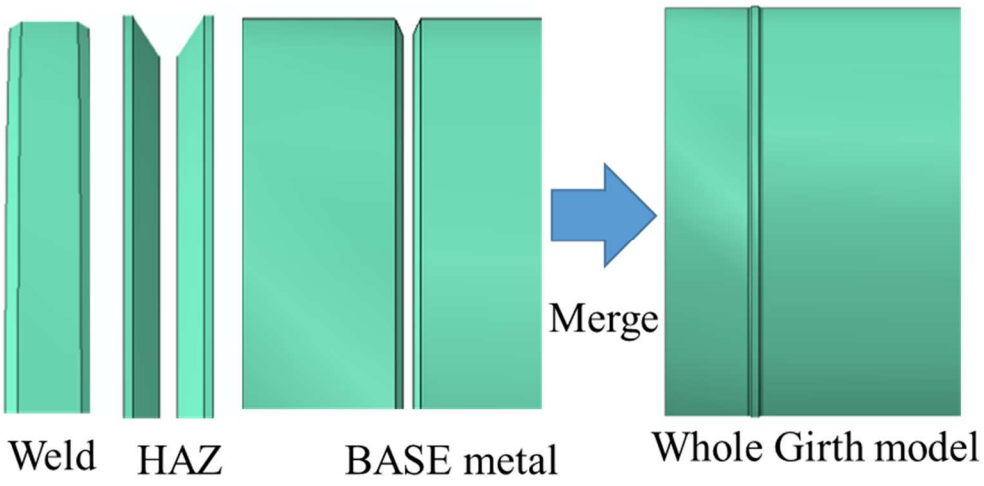

Fig. 3.28. Detail modeling of crack propagation with girth weld

The material properties were used in Table 3.9 for base metal, weld, and HAZ at 207,000 MPa of Elastic, 0.3 of Poisson's ratio and 7680 kg/m^3 of density. The model of girth weld based on the experiment data from API X70 pipe with manual weldment for HAZ and gas tungsten arc welding and shield metal arc welding for girth weld as shown in Fig. 3.29 [74].

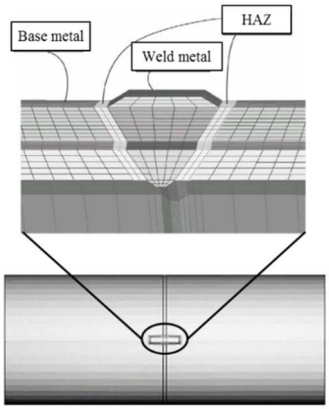

Fig. 3.29. FEA schematic diagrams of girth weld

Table 3.9. Material properties of API X70 pipe for damage theory in FEA.

Material	MaxS Damage (MPa)			Fracture toughness (MPa·mm)	Elastic modulus (MPa)		
	Normal	1st	2nd	Linear	K_{nn}	K_{ss}	K_{tt}
Base	1,746	1,310	1,310	12.99	10,000,000	3,846,154	
HAZ	1,584	1,188	1,188	11.78	10,000,000	3,846,154	
Weld	1,989	1,492	1,492	14.80	10,000,000	3,846,154	

In the case of fluid analysis CO_2, the simulation condition is equivalent to the analysis of different crack sizes studies with inlet, outlet, and wall conditions. The fluid analysis was considered with Real Peng-Robison, enhanced wall treatment, and HEM [47].

The model of the fluid was created by ABAQUS CAE with SAT file in order to import through to Fluent. The inside of structure and outside of fluid mesh has to be consistent for FSI. The fluid geometry had diameter of 730.2 mm and length of 15,050 mm. The element type is hexagonal with numbers of 952,960. The fluid model was imported into ANSYS mesh in order to create the element and boundary conditions at 1/2 scale, as shown in Fig. 3.30. (a). and fluid results in Fig. 3.30 (b).

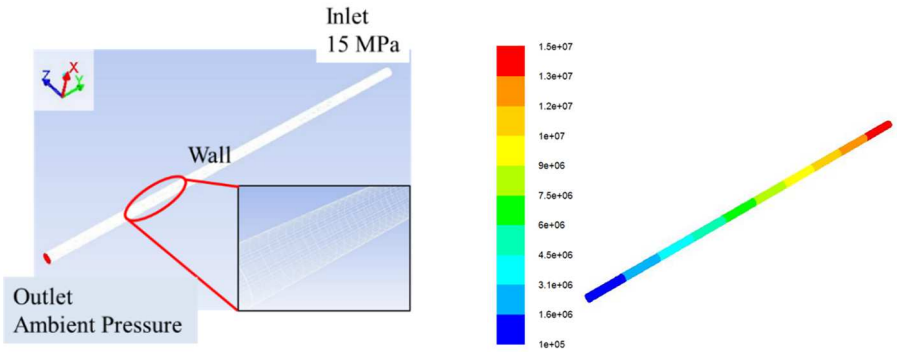

(a) Condition of Fluent (b) Result of Fluent

Fig. 3.30. 100% CO_2 fluid analysis of API X70 pipe by Fluent.

4. Results and discussion

4.1 Basic crack analysis of CO_2 pipeline

There are some agued with differences of NG and CO_2 pipeline. Decompression curve analysis by BTCM assumes with started equivalent pressure and temperature for CO_2 and NG. The comparison with decompression curve of condition is with 100 % CH_4, 100% CO_2, 20 ^oC, and start 15 MPa as shown in Fig. 4.1.

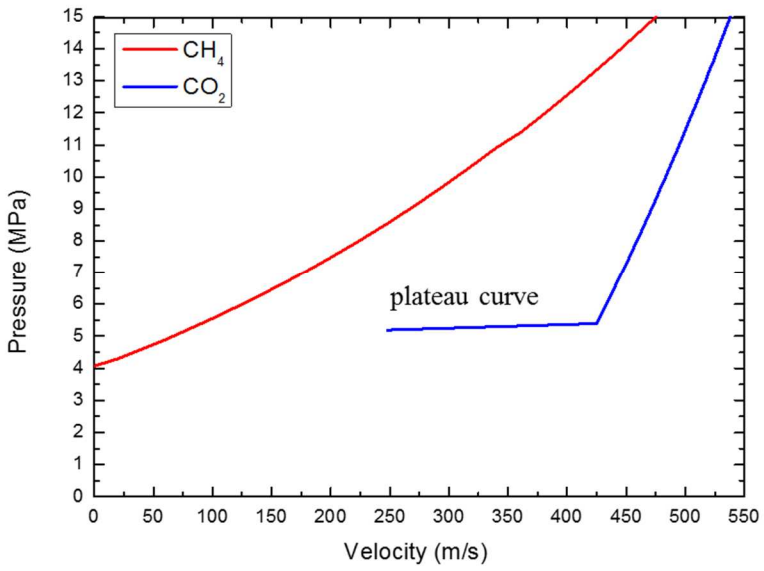

Fig. 4.1. The comparisons with NG and CO_2 by BTCM

The results of decompression curve with CH_4 is gradually decreased. Otherwise, CO_2 is plateau curve occurred caused phase transition it causes the pressure suddenly drop and crack propagation when the crack propagation takes place.

The different CO_2 and NG flow was analyzed with Fluent which 100 % CO_2 is used by used Homogeneous Equilibrium Method, Real Peng-Robison EOS and other simulation conditions. The 100 iteration is conducted for two cases as shown in Fig. 4.2.

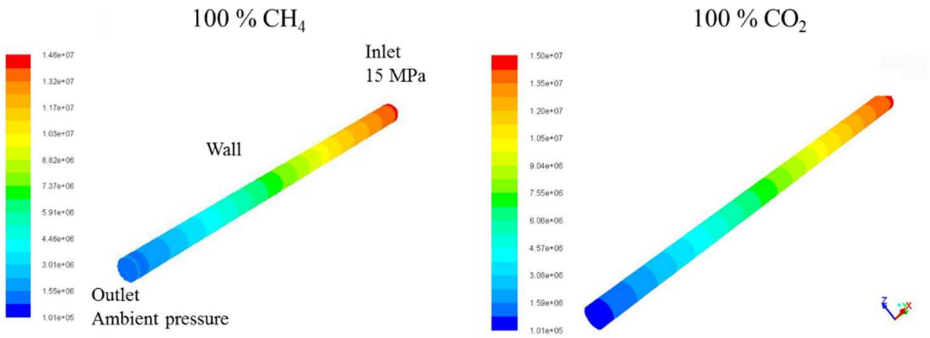

Fig. 4.2. The comparison with 100 % CH_4 and CO_2 with 100 iteration of fluid analysis

Because of short iteration, the pressure drop of CH_4 is higher than CO_2. The comparisons with BTCM and Fluent analysis, the phase transition predicts during operation of pipeline when the pipeline occurs the crack propagation.

This result was correlated with hoop stress law and FEM result. The crack initiation of API X70 was simulated without crack by XFEM in API X70 pipe. The model of crack in API X70 is two-dimensional, symmetry condition. STATUSXFEM is defined in ABAQUS field output [77]. The status of an enriched element is 1.0 when the element is crack and 0.0 when the element is not initiated in XFEM. As shown in Fig. 4.3 the result shows that there was no crack propagation in XFEM if there is no crack in pipes until internal pressure reached 8 MPa and more.

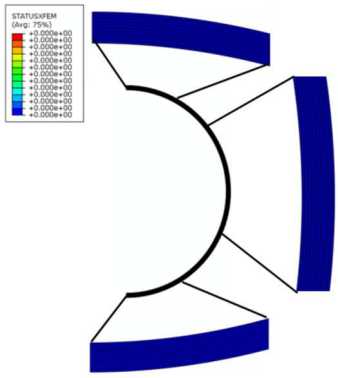

Fig. 4.3. Crack initiation with XFEM in API X70 pipeline.

4.2.1 Crack propagation

In order to analyze the crack propagation, the crack depths were varied from 10 % to 90 % of pipeline thickness as shown Table 1. The true stress-strain curve and fracture energy were applied to resistance with a variety of crack depths. According to the true stress-strain curve, the maximum stress of API X70 pipe was 532 MPa for crack propagation. The maximum pressure was predicted by constant internal pressure as 4 MPa as shown Fig. 4.4. The 10 %, 50% and 90% crack depths of pipelines thickness were compared with maximum principle stress. The stress of 10% crack depth was not reached maximum stress of API X70 pipe, which means the crack was not propagated. Otherwise, stress of 50 % and 90 % of crack depth were exceeded 532 MPa and already propagated.

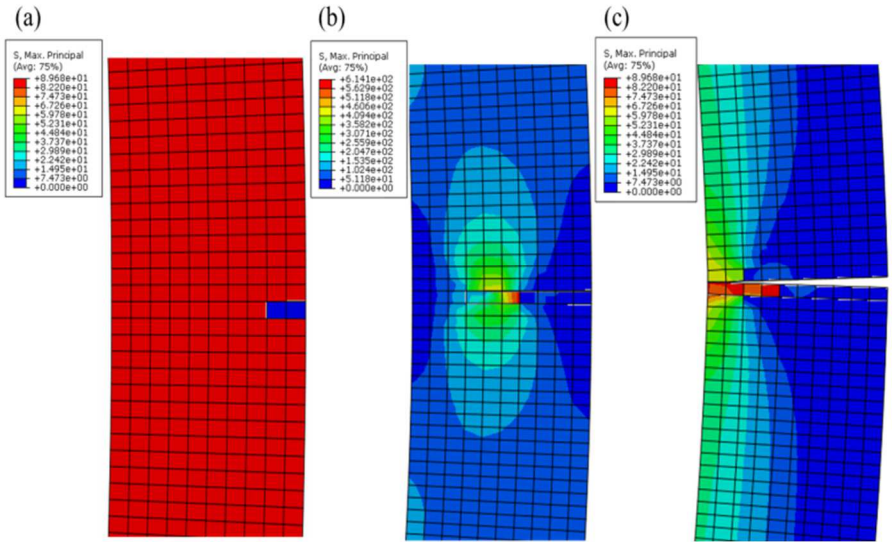

Fig. 4.4. Maximum principle stress analysis with constant internal pressure at 4 MPa with (a) 10 %, (b) 50 %, and (c) 90 % of crack depths with pipelines thickness.

The stress distribution is depending on the pipelines thickness when the 10 %, 50 % and 90 % crack depths of pipeline thickness shown as in Fig. 4.5. The 50 % crack size of pipeline thickness reached 430 MPa and maximum principle stress of 90 % reached more than 532 MPa as 550 MPa. The 50 % was not reached the maximum principle stress and was not propagated but the 90 % was already propagated. The results of critical internal pressure are shown as in Table 5.1 with varied crack depths ratio. The crack propagation of API X70 with varied of crack depths could obtain

results that maximum principle stress affect pipeline thickness with crack size and collated with the maximum stress position and crack position in pipeline.

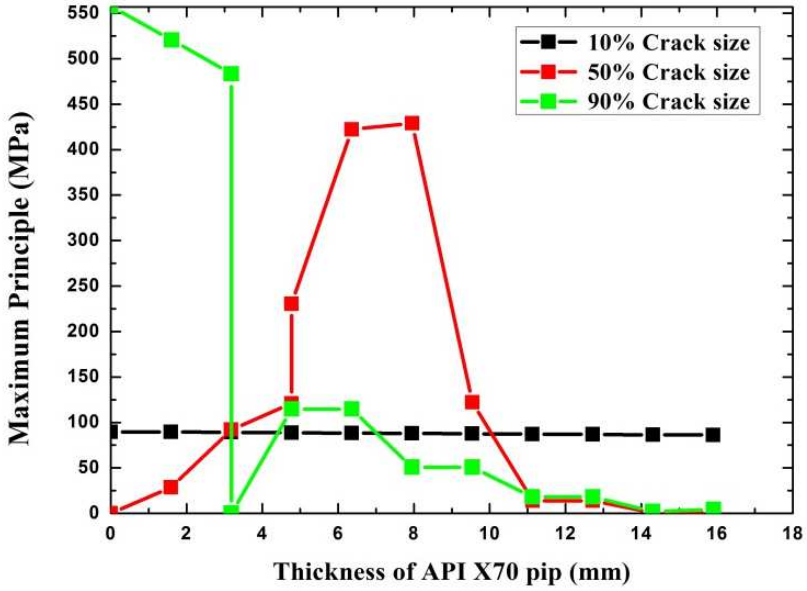

Fig. 4.5. Stress distribution of API X70 by XFEM with 10%, 50%, and 90% crack depths of pipelines thickness.

Table 4.1 Result of critical internal pressure with different crack ratios in API X70 pipeline.

Crack size ratio of thickness (%)								
10	20	30	40	50	60	70	80	90
Critical internal pressure (MPa)								
22.65	9.00	5.18	5.17	5.15	4.30	3.87	3.65	3.44

4.2.1.2 Seam crack

In this study, the seam crack was analyzed for confirming crack propagation behavior by comparisons with XFEM. The seam crack is known to conduct the crack propagation with independent on the direction of the crack as shown in Fig. 4.6.

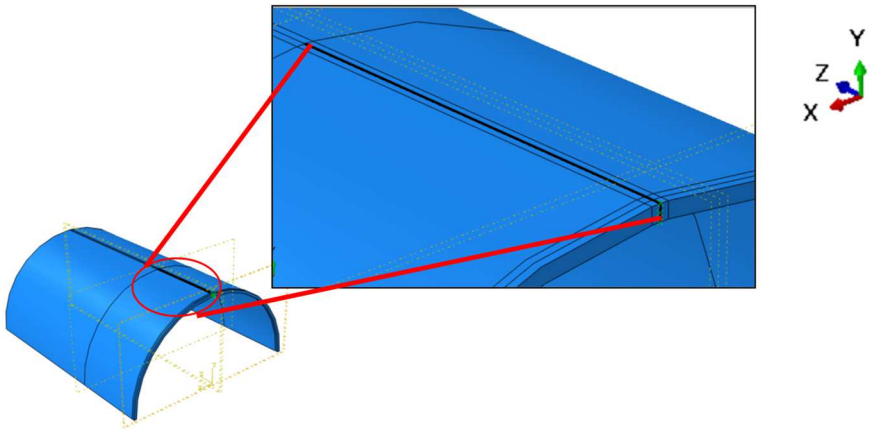

Fig. 4.6. Initial crack test condition of FEM for seam crack

For the modeling and meshed with FEM, the seam crack is modeled with 1/2 scale, three-dimension, z symmetry condition. The element is used C3D8R (element is a general-purpose linear brick element, with reduced integration). The material properties of API X70 used equal as the chapter 4.1.

Structure analysis of seam crack is described as below sequences.

1) use q vector in seam crack which could select crack length and crack direction

2) choose the crack length, set the condition of crack propagation

3) set the initial crack length as 50 mm with seam direction in pipe

The results of seam crack with structural analysis is descried as shown in Fig. 4.7.

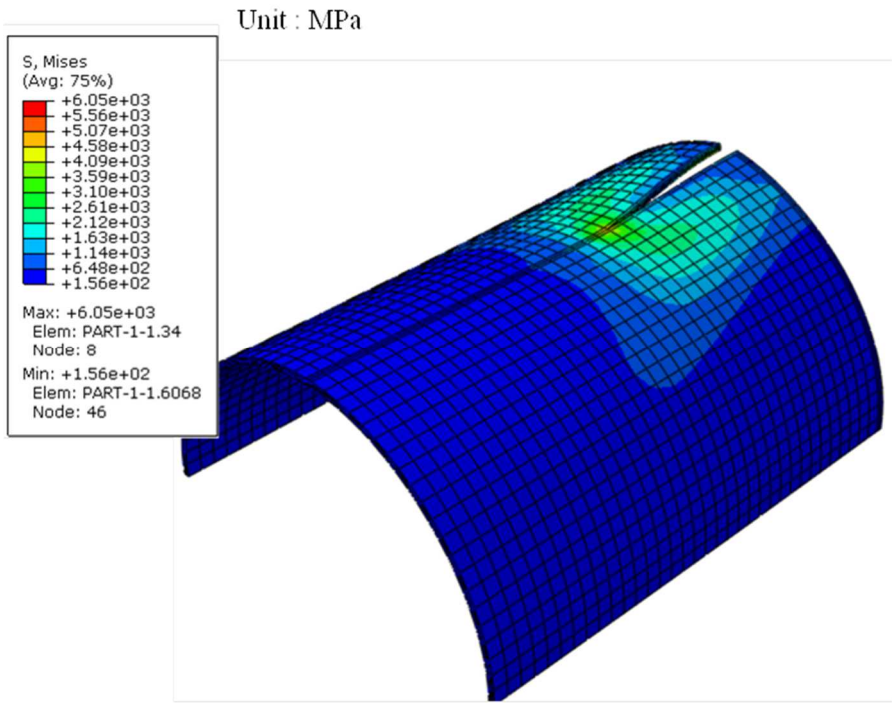

Fig. 4.7. The result of seam crack for structure analysis.

It appears the most concentrated stress is 605 MPa with end of crack propagation. The seam crack only considers the specified with select crack lengths for analysis of J-integral, stress intensity factor. It concluded that seam crack only considered the selected crack length and position, although the real crack propagation of HLP condition propagated along with different CVN energy and lengths.

In part of fluid analysis uses dynamic mesh in order to consider the remised near crack position when crack is propagated. The condition of flow considered with energy equation, Air (Ideal gas), Enhanced wall, flow inlet is 11.6 MPa, K-epsilon behavior with standard model, and standard wall function. The fluid model is considered to flow of 100% CO_2 with ideal gas and modeled 365.1 mm in diameter. The model generated by ABAQUS CAE for contained consistency of ABAQUS and Fluent model and condition. If the mesh between ABAQUS and Fluent has inconsistence, the FSI could not run the simulation. The model and fluid analysis is shown in Fig. 4.8.

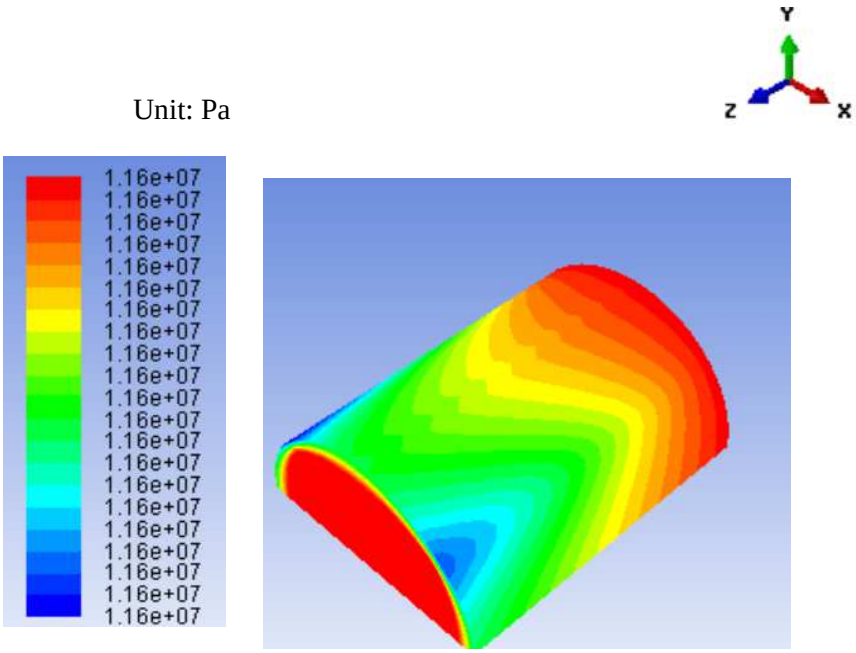

Fig. 4.8. The results of fluid analysis by Fluent.

The interval time is set as ‘1.0’ and number of iterations is set more than 100. The more mesh used in fluid model, the more number of interactions need to calculate. Above the figure, the scale is set as 20 counts and there is no difference of decompression behavior. The results of FSI with seam crack in ABAQUS and Fluent is shown in Fig.4.9. The maximum stress point of FSI and structure results was found 605 MPa and 50 MPa difference. The crack is not propagated as shown in Fig. 4.9; other analysis approach is needed for analysis of crack propagation.

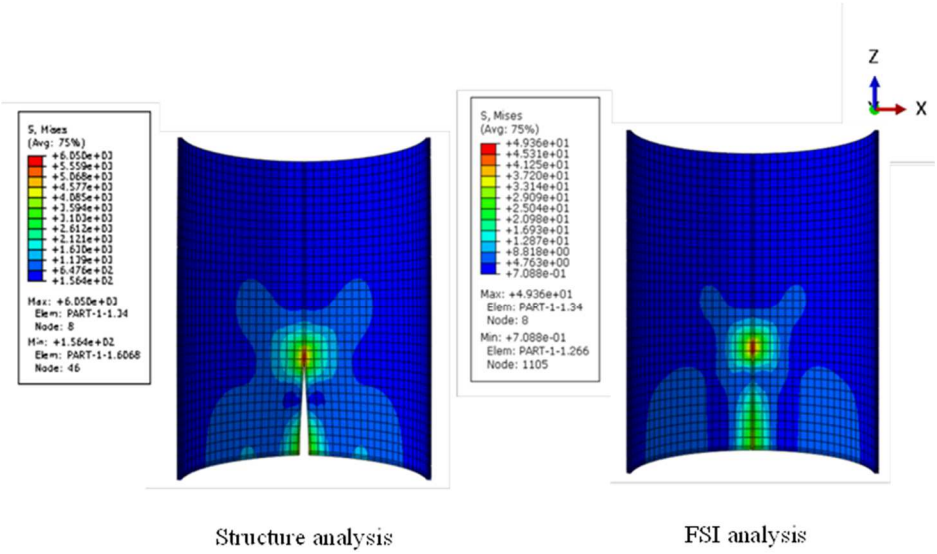

Fig. 4.9. The maximum stress point of FSI and structure results differences.

4.2.1.2 XFEM

The structure and fluid analysis applied surface were confirmed by applied with inner surface of structure and outer surface of fluid. In order to study the mesh sensitivity, the mesh element study of the structure analysis performed as shown in Fig. 4.10.

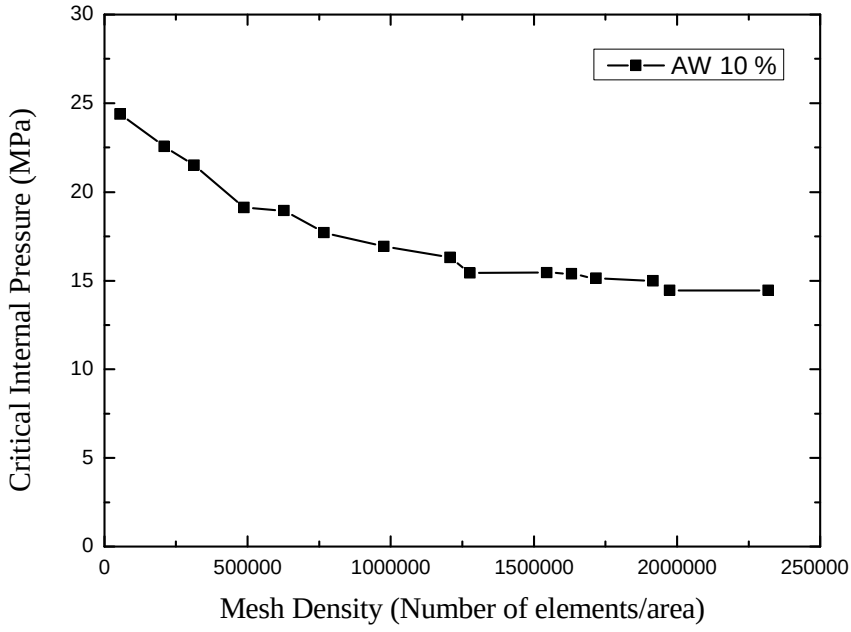

Fig. 4.10 Element study for element size at 10 % crack size.

The condition of boundary and load were equivalent with hoop stress verification as shown in Fig. 4.11.

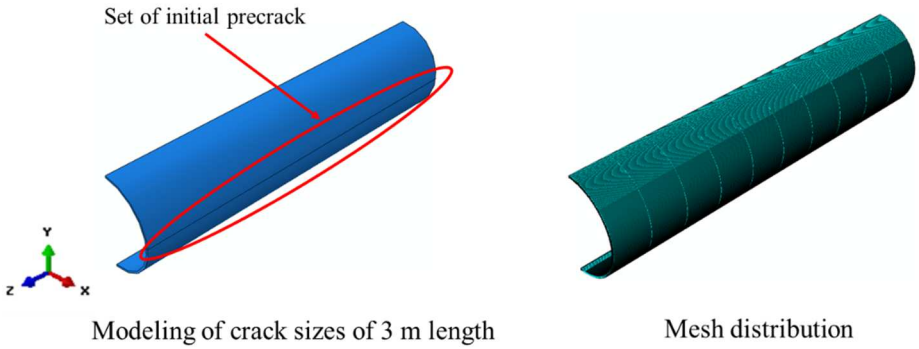

Fig. 4.11. Modeling and mesh distribution of different crack sizes ratio.

When the crack exists in pipe, the critical internal pressure was affected crack propagation even though 10% crack depth is existed based on the results in Fig. 4.12. The critical internal pressure with varied crack depth ratios were derived as shown in Table 4.2. This study is based on the comparison with FSI study.

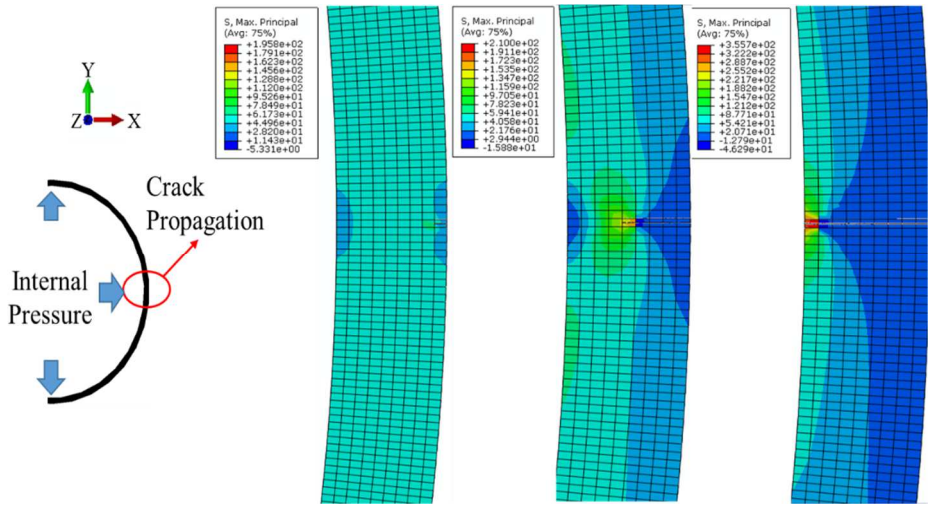

(a) (b) (c) (d)

Fig. 4.12. Schematic model of pipe and crack location (a) for maximum principle stress analysis at constant internal pressure of 8 MPa at (b) 10 %, (c) 30 %, and (d) 50 % crack depths of pipe thickness.

Table 4.2 Results for critical internal pressure at different crack ratios of thickness.

Critical Internal Pressure (CIP) (MPa)	Crack size from outside of diameter								
	10	20	30	40	50	60	70	80	90
Structure (1)	14.44	13.41	10.53	6.81	5.31	4.17	2.2	1.7	1.78
FSI (2)	9.23	8.75	7.03	4.55	3.56	1.49	0.42	1.15	0.99
(1)-(2)	5.21	4.66	3.5	2.26	1.75	2.68	1.78	0.55	0.79

The pipeline was successfully propagated at the crack with girth welds of two sections. Two girth weld sections were analyzed with maximum principle stress and STATUSXFEM, which predict that the crack is propagated or not propagated at value ‘1.0.’ Value ‘1.0’ is defined as full crack propagation. The two section of the girth weld model and full propagation are shown in Fig. 4.13 (a) by STATUSXFEM mode in ABAQUS at 13.97 MPa of internal pressure and detail of girth weld modeling. Fig. 4.13 (b) shows the stress distribution before cracking due to crack propagation at 13.98 MPa. Finally, Fig. 4.13. (c) is the stress distribution after the final time step of a full crack propagation. Therefore, the maximum principle stress is predicted to be higher than the base metal of API X70 pipe at 532 MPa, which is expected to cause sufficient internal pressure propagation. Based on this structural analysis, CO_2 pipeline was analyzed optimum toughness requirement by performing CO_2 flow analysis, and FSI with structure and fluid in cooperation.

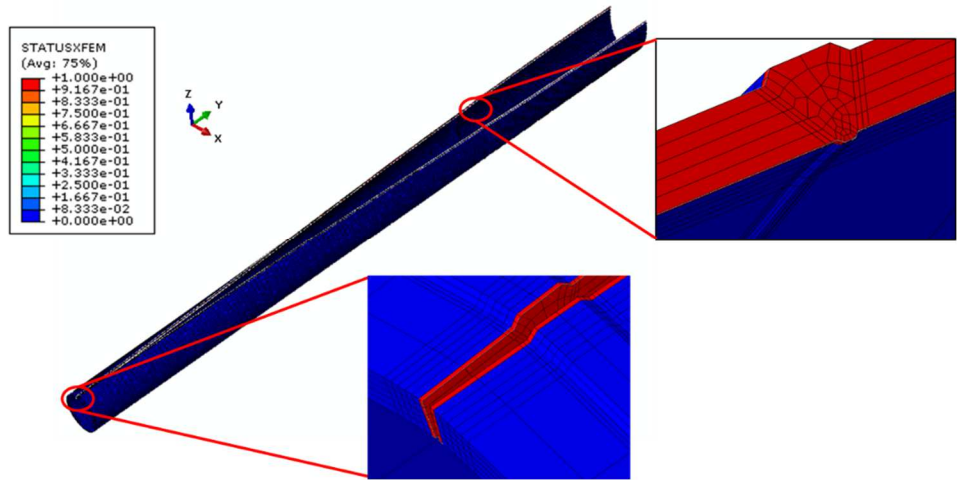

(a) Crack propagation results of two section with girth welds in part of structure.

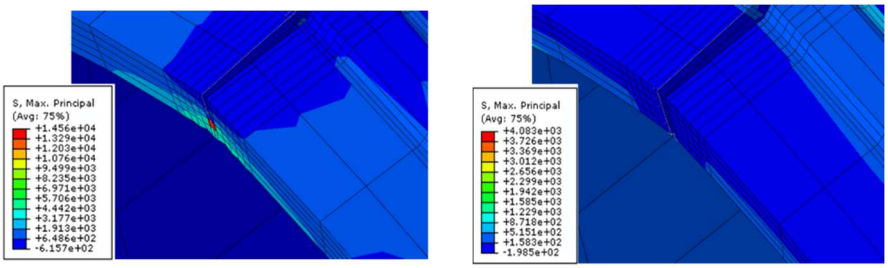

(b) Before detached thickness (c) After detached thickness

Fig. 4.13. Result of crack propagation with structure analysis of API X70 pipe.

4.3 Fluid analysis

This study used Fluent, which is capable of applying various EOS, for part of the fluid analysis [47]. The computational fluid dynamics package ANSYS-Fluent can simulate laminar and turbulent multi-dimensional geometries. Fluid simulation was performed using Fluent 15.0 while the model and mesh of fluid were created by ABAQUS CAE. The fluid model was considered at 1/2 scale in order to apply the boundary conditions with inlet, outlet, wall and symmetry condition. The diameter of the API X70 pipe was 365.1 mm in the 3D fluid simulation. The element type used hexagonal, which is identical with the structure model that has a number of 3,019,997. The turbulence model for 100 % CO_2 assumed at 330 K. The pressure inlet was 15 MPa for dense phase transportation of CO_2 [78]. The boundary condition is considered with 15 MPa for inlet and atmospheric pressure for outlet. The fluid utilized the K-epsilon model with enhanced wall treatment. Furthermore, the boundary condition wall was a stationary wall with no slip for the shear condition. The EOS used the Robin-Pension [79], which is validly used for the thermophysical properties of liquid densities [47], and CO_2 [78]. The CO_2 fluid is treated as homogenous gas phase while the mixture is considered a species model in Fluent and equivalent phase with mixture fluid [47]. The results of the fluid simulation are shown in Fig. 4.14. The FSI simulation was first performed for fluid analysis with CO_2 flow and the fluid information was used for structural analysis [81].

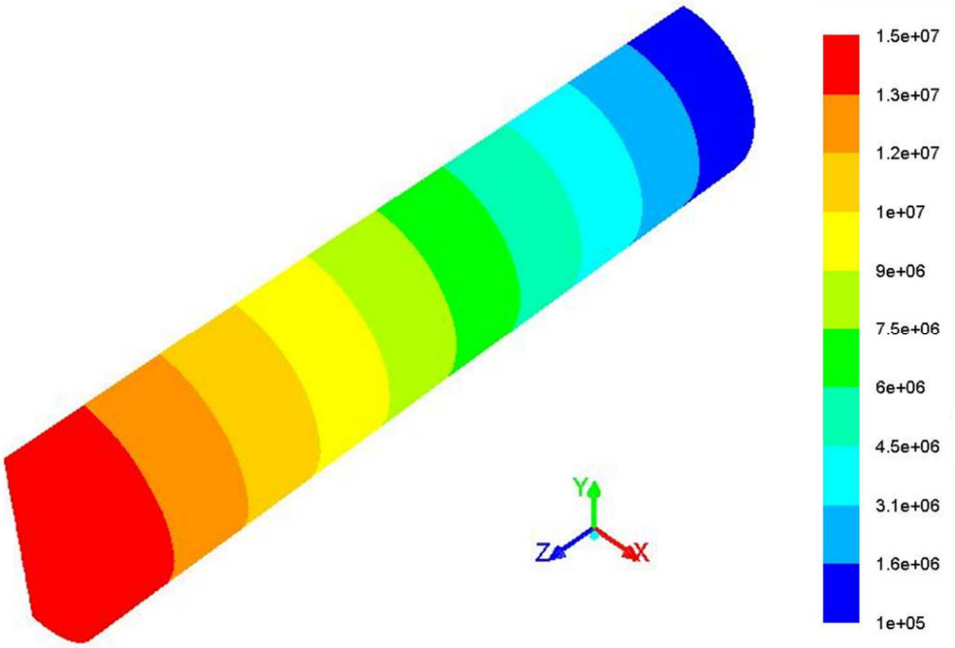

Fig. 4.14. Result of CO_2 flow by Fluent.

4.4 Crack analysis of CO_2 pipeline using FSI

The CO_2 pipeline was considered with understanding the behavior depending on the crack depths using MpCCI, which facilitated cooperation between ABAQUS and Fluent. The comparison of the results for the FSI analysis are shown in Fig. 4.14 at constant 8 MPa of internal pressure. The highest stress region was the same in the FSI and the structure results. The fracture theory applied the equivalent maximum principle stress as the XFEM results. The critical internal pressure when using FSI to understand the CO_2 flow and structure effect is described in Table 4.2. A comparison of Table 4.2 of structure results FSI results shows effect of critical internal pressure is noticeable when the flow is considered. The FSI analysis result shows that the critical internal pressure value decreases as compared with the structural analysis [82]. Therefore, it is found that the influence of the cracks in the fluid is large, which can be distinguished from the results of structure and FSI in the same internal pressure condition as shown in Fig. 4.12. and 4.15.

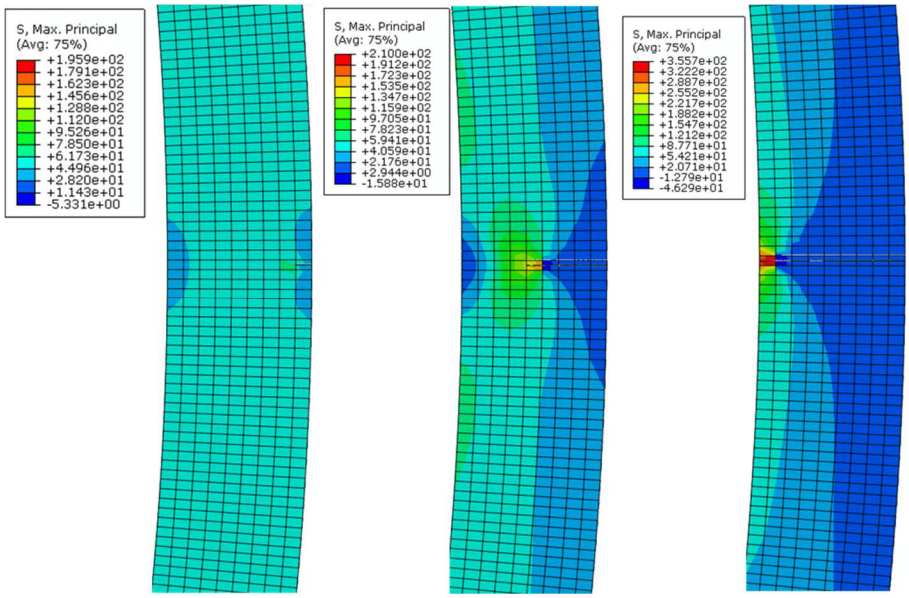

(a) (b) (c)

Fig. 4.15. The results of FSI with maximum principle stress analysis at constant internal pressure of 8 MPa at (a) 10 %, (b) 30 %, and (c) 50 % crack depths of pipe thickness.

This is the results of FSI with successive two sections of girth weld. In the case of assessment of CO_2 pipeline for requirement toughness, FSI was considered by serial coupling method uses for Gauss-Seidel Algorithm which one code runs the other code waits for simulation between structure and fluid. The structure and fluid analysis are simultaneously considered in order to use the FSI method for analysis of crack propagation with CO_2 pipeline. The FSI simulation was first performed for

fluid analysis with CO_2 flow and the fluid information was used for structure analysis [81].

The results for the FSI analysis are shown in Fig. 4.16. Fig. 4.16 (a) confirmed that the crack propagation went completely through the thickness of CO_2 pipeline via the STATUSXFEM mode. Fig. 4.16 (b) and (c) analyzed the CO_2 pipeline fracture before and after cracks, reflectively, by the maximum principle stress according to the time step in ABAQUS. As a result, the internal pressure for crack propagation of CO_2 pipelines was analyzed with at 13.99 MPa.

In the case of the fluid analysis, the highest pressure was generated at the inlet due to inlet and outlet boundary conditions. This result was analyzed at a pressure 0.02 MPa different from the structural analysis results [82]. The crack propagation could be predicted through FSI analysis.

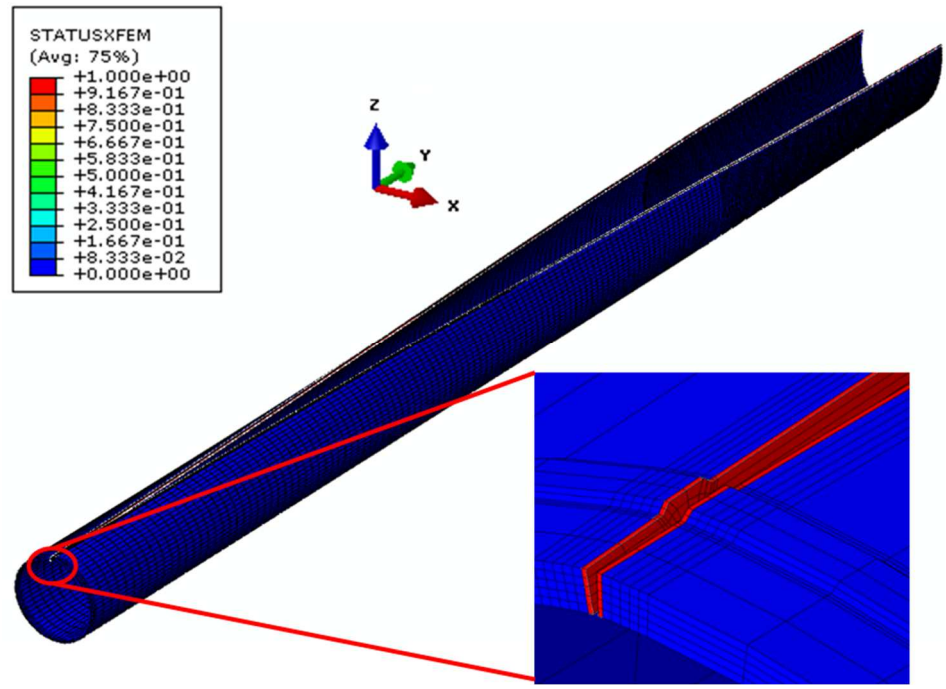

(a) Crack propagation results of 2 sections with girth welds in part of FSI.

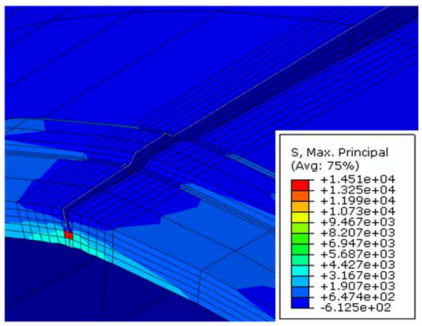

(b) Before detached thickness

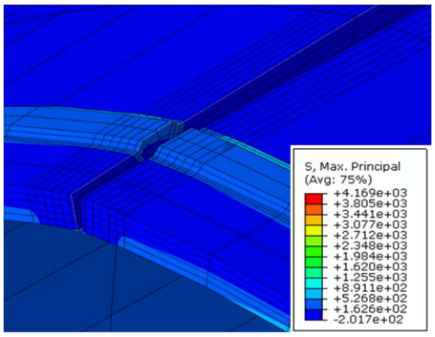

(c) After detached thickness

Fig. 4.16. Results of crack propagation with FSI analysis of API X70 pipe.

5. Further study

Verification of West Jefferson Tests

The CO_2 pipeline with buried depths was experiment by National grid. The pipeline of tests was used API X65 which is equal to Grade L450 with varied types of composition of CO_2 and NO_2. The dimeter of pipe was 914mm, and thickness was 25.4 mm. Test 1 was concerned with 100 % CO_2 with 1.0 m buried depth. The test 02 and 03 was 95 % CO_2 and 5 % NO_2 with 1.0 m, and was 95 % CO_2 and 5 % NO_2 with 1.0 m.

The explosive charger was set to middle of CO_2 pipeline with 0.7 m for Test 01, 3.0 m for Test 02, and 1.8 m for Test 03. The explosive charger assumed through thickness of pipeline for crack propagation. The CVN test conducted xx tester with full size of CVN specimen with upper shelf. The CVN energy was 225 Joule for Test 01, 205 Joule for Test 02, and 217 Joule for Test 03.

The result was successful for burst tests and acquired appropriated shapes of burst with CO_2 pipeline. The tests 01 and 02 of burst results were ring off and Test 03 was propagated.

The sequence of verification was described in Table 5.1 by FSI method in this paper. For the conducting of FSI verification, the analysis of crack propagation in structure part consider simulating at the first in order to acquire the appropriate verification.

The structure part of analysis of crack propagation was used ABAQUS 6.12 and 1/2 scale considered in order to apply boundary and load condition. The element of CO_2 pipeline used C3D8R (element). The density of pipeline 7.85 x 10^{-9} kg/m2 and gravity was used. The fracture energy was converted to use the below equations in decried with BS 7910 [64] equation J.6.

$$K_{J0.2} = \sqrt{\frac{E\left(0.53C_{V_{us}}^{1.28}\right)\left(0.2^{0.133C_{v_{us}}^{0.256}}\right)}{1000\left(1-\nu^2\right)}}$$

$K_{J0.2}$: MPa√m

C_V : Charpy upper shelf energy (J)

E : Young's Modulus (MPa)

ν : Poisson’s Ratio

In order to apply the fracture energy of CVN, the unit needs to covert to ABAQUS based on the equation of energy released rate equation. This equation established with elastic crack-tip solution and the energy theory with relationship between K_I and G [40].

$$G = \frac{K_I^2}{E'}$$

K_I : Stress intensity factor

G : Elastic energy release rate

E' : E for plane stress conditions

Table 5.1. The fracture energy conversion based on the CVN energy by West Jefferson Test of CO_2 pipeline.

CVN (J)	SIF (MPa√m)	G (MPA.mm)
201	216	225
184	206	205
194	212	217

Using the sequence of simulation for verification of West Jefferson tests is described in Table 5.2.

Table. 5.2 The process of simulation sequences for verification method.

Sequences	Simulation
1	Analysis of pipe (applied internal pressure)
2	Crack Propagation of pipe
3	Pipe+Gravity
4	Pipe+Gravity+Soil pressure
5	Pipe+Gravity+Soil pressure +Crack Propagation

The sequences of number 1 and 2 have to conduct basic analysis of crack propagation before considering of buried depth effect as shown in Fig. 5.1.

The soil pressure is calculated with this equation to predict of actual soil load experienced by a pipe [83].

$P_{sp} = (9.81)(\gamma_S)[H + 1.1 \times 10^{-4}(OD)]$

P_{sp} : Geostatic load, MPa

H : Burial depth to top of pipe, m

γ_S : Soil density, kg/m^3 (Sand, dry : 1550 kg/m^3)

OD : Outside diameter of pipe, m

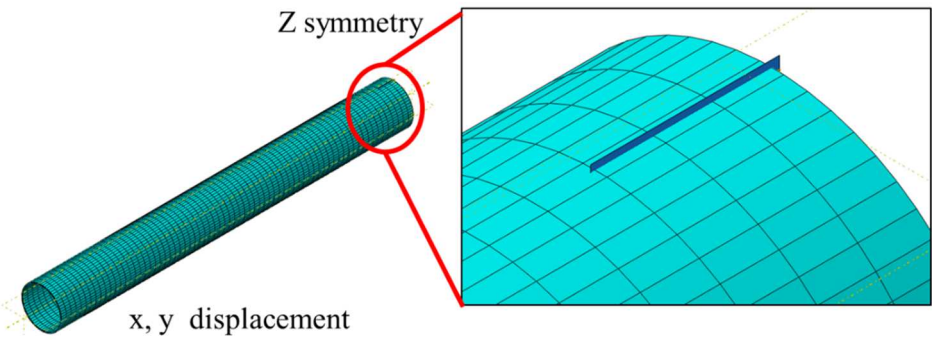

(a) Modeling of crack propagation (b) Detail of crack position

Fig. 5.1. The model of verification with West Jefferson tests.

New consideration of crack propagation for Test 03 has been proposed in this study. The pressure decay from initial pressure (14.9 MPa) to end of test (8.2 MPa) has set up for verification. The difference CVN energy applied with 5.955+5.4m (1/2 scale model) ((total length: 22.71m (5.955+10.80+5.955)). The wet sand density was applied with value of 1905 kg/m^3 as shown in Fig. 5.2.

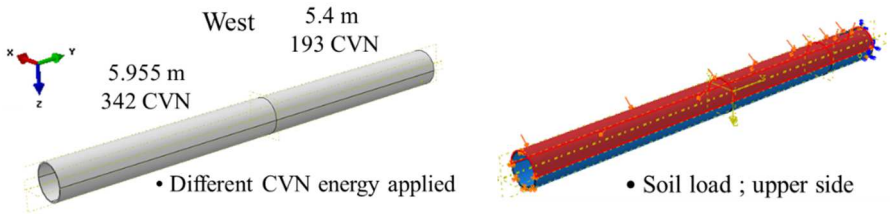

Fig. 5.2. The applied value of CVN and soil effect of West Jefferson tests.

Crack propagation verification of test 03 conducted as shown in Fig. 5.3. The simulation was fully crack propagation. The end of tip internal pressure acquired with 13.89736 MPa. As the results expectation of crack propagation, the internal pressure was not dropped at 8.2 MPa. The simulation has to extend the time step with 50 m/s. Besides, the increment of internal pressure was 4.73671 MPa.

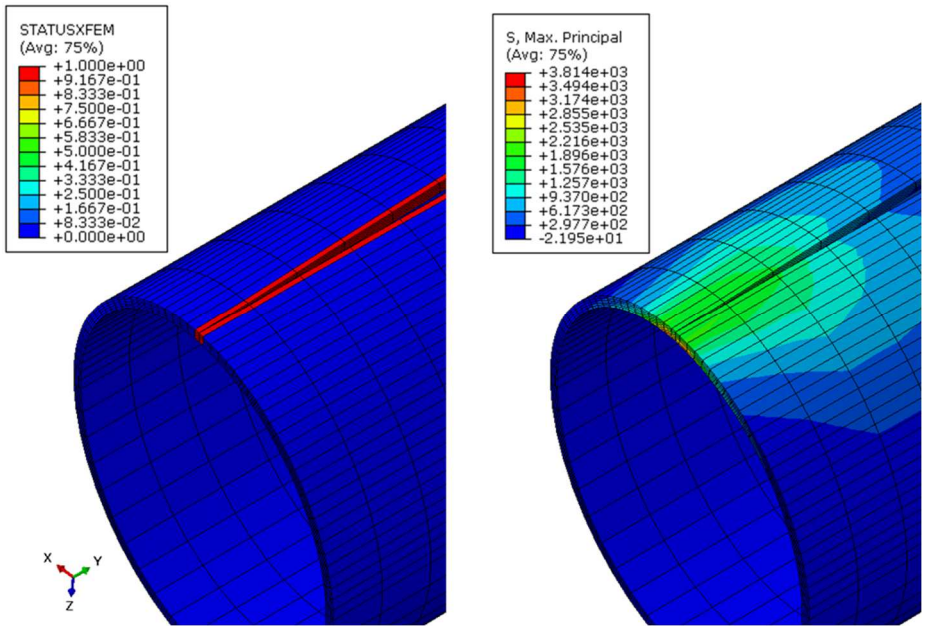

Fig. 5.3. The results of crack propagation verification of West Jefferson Test.

The length of crack initiation is equal to direction of crack propagation with 1.3 m length for crack deviation as shown in Fig. 5.4. The simulation was running and did not increase the time step. It seems the crack deviation is delicate to the mesh condition. The results of Fig. 5.4 (a) was applied with 35 seeds in hoop direction,

170 seeds in longitudinal direction. Otherwise Fig. 5.4 (b) was 43, and 170 seed. Need to study of verification with mesh density study.

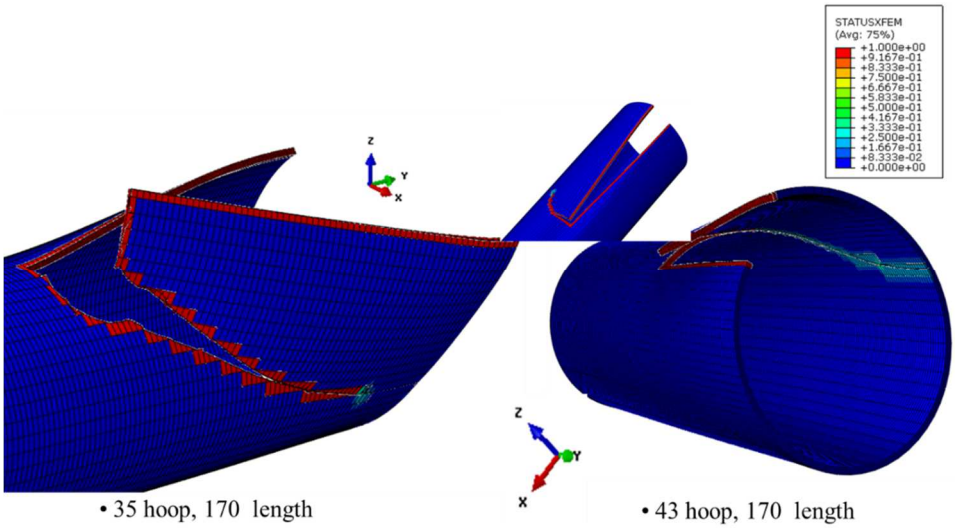

Fig. 5.4. The result of crack deviation with West Jefferson Tests.

6. Summary

The ductile fracture analysis is important to prevent from the catastrophic fracture. In order to assess the ductile fracture, the assessment of BTCM is predicted whether crack is propagated or not. However, this method was based on the low strength and toughness of NG pipeline lower than API X65 with 100 Joule of fracture energy. This method has limitation of using CO_2 pipeline and high strength, toughness. When NG is dropped pressure, the single phase has occurred with low speed. The two phase of CO_2 flow behaved the plateau curve which it causes phase transition with dropped the pressure of pipeline.

In order to develop the crack propagation of CO_2 pipeline, the FSI simulation has conduct to combine structure and fluid behavior. The different crack size ratio considered for acquired critical internal pressure with failure theory of maximum principle stress. The study of crack propagation recognized with girth weld effect based on confirmation of experiment and simulation which is results of CTOD with load and displacement curve. The FSI results tended to be lower than structure results because it may affect high pressure with started in inlet of fluid analysis.

The verification of method with crack size ratio and crack propagation with two successive section of girth weld may influence the cost of construction if the simulation is preceded with Front End Engineering Design (FEED). According to the results of FSI, the length of pipeline or different CVN energy with each section

of pipeline would have extended for actual FEED system in order to assess the appropriate required toughness of CO_2 pipeline. The soil effect of pipeline could be expected to apply above the pipeline to simulate the crack propagation.

7. References

[1] Cosham, Andrew, et al. (2012), 'Ruptures in gas pipelines, liquid pipelines and dense phase carbon dioxide pipelines', *2012 9th International Pipeline Conference* (American Society of Mechanical Engineers), 465-82.

[2] DNV (2010), 'Design and Operation of CO 2 Pipelines', *DNV RP-J202, Bærum, Norway*, 1-42.

[3] Metz, Bert, et al. (2005), 'IPCC special report on carbon dioxide capture and storage', (Intergovernmental Panel on Climate Change, Geneva (Switzerland). Working Group III).

[4] Mannucci, Gianluca and Demofonti, Giuseppe (2011), 'Control of ductile facture propagation in X80 gas linepipe', *Journal of Pipeline Engineering*, 10 (3).

[5] Skovholt, Otto (1993), 'CO2 transportation system', *Energy Conversion and Management*, 34 (9), 1095-103.

[6] Chrysostomidis, Ioannis, et al. (2009), 'Assessing issues of financing a CO2 transportation pipeline infrastructure', *Energy Procedia*, 1 (1), 1625-32.

[7] Noothout, Paul, et al. (2014), 'CO2 Pipeline infrastructure–lessons learnt', *Energy Procedia*, 63, 2481-92.

[8] Seevam, Patricia N, et al. 'Transporting the next generation of CO2 for carbon capture and storage: the impact of impurities on supercritical CO2 pipelines'.

[9] DNV, (2007), 'Submarine Pipeline Systems', (DNV-OS-F101)

.

[10] DOT, US 'CFR Part 195, Transportation of Hazardous Liquids by Pipeline. 2004', *Washington, DC: US Dept. of Transportation*.

[11] ASME B31.4, (2009), 'Pipeline Transportation Systems for Liquids and Slurries', *American Society of Mechanical Engineers*.

[12] ASME B31.8, (2010), *Gas transmission and distribution piping systems* (American Society of Mechanical Engineers).

[13] ISO 13623, (2009), 'Petroleum and Natural Gas industries–Pipeline Transportation Systems'.

[14] Vermeulen, TN (2011), 'Knowledge sharing report-CO2 liquid logistics shipping concept (LLSC): Overall supply chain optimization', *Tebodin Netherlands BV, The Hague*.

[15] Heddle, Gemma, Herzog, Howard, and Klett, Michael (2003), 'The economics of CO2 storage', *Massachusetts Institute of Technology, Laboratory for Energy and the Environment*.

[16] ANSI (1991), *Manual for Determining the Remaining Strength of Corroded Pipelines: A Supplement to ASME B31 Code for Pressure Piping* (American Society of Mechanical Engineers).

[17] British Standard, (1993), 'BS 8010: code of practice for pipelines'.

[18] API 5L, (2004), 'Specification for Line Pipe', *American Piping Institute*.

[19] E On, 'Kingsnorth Carbon Capture & Storage Project Consequence Assessment of CO2 Pipeline Releases.

[20] Maxey, WA, Kiefner, JF, and Eiber, RJ (1983), 'Brittle Fracture Arrest in Gas Pipelines', *American Gas Association, NG-18 Report*, (135).

[21] Meyers, MA and Chawla, KK 'Mechanical behavior of materials, 2009', (Cambridge University Press).

[22] Burdekin, F Mo and Stone, DEW (1966), 'The crack opening displacement approach to fracture mechanics in yielding materials', *Journal of strain Analysis*, 1 (2), 145-53.

[23] Wells, AA (1963), 'Application of fracture mechanics at and beyond general yielding', *British Welding Journal*, 10 (11), 563-70.

[24] BS 7448-3:2005, (2005), 'Fracture mechanics toughness tests. Method for determination of fracture toughness of metallic materials at rates of increase in stress intensity factor greater than 3.0 MPa m0.5 s-1', (British Standard).

[25] ASTM E1290-08 (2008), Standard test Method for crack-tip opening displacement (CTOD) fracture toughness measurement'.

[26] ASTM A370-17, (2017), 'Standard Test Methods and Definitions for Mechanical Testing of Steel Products'.

[27] Anderson, Ted L (2017), *Fracture mechanics: fundamentals and applications* (CRC press).

[28] Dunbar, Andrew, et al. (2012), 'Simulation of ductile crack propagation in pipeline steels using cohesive zone modeling', *ASME 2012 Pressure Vessels and Piping Conference* (American Society of Mechanical Engineers), 917-26.

[29] Zerbst, Uwe, Heerens, Jürgen, and Schwalbe, K-H (1995), 'Fracture mechanics analysis based on a local simulation principle', *Fatigue & Fracture of Engineering Materials & Structures*, 18 (3), 371-76.

[30] Erdelen-Peppler, M, et al. (2005), 'Significance of DWT testing for line pipe safety', *11th International Conference on Fracture ICF11, Turin, IT*.

[31] API RP 5L3 (1996), *Recommended Practice for Conducting Drop-Weight Tear Tests on Line Pipe", 3rd edition, American Petroleum Institut API*.

[32] Parmar, Shreya, et al. (2015), 'Simulation of Ductile Fracture in Pipeline Steels Under Varying Constraint Conditions Using Cohesive Zone Modeling', *ASME 2015 Pressure Vessels and Piping Conference* (American Society of Mechanical Engineers).

[33] Tvergaard, Viggo and Hutchinson, John W (1992), 'The relation between crack growth resistance and fracture process parameters in elastic-plastic solids', *Journal of the Mechanics and Physics of Solids*, 40 (6), 1377-97.

[34] Wilkowski, G, et al. (2006), 'Effect of grade on ductile fracture arrest criteria for gas pipelines', *analysis*, 6 (1), 1.

[35] Leis, BN, et al. (2005), 'Modeling running fracture in pipelines-past, present, and plausible future directions', *11th International Conference on Fracture, ICF11* (8), 5759-64.

[36] Jones, DG, et al. (2013), 'Fracture-propagation control in dense-phase CO2 pipelines', *Proceedings of the 6th International Pipeline Technology Conference*, 7-9.

[37] Sugie, E, et al. (1982), 'A study of shear crack propagation in gas-pressurized pipelines', *Journal of Pressure Vessel Technology*, 104 (4), 338-43.

[38] Makino, Hiroyuki, et al. (2001), 'Prediction for crack propagation and arrest of shear fracture in ultra-high pressure natural gas pipelines', *ISIJ international*, 41 (4), 381-88.

[39] Makino, Haroyuki, Takeuchi, Izumi, and Higuchi, Ryouta (2008), 'Fracture propagation and arrest in high-pressure gas transmission pipeline by ultra high strength line pipes', *IPC2008-64078, Proc. of International Pipeline Conference*.

[40] Zhu, Xian-Kui (2015), 'State-of-the-art review of fracture control technology for modern and vintage gas transmission pipelines', *Engineering Fracture Mechanics*, 148, 260-80.

[41] Aursand, Eskil, et al. (2014), 'CO2 pipeline integrity: Comparison of a coupled fluid-structure model and uncoupled two-curve methods', *Energy Procedia*, 51, 382-91.

[42] G. Demofonti, G. Mannucci, H. G. Hillenbrand, D. Harris (2004), 'Evaluation of the suitability of X100 steel pipes for high pressure gas transportation pipelines

by full scale tests', *Proceedings of 6th International Pipeline Conference, Calgary, Canada*, 2004-145.

[43] Demofonti, G and Spinelli, CM (2011), 'Technical challenges facing the transport of anthropogenic CO2 by pipeline for carbon capture and storage purposes', *PTC 6th Pipeline Technology Conference*.

[44] Meleddu, A, et al. (2014), 'CO2 decompression modeling for ductile fracture propagation control in deepwater pipelines', *The Twenty-fourth International Ocean and Polar Engineering Conference* (International Society of Offshore and Polar Engineers).

[45] King, Graeme G and Kumar, Satish (2010), 'How to select wall thickness, steel toughness, and operating pressure for long CO 2 pipelines', *Journal of Pipeline Engineering*, 9 (4).

[46] Poling, Bruce E, Prausnitz, John M, and O'connell, John P (2001), *The properties of gases and liquids* (5: Mcgraw-hill New York).

[47] Fluent, ANSYS (2013), 'Release 15.0', *Theory Guide, November*.

[48] Edwards, DK, Denny, VE, and Mills, AF (1973), 'Transfer Processes, Holt, Rinehart and Winston', *Inc., New York*.

[49] Hirschfelder, Joseph O, Bird, R Byron, and Spotz, Ellen L (1949), 'The Transport Properties of Gases and Gaseous Mixtures. II', *Chemical Reviews*, 44 (1), 205-31.

[50] Van Wylen, Gordon J and Sonntag, Richard E 'Fundamentals of classical thermodynamics 1985', (John Wiley and Sons).

[51] Saraswat, Rajil and Mirzaee-Sisan, Ali (2013), 'Comparison of Plastic Collapse Solutions for Surface Breaking Flaws in Standard Assessment Procedures with FEA', *ASME 2013 32nd International Conference on Ocean, Offshore and Arctic Engineering* (American Society of Mechanical Engineers), V04BT04A052-V04BT04A52.

[52] Glinka, G (1996), 'Development of weight functions and computer integration procedures for calculating stress intensity factors around cracks subjected to complex stress fields', *Stress and Fatigue-Fracture Design, Petersburg Ontario, Canada, Progress Report*, 1 (1), 1.

[53] Gajdos, L and Sperl, M (2013), 'Critical Conditions of Pressurized Pipes', *Engineering Mechanics*, 20 (5).

[54] Folias, ES (1970), 'On the theory of fracture of curved sheets', *Engineering fracture mechanics*, 2 (2), 151-64.

[55] Berstad, T, et al. (2011), 'CO2 pipeline integrity: A new evaluation methodology', *Energy Procedia*, 4, 3000-07.

[56] Du, Yang, et al. (2016), 'Coupled simulation of explosion-driven fracture of cylindrical shell using SPH-FEM method', *International Journal of Pressure Vessels and Piping*, 139-140 (Supplement C), 28-35.

[57] Zargarzadeh, Payam (2013), 'Structural integrity of CO2 transportation infrastructures', *England: Cranfield University*.

[58] Elshahomi, Alhoush Mohmed (2015), 'Modelling of gas decompression process for CO2 transmission pipeline'.

[59] O'Donoghue, PE, et al. (1997), 'The development and validation of a dynamic fracture propagation model for gas transmission pipelines', *International Journal of Pressure Vessels and Piping*, 70 (1), 11-25.

[60] Makino, Hiroyuki, et al. (2001), 'Natural gas decompression behavior in high pressure pipelines', *ISIJ international*, 41 (4), 389-95.

[61] Terenzi, A (2005), 'Influence of real-fluid properties in modeling decompression wave interacting with ductile fracture propagation', *Oil & Gas Science and Technology*, 60 (4), 711-19.

[62] Cheng, Weili and Finnie, Iain (1986), 'Measurement of residual hoop stresses in cylinders using the compliance method', *Journal of engineering materials and technology*, 108 (2), 87-92.

[63] Zhu, Xian-Kui and Joyce, James A (2012), 'Review of fracture toughness (G, K, J, CTOD, CTOA) testing and standardization', *Engineering Fracture Mechanics*, 85, 1-46.

[64] BSI, BS (2013), '7910: 2013+ A1: 2015: Guide to Methods for Assessing the Acceptability of Flaws in Metallic Structures', (December).

[65] Bannister, AC (1998), *Structural Integrity Assessment Procedures for European Industry: SINTAP: Sub-task 3.3 Report: Final Issue Determination of Fracture Toughness from Charpy Impact Energy: Procedure and Validation* (British Steel plc).

[67] Liu, Guowei, et al. (2013), 'XFEM for thermal crack of massive concrete', *Mathematical Problems in Engineering*, 2013.

[68] American National Standards Institute (1991), *Manual for Determining the Remaining Strength of Corroded Pipelines: A Supplement to ASME B31 Code for Pressure Piping* (American Society of Mechanical Engineers).

[69] Bickell, MB and Ruiz, C (1967), 'Stress Analysis of Piping Systems', *Pressure Vessel Design and Analysis* (Springer), 341-62.

[70] Liu, PF, Zhang, BJ, and Zheng, JY (2012), 'Finite element analysis of plastic collapse and crack behavior of steel pressure vessels and piping using XFEM', *Journal of failure analysis and prevention*, 12 (6), 707-18.

[71] Fraunhofer SCAI, (2014), 'MpCCI 4.3.1-2 Documentation, Part I Overview. Sankt Augustin: Fraunhofer SCAI.

[72] Talemi, Reza H, et al. (2016), 'Assessment of brittle fractures in CO 2 transportation pipelines: A hybrid fluid-structure interaction model', *Procedia Structural Integrity*, 2, 2439-46.

[73] Oh, Chang-Kyun, et al. (2007), 'Development of stress-modified fracture strain for ductile failure of API X65 steel', *International Journal of Fracture,* 143 (2), 119-33.

[74] Yeom, Kyu Jung, Kim, Woo Sik, and Oh, Kyu Hwan (2016), 'Integrity assessment of API X70 pipe with corroded girth and seam welds via numerical simulation and burst test experiments', *Engineering Failure Analysis,* 70, 375-86.

[75] Makino, Hiroyuki, et al. (2001), 'Study on the propagating shear fracture in high strength line pipes by partial-gas burst test', *ISIJ international,* 41 (7), 788-94.

[76] François, Dominique, Pineau, André, and Zaoui, André (1998), *Mechanical behaviour of materials* (Springer).

[77] Simulia, Dassault Systemes (2012), 'Abaqus 6.12 documentation', *Providence, Rhode Island, US.*

[78] Chandel, Munish Kumar, Pratson, Lincoln F, and Williams, Eric (2010), 'Potential economies of scale in CO2 transport through use of a trunk pipeline', *Energy Conversion and Management,* 51 (12), 2825-34.

[79] Span, Roland and Wagner, Wolfgang (1996), 'A new equation of state for carbon dioxide covering the fluid region from the triple-point temperature to 1100 K at pressures up to 800 MPa', *Journal of physical and chemical reference data,* 25 (6), 1509-96.

[80] Zhao, Qing and Li, Yu-Xing (2014), 'The influence of impurities on the transportation safety of an anthropogenic CO2 pipeline', *Process Safety and Environmental Protection,* 92 (1), 80-92.

[81] Fluent, Inc. (2006), 'FLUENT 6.3 user's guide', *Fluent documentation*.

[82] Mitsuya, Masaki, et al. (2014), 'Calculation of dynamic stress intensity factors for pipes during crack propagation by dynamic finite element analysis', *Journal of Pressure Vessel Technology,* 136 (1), 011207.

[83] Babu, GL Sivakumar and Srivastava, Amit (2010), 'Reliability analysis of buried flexible pipe-soil systems', *Journal of pipeline systems engineering and practice,* 1 (1), 33-41.

요약 (국문초록)

본 학위논문에서는 CO_2 배관의 최소 인성 요구치 분석을 수행하였다. 이를 위해서 유동 구조 연계 해석을 통한 균열 크기에 따른 임계내압치를 분석하였으며, 균열 전파에 따른 인성치를 분석하였다.

일반적으로 미국 Battelle 연구소에서 1970 년대에 개발한 Battelle two curve method 법을 이용하여 배관의 균열 전파를 분석하였다. 이는 Crack resistance curve 를 API X65 및 파괴 인성이 100 Joule 이하의 배관을 통한 파열 실험을 이용, semi-empirical 방법을 통하여 수식을 얻었으며, BWRS 의 상태방정식을 통한 Gas decompression curve 를 배관의 유동 조건에 따라 얻었다. 만약 이 두 선이 겹치면 균열이 전파된다고 가정하였다. 하지만 높은 인성 및 응력, CO_2 배관을 균열전파 여부를 평가한다면, 수정된 계수를 적용한 BTCM 을 사용한다 하더라도 균열전파 평가를 적절하게 못하는 것으로 판단된다. 또한 천연가스 및 CO_2 배관을 설계할 때 환경 및 배관 조건에 따라 달라지기 때문에 개선이 필요하다고 판단된다.

이를 위해 본 연구에서는 유동 구조 연계 해석을 적용하였다. 균열전파 구동력이 유동의 감압곡선보다 크다면 균열이 계속해서 발전하고, 천연가스와 다르게 CO_2 는 감압되는 속도가 느리며, Plateau 곡선이 발생하므로, 파열이 된다면 공기보다 무겁고, CO_2 의 독성이 심각하기

때문에 인간 및 자연에 심각한 영향이 발생할 수 있다. 이를 방지하기 위해, 높은 밀도와 낮은 점성을 가지는 조밀상 및 초임계상을 모사할 수 있도록 Fluent 를 이용하여, 원하는 점성 등의 유동 물성을 계산하고, 유동의 압력과 위치 정보를 구조 해석에 송부하여, 실제 유동 및 구조의 파괴를 연계하여 좀 더 정확하고, 실제 상황에 맞게 예측이 가능할 것이라 판단된다.

균열 크기의 경우 charpy v-notch Impact 실험을 통해 실제 API X70 배관에서 실제 시편을 채취하여 Fracture toughness 를 측정하였으며, 이를 통해 Fracture energy 변환하여 적용하였다. 또한 균열 크기는 10 % 단위로 10 % 에서 90 %를 고려하였다. 균열의 위치는 길이 방향으로 두께의 바깥에서 안쪽 부분을 고려 하였다.

구조해석의 경우 Seam crack 과 같이 균열의 방향 및 거리를 사용자의 임의로 적용하는 것이 아니라, 본 연구에서는 확장유한요소해석을 이용하여, 균열 조건 및 유동에 따라 균열이 전파 되는 것을 모사할 수 있다. 이는 특히 Mesh 를 재생성하는 것이 아니기 때문에 균열 전파를 예측하는데 있어서 효과적일 것이라 판단된다.

균열 전파 모사를 위해 crack tip opening displacement (CTOD) 법을 이용하였다. 3 축을 통한 균열 전파를 시험하는 것으로 2 개의 홀더와 균열을 전파하는 홀더를 이용하여, 균열의 진전을 모사하여 배관의 적정 CTOD 값을 예측할 수 있다. 이를 이용하여 Traction-separation

이론치와 해석치를 비교 분석하였으며, 이를 균열 전파 모사를 위해서 적용하였다. 또한 원주 용접부 물성 및 형상을 적용하였다. API X70 배관의 실제 원주 용접을 통하여 100 % 원주 용접, 모재, 열영향부의 시편을 채취하여 인장 실험을 통하여 물성을 얻었다. 실제 실험 부분을 정확하게 해석에 모사 및 물성을 적용하여 균열 전파에 미치는 영향을 분석하였다.

균열 크기에 따른 임계내압을 분석을 통해서 균열이 두께 방향으로부터 바깥 크기가 10 %의 균열이 존재하더라도, 영향을 미치는 것을 알 수 있었으며, 균열 전파 분석의 경우 0.02 MPa 차이가 나는 것을 판단할 수 있다. 이를 통해, 추후 실제 CO_2 배관을 설계 할 때 중요한 요소가 될 것이라 판단되며, 해석에서의 배관의 길이를 연속적으로 늘리거나, 다른 CVN energy, 토양의 밀도를 적용하여 해석한다면, 실제 설계와 해석의 차이 분석을 통하여 상당의 설계 소요 금액을 줄 일 수 있을 것이라 판단된다.

핵심어: 균열 전파, 유동 구조 연계 해석, 임계 내압, CTOD, Traction-separation, Charpy v-notch impact test, CO2 배관, XFEM, 주응력, 원주 용접, Fracture energy

학번: 2010-20616